UNIVERSIDAD DE CHILE
FACULTAD DE CIENCIAS FÍSICAS Y MATEMÁTICAS
DEPARTAMENTO DE FÍSICA

TOPOLOGICAL MECHANICS OF HYPERSTATIC METAMATERIALS

TESIS PARA OPTAR AL GRADO DE MAGÍSTER EN CIENCIAS, MENCIÓN FÍSICA

FERNANDO ELADIO VERGARA ARREDONDO

PROFESOR GUÍA:
CLAUDIO MOISÉS FALCÓN BEAS

PROFESOR CO-GUÍA:
CARLOS ALBERTO CÁRDENAS VALENCIA

MIEMBROS DE LA COMISIÓN:
ÁLVARO SEBASTIÁN NÚÑEZ VÁSQUEZ
GUSTAVO ALBERTO DÜRING HIDALGO

Este trabajo ha sido parcialmente financiado por FONDECYT Regular - N. 1210656

SANTIAGO DE CHILE
2023

RESUMEN DE LA TESIS PARA OPTAR
AL GRADO DE MAGÍSTER EN CIENCIAS
MENCIÓN FÍSICA
POR: FERNANDO ELADIO VERGARA ARREDONDO
FECHA: 2023
PROF. GUÍA: CLAUDIO MOISÉS FALCÓN BEAS
PROF. CO-GUÍA: CARLOS ALBERTO CÁRDENAS VALENCIA

MECÁNICA TOPOLÓGICA DE METAMATERIALES HIPERESTÁTICOS

La mecánica topológica es un campo emergente que combina conceptos de la mecánica clásica y las fases topológicas de la materia estudiadas en la teoría de la materia condensada. En este campo, la topología no trivial de la materia y los estados topológicamente protegidos se extienden a sistemas mecánicos diseñados artificialmente para mostrar respuestas mecánicas específicas, denominados metamateriales mecánicos. Dentro de este contexto, el estudio de los modos topológicamente protegidos a frecuencia cero ha recibido un interés particular, típicamente en sistemas en los que el número de restricciones está equilibrado con el número de grados de libertad, denominados sistemas isostáticos. En cambio, en esta tesis nos centramos en sistemas que tienen más restricciones que grados de libertad, denominados sistemas hiperestáticos, que son más rígidos y estables que los isostáticos.

Comenzamos revisando el marco topológico de los modos de frecuencia cero y, en concreto, revisamos la cadena isostática, que admite modos topológicamente protegidos a frecuencia cero y surge como un análogo mecánico para un modelo de aislante topológico prototípico, el modelo Su-Schrieffer-Heeger, el cual admite estados de energía cero. Más adelante introducimos la cadena hiperestática, un sistema hiperestático inspirado en la cadena isostática que también puede caracterizarse topológicamente por un número de enrollamiento, y donde la interfaz entre dos cadenas topológicamente distintas, el sistema admite modos topológicamente protegidos de baja frecuencia exponencialmente localizados en la interfaz. A continuación, introducimos la generalización de la cadena hiperestática a un sistema compuesto por una superposición de múltiples cadenas hiperestáticas. Aqui concluimos que es posible caracterizar topológicamente el sistema siempre que las cadenas en la composición compartan ciertas relaciones geométricas y como consecuencia de esto, cada cadena en la composición diferirá en su rigidez. En este contexto, una interfaz entre dos sistemas de cadenas múltiples topológicamente distintos, admite estados topológicamente protegidos de baja frecuencia , independientemente del número de cadenas en la composición. Por último, estudiamos un sistema compuesto por una cadena hiperestática geométricamente uniforme pero con una interfaz de elasticidad que también admite un estado exponencialmente localizado en la interfaz y que proponemos pueda clasificarse topológicamente a futuro. Finalmente, en el régimen no lineal, se muestra que la cadena hiperestática exhibe un comportamiento solitónico en el límite de rigidez total de un resorte, como también se encontró en la versión isostática.

Hemos demostrado la existencia de modos topológicamente protegidos en un sistema donde el número de restricciones puede ser indefinidamente mayor que el número de grados de libertad y esperamos que nuestro trabajo pueda servir para explorar nuevos sistemas topológicos en el régimen hiperestático.

RESUMEN DE LA TESIS PARA OPTAR
AL GRADO DE MAGÍSTER EN CIENCIAS
MENCIÓN FÍSICA
POR: FERNANDO ELADIO VERGARA ARREDONDO
FECHA: 2023
PROF. GUÍA: CLAUDIO MOISÉS FALCÓN BEAS
PROF. CO-GUÍA: CARLOS ALBERTO CÁRDENAS VALENCIA

TOPOLOGICAL MECHANICS OF HYPERSTATIC METAMATERIALS

Topological mechanics is an emerging field that combines concepts of classical mechanics and the topological phases of matter encountered in condensed matter theory. In this field, the non-trivial bulk topology and the topologically protected states are extended to mechanical systems artificially designed to exhibit specific mechanical responses, called mechanical metamaterials. Within this context, the study of topologically protected zero-frequency modes has received particular interest, typically in systems where the number of constraints is balanced with the number of degrees of freedom, which are called isostatic systems. In contrast, in this thesis, we focus on systems that have more constraints than degrees of freedom, called hyperstatic systems, which are more rigid and stable than isostatic ones.

We start by reviewing the zero-frequency modes topological framework and specifically, we review the isostatic chain, which supports topologically protected zero-frequency modes and emerges as a mechanical analog for a prototypical topological insulator model, the Su-Schrieffer-Heeger model, which supports zero-energy states. Later we introduce the hyperstatic chain, which recently was introduced as a hyperstatic system inspired by the isostatic chain that also can be topologically characterized by a winding number, and where the interface between two topologically distinct hyperstatic chains, the system supports low-frequency topologically protected modes that are exponentially localized. Next, we introduce the generalization of this hyperstatic chain to a system that is composed of the superposition of multiple hyperstatic chains, which we call a multiple-chain system. First, we conclude that is possible to topologically characterize the system as long as the chains in the composition share certain geometrical relations. To follow this topological characterization every chain in the composition will differ in their stiffness. Regarding this, at an interface between two topologically distinct multiple-chain systems, topologically protected low-frequency states are supported, regardless of the number of chains in the composition. In addition, we studied a system composed of a geometrically uniform hyperstatic chain but with an elasticity interface that also supports an exponentially localized state in the interface which we propose can be topologically classified in future work. Finally, in the non-linear regime, it is shown that the hyperstatic chain exhibits a solitonic behavior in the limit of total rigidity of one spring, as was also encountered in the isostatic version, that supports a zero-energy propagative solution. We replicate the analyses in the hyperstatic case where we show that only finite energy solutions are supported.

We have shown the existence of topologically protected modes in a system where the number of constraints can be indefinitely larger than the number of degrees of freedom and we expect that our work can serve to explore new topological systems in the hyperstatic regime.

Para mi abuelita Sesia Salinas

In opposition to the foolish ignorabimus our slogan shall be “We must know – we will know”

David Hilbert

Acknowledgments

When I started this process, along with a global pandemic and into a subject I had not previously studied, I knew it was going to be difficult. However, now in retrospect, I learned things and solved problems that I saw as impossible at first, and that even led me to travel to Brazil and the USA. All this would have been impossible without the guidance and willingness of Professor Claudio Falcon, whom I bothered countless times in and out of work hours, during weekends and vacations, and where there was always the willingness to help me. During this process, when problems seemed to have no solution or when the impostor syndrome appeared, he always knew how to support and encourage me. I would also like to thank Professor Carlos Cardenas, without whom I would probably be doing something else if he had not shown me this research topic during my undergraduate studies. I would also like to thank Professors Xiaoming Mao, Corentin Coulais, Zeb Rocklin and Anton Souslov all of whom are experienced in the subject and with whom I have had interesting discussions.

Thanks to all my family for helping me directly and indirectly up to this point. To my parents Olga Arredondo and Eladio Vergara who took care of my early education, and who have also supported my formation as a scientist. To my *abuelita* Sesia Salinas, who without understanding much of what I do has always been proud. I thank my sisters Dominique and Alison Vergara (as long as she does not believe in horoscopes), my niece Renata Cabala, and my aunts Celeste Arredondo and Maximiliano Sanchez who fostered my scientific spirit since I was a child. I also thank Luz Diaz and Valeria Toro who have also been important to me and my father. And because they are also like my family, to my cat Pepa who was by my side every night I wrote this and to my dogs Bloom and Jack (who barked every day I wrote this).

Certainly, I thank my best friend Trinidad Novoa, who despite the distance has been able to be present in this process, and also all the friends from the university, Ivan Gallo, Jaime Clark, Maricarmen Winkler, Edgar Barriga, Javier Silva, Nayadeth Villarroel, Nicole Diaz, Karol Rapunzel and Jose Mella, who are still there despite the lack of time and that many of us follow different paths.

Thanks to BaityBait and Joseju, who recommended *Outer Wilds*, and who have accompanied me during this stage.

Finally, thank to Pedro Rojas, a friend since I can remember, and the rest of the group *piamartinos de corazón* Bastian Meza, Esteban Perez, Marco Cumian, Nicolas Sandoval and Diego Kaeri.

Table of Content

List of Figures

Chapter 1

Introduction

The new field of topological mechanics combines principles of classical mechanics, and topological phenomena inherited and inspired by condensed matter theory, where a novel class of fashioned-designed mechanical materials called metamaterials, fit as a spontaneous link between these two fields. In this chapter, we will review the basics of classical mechanics, and topological condensed matter theory, starting by introducing the fundamental topology concepts. Later we review some examples on topological condensed matter theory including a specific model that is important in the problems treated in this thesis. After this we present the concept of mechanical metamaterials and why there are a good platform to study topological mechanics problems. We recommend some remarkable books and reviews such as [1–9] and [10–18] for a detailed discussion on the topics treated in this chapter, and also many tangential study problems.

1.1 On Topology

In mathematics, a circumference or a sphere are examples of spaces that locally look like $\mathbb{R}^n$, but not necessarily globally[1], which are called *manifolds*[1], and the mathematics branch called *Topology* deals with the properties and classification of these spaces under continuous deformations. Beyond the formal definition of what is a continuous deformation, it could be more intuitive to think first of some examples. A spherical surface can be continuously stretched to obtain, for instance, an ellipsoid. In contrast, when considering the surface of a plane, is not possible to deform it to get a sphere unless we "glue it", that is, to glue the plane boundaries and obtain a closed surface as the sphere. The opposite is also not possible: the spherical surface cannot be deformed to obtain a plane without "cutting" the sphere at some point(see Fig. 1.1). All these manifolds are *topological spaces*[2], and in the case of the sphere and ellipsoid, they are set to be *topologically equivalent*, while the sphere and the plane are not. Stretch, bend, and twist, as we usually encounter in mechanics, are particular cases of *homeomorphisms*, which are continuous maps with a continuous inverse map[1, 2], and

[1] $n = 1$ for the circumference and $n = 2$ for the sphere

[2] In this thesis we will assume the term without formally defining what a topological space is or that every mentioned space is indeed a topological space, since in general, we will deal with well-known spaces.

consequently one says that two topological spaces are equivalent if there a homeomorphism between them.

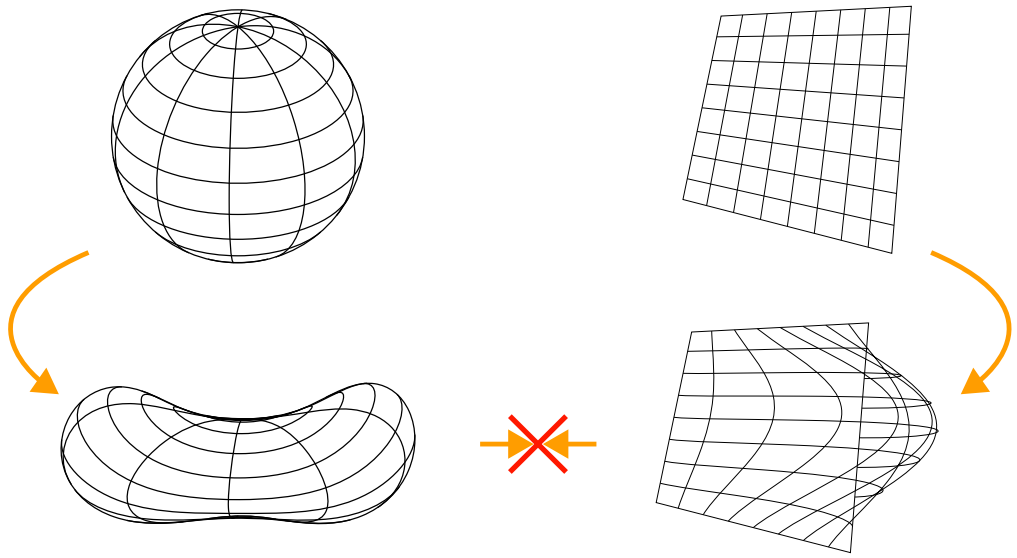

Fig. 1.1: *Topological difference between a spherical and plane surface. The spherical surface (top left) can be continuously deformed to shapes like the one at the bottom left. Similarly, the plane surface (top right) can be continuously deformed to shapes like the one at the bottom right. However, by only considering continuous deformations, the deformed sphere cannot become the deformed plane and vice versa.*

Despite that sometimes it is trivial to know if there is a continuum transformation between spaces, as in the case of the sphere and the ellipsoid, it would be useful to have a method to evaluate systematically the existence of a continuous transformation between two spaces. This goal is, nevertheless, too ambitious[1]. Instead, it is possible to partially address the problem, by knowing when two spaces are not topologically equivalent. For that purpose, one classifies the spaces with a certain *topological invariant* that is preserved by continuous transformations and therefore allows us to assert that two spaces with a different topological invariant are not equivalent. Some of these invariants can be elemental topological properties, like space compactness, which refers to the closed and bounded condition of a space, or space connectedness, which refers to the union of disjoint open sets. However, it must be noted that the equivalence between spaces can be broken if any invariant differs in two topological spaces[1, 2]. Notice that the inverse affirmation, that is, that two spaces that share a topological invariant imply the existence of an homeomorphism between them, is not true in general, because there could be another invariant where they differ.

So far, treating only elemental topological properties, like the aforementioned ones, does not allow us to classify some of the most common topological spaces, e.g. the compactness of a sphere and a torus are similar, when they are topologically different. For this purpose, the *algebraic topology* uses algebraic expressions to classify the spaces and instead of the homeomorphism formulation, it uses broader formulations. For instance, it can be shown that the genus number (roughly speaking, the number of holes in a surface), is a topological invariant of two surfaces as long as these spaces are homeomorphic[1]. With this invariant,

which is obtained from an algebraic expression over the surface, is clear that a sphere S^2 with genus number zero is not equivalent to a torus T^2(e.g. a doughnut) with genus number one. This can be also understood by realizing that it is not possible to transform one space to the other without closing or opening a hole(see Fig. 1.2). The above comparison leads to the most common and overused example in topology, referred in the mathematical joke[19]

> Q: "What is a topologist? "
> A: "Someone who cannot distinguish between a doughnut and a coffee cup"

because the surface of a "coffee cup" and the torus surface have the same genus number. Finally, for this thesis, it is important to mention a last invariant that will be relevant in the next discussions: the *homotopy groups* of a topological space. Again, avoiding a formal definition, in a topological space X, the n-th order homotopy group is composed of the continuous mappings of the S^n sphere onto X, $S^n \to X$. The most elemental homotopy group is the fundamental one denoted as $\pi_1(X)$ which characterizes the closed loops that are equivalent between each other[2], where two loops are equivalent if it is possible to continuously deform one loop into the other. The simplest case is the fundamental group of a circle $\pi_1(S^1)$, where every closed loop can be "drawn" just along the circle line, and considering that every loop can roll up a different number of times and orientations, thus $\pi_1(S^1) \cong \mathbb{Z}$. Here "$\cong$" refers to an isomorphism, which is a bijective map between two groups that preserve its topology, but also it is common to use just "$=$".

To exemplify the concept, it can be helpful to think of two spaces that do not share their fundamental group. In the sphere, we have that $\pi_1(S^2) \cong 0$ since any loop that lies on the surface can be contracted along the surface until reaching a single point as shown in Fig. 1.2. Instead in the torus $T^2 = S^1 \times S^1$, the fundamental group is more complex, since it is possible to draw loops over the two independent sections of the surface(see Fig. 1.2), which are just the two circles that define the torus, and therefore $\pi_1(T^2) \cong \pi_1(S^1) \oplus \pi_1(S^1) \cong \mathbb{Z} \oplus \mathbb{Z} = \mathbb{Z}^2$. Consequently, this invariant also indicates a topological difference between the sphere and the torus.

The first homotopy group of a certain space X is usually the most intuitive one, but in contrast, their higher order homotopy groups, $\pi_n(X)$ $n > 1$, can be hard to understand even at low orders, because $\pi_n(X)$ requires to consider a deformable n-sphere S^n over the space X, which deals with higher dimensional reasoning. The simplest case that does not require going further from the three-dimensional space is $\pi_2(S^2)$, which is the mapping of the deformable closed spheres, over the spherical surface. This surface can wrap around the sphere(as it also happened with the loops in the circle) multiple times and orientations(see Fig. 1.2), and therefore $\pi_2(S^2) \cong \mathbb{Z}$. On account of this, and in favor of reducing to essentials, we will only deal with problems where the fundamental group can be used to compare the topology of different topological spaces.

Up to this point, no physics problems have been discussed. Regarding its mathematical formulation, it is possible to study the topology of many physical systems. Nevertheless, if there are topological properties, does it have physical meaning? and if they do, what consequences could we draw about that? As we will review, there are several physics problems where the topological properties and topological invariants are key features of the study.

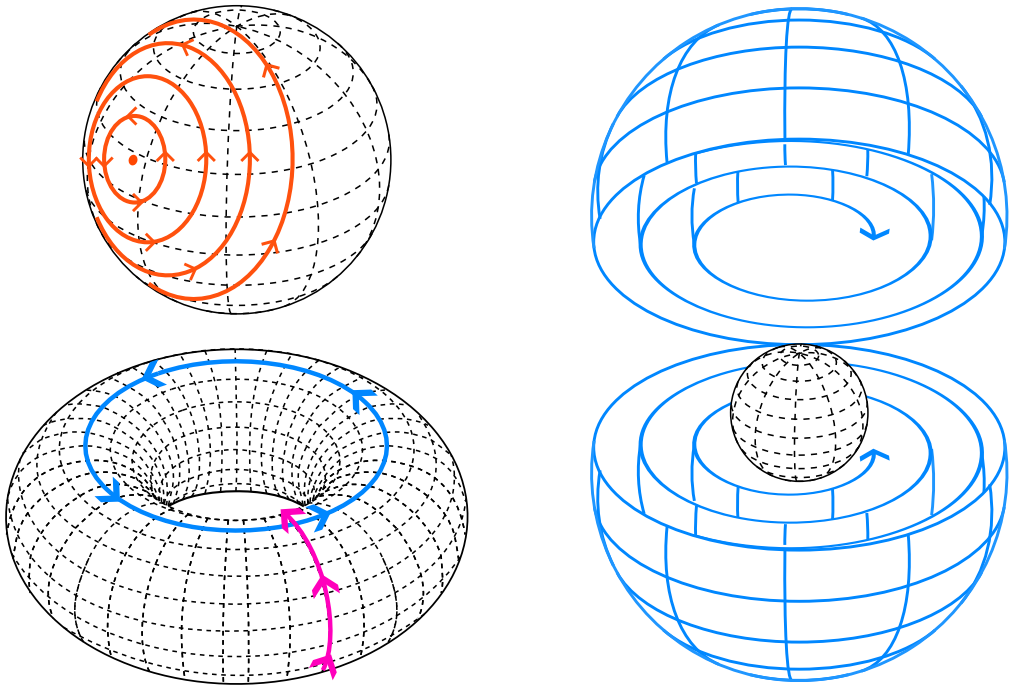

Fig. 1.2: *The spherical surface(top left), has a genus number zero, while a torus surface(bottom left) has a genus number of one. In addition, these figures also show the closed loops in the surfaces(solid directed lines) which compose the fundamental homotopy group. In the sphere, every closed loop can be contracted to a single point. In contrast, in a torus, there are closed loops in two independent sections of the surface, that cannot be contracted. On the right, the figure shows a schematic view of the second homotopy group of a sphere. The spherical closed surface mapping (solid lines surface), can roll up an integer number of times to the inner spherical surface(dashed lines surface).*

1.2 Topology in Condensed Matter Theory

In 1980 K. Von Klitzig observed that in a two-dimensional electron gas under a strong external magnetic field at low temperature(> 1 T and ~ 2 K respectively), the Hall resistivity becomes quantized in units of h/e^2, while the longitudinal resistance dropped to zero[20]. This phenomenon is known as the *quantum Hall effect* (QHE)(see Fig. 1.3), and its quantization showed to be highly accurate and robust to microscopic details[21]. A few years later, Thouless et.al.[22], prove that this resistance quantization can be explained by a topological invariant, the *Chern number*, where aspects like the microscopic defects act as "continuous deformations" of the system, and the quantized response(Hall resistivity) relies on the invariance of the Chern number. This number is obtained from the system *bulk*, where the bulk is the material zone where the interfaces or surfaces are not influential. While the aforementioned deformations can change the bulk, its Chern number remains invariant[5]. The discovery and the explanation of the QHE were meritorious of two different Nobel prizes[3], and are one of the most important physics phenomena dealing with topological properties.

The QHE involves two features, the quantized Hall resistivity, explained by a topological property that endows its robustness, but also a boundary of zero longitudinal resistance.

[3]In 1985 the prize for Von Klitzig, and 2016 the shared prize for Thouless, Haldane and Kosterlitz

These two features, bulk and boundary resistivity, appear to be related in some manner. This relation is one of the most important concepts in the study of topological states of matter, known as the *bulk-boundary* correspondence[4, 5]. The correspondence can also be seen by noting that the bulk shares its robustness with the states on the edge, which are known as *topologically protected states* and will remain in the system as long as the bulk holds this non-trivial Chern number[5].

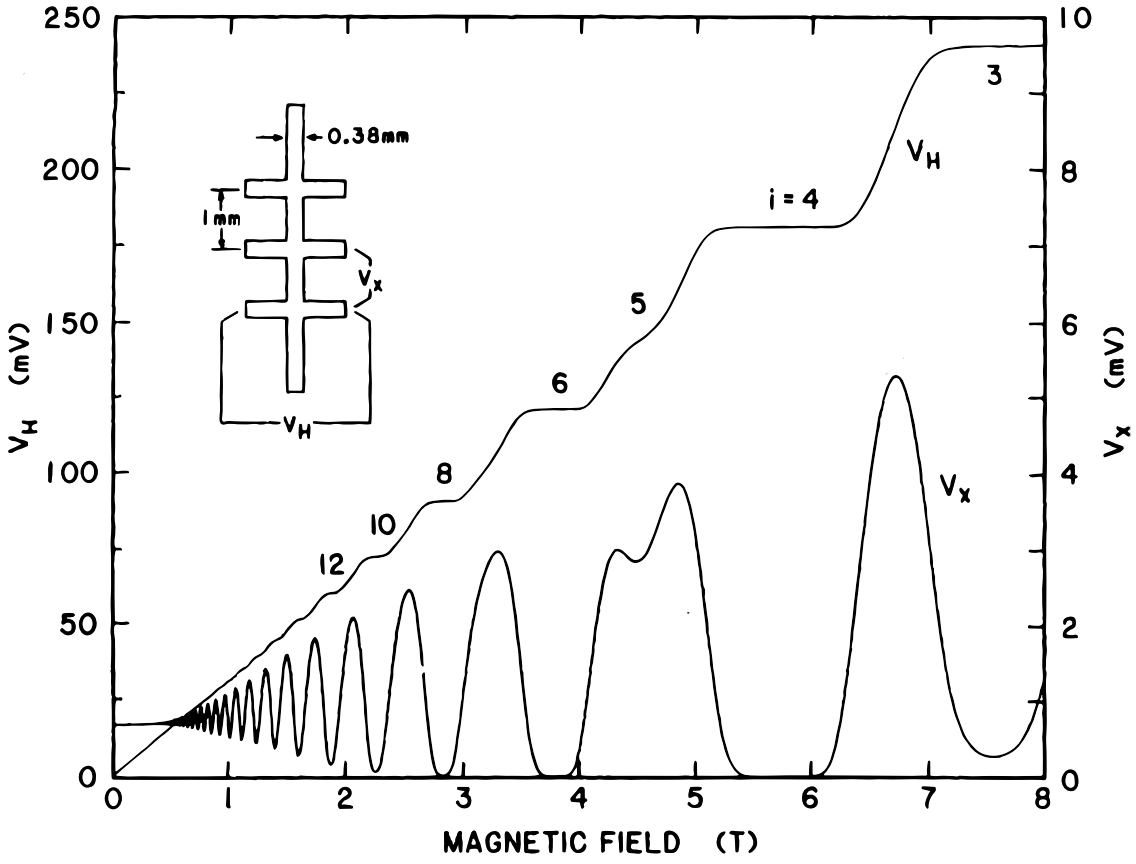

Fig. 1.3: *Measurement of the Hall voltage V_H, and the longitudinal voltage V_x in a two-dimensional electron gas(see inset) cooled to* 1.2 *K as a function of the external magnetic field. The Hall or transversal resistivity $R_H = \frac{V_H}{I} = \frac{h}{e^2 i}$, is quantized for the integer i, while the longitudinal resistance drops to zero[21], for a current $I = 22.5\mu A$. Reprinted from Ref. [23] with permission from IEE.*

Inspired by this discovery, there have been additional topological phases of matter discovered in condensed matter, such as *topological insulators*. Different from the QHE where the external magnetic field is required to reach the topological quantized phase, in topological insulators there are topologically protected states where the bulk topology relies on the system's *symmetry*. What represents these symmetries and how they are related to the system will be treated in the following section, where we will discuss one of the most extended examples of a topological insulator, which also is intimately related to the specific problems of this thesis.

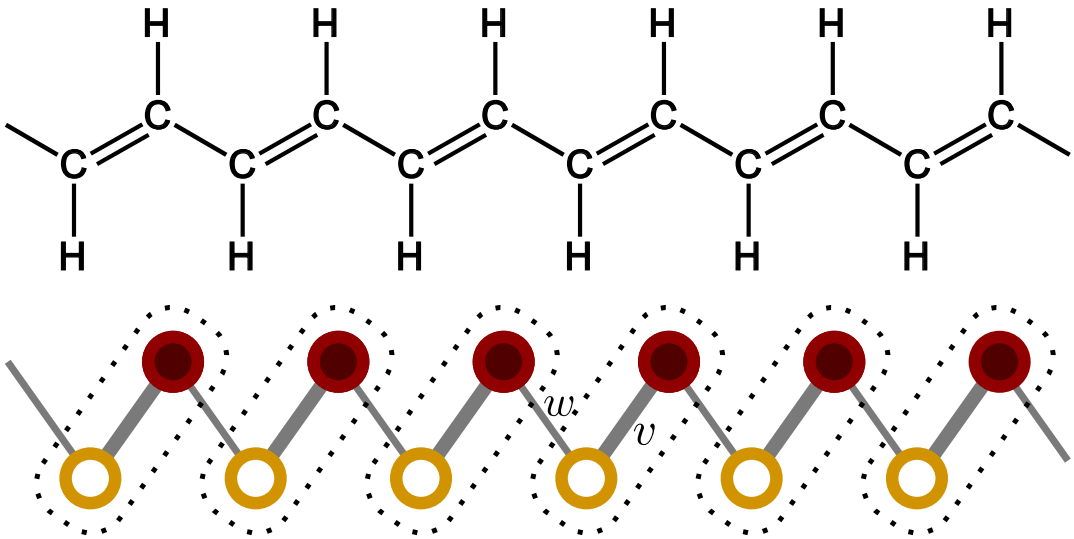

Fig. 1.4: *The structural diagram of a polyacetylene molecule (top), and the diagram of the SSH model (bottom). In the SSH model, every unit cell is composed of two sites, in the sub-lattice A and B, represented by empty circles and filled circles respectively. The sites are coupled by an intra-cell hopping v and an inter-cell hopping w, and the line thickness between sites represents the strength of these couplings(in this case $v > w$).*

1.2.1 The Su-Schrieffer-Heeger Model

The Su-Schrieffer-Heeger model (SSH)[24] is a prototypical example of a topological insulator, and emerges as a tight binding model to describe the electronic conduction along the polyacetylene molecule, an organic polymer composed of carbon and hydrogen atoms, with an alternating double and single bond between the carbon ones (see Fig. 1.4). The model describes spin-less charged particles on a one-dimensional lattice where each unit cell host two sites A and B with an inter-cell hopping v and an intra-cell hopping w, as shown in Fig. 1.4. A bulk Hamiltonian can be written to describe its bulk electronic conduction od these particles and can be addressed by considering a lattice under periodic boundary conditions(PBC). From the stationary Schrödinger equation describing the evolution of these particles along the periodic lattice, the following eigenvalue equation is obtained,

$$\hat{H}(k)\,|u_n(k)\rangle = E_n(k)\,|u_n(k)\rangle \qquad |u_n(k)\rangle = a_n(k)\,|A\rangle + b_n(k)\,|B\rangle$$

where $\hat{H}(k)$ and $|u_n(k)\rangle$ are the bulk k-space Hamiltonian and the k-space eigenstate of energy $E_n(k)$ respectively, and $|A\rangle(|B\rangle)$ denotes the state of the chain for the particles in sublattice $A(B)$. The above equation can be written in a matrix form as

$$H(k)\begin{pmatrix} a(k) \\ b(k) \end{pmatrix} = E(k)\begin{pmatrix} a(k) \\ b(k) \end{pmatrix}$$

where $H(k)$ is the bulk k-space Hamiltonian matrix:

$$H(k) = \begin{pmatrix} 0 & v + w\, e^{-ik} \\ v + w\, e^{-ik} & 0 \end{pmatrix} = \begin{pmatrix} 0 & h(k) \\ h^*(k) & 0 \end{pmatrix}$$

From the above equation, the dispersion relation $E(k)$ is obtained

$$E(k) = \pm\sqrt{v^2 + w^2 + 2vw\cos k}$$

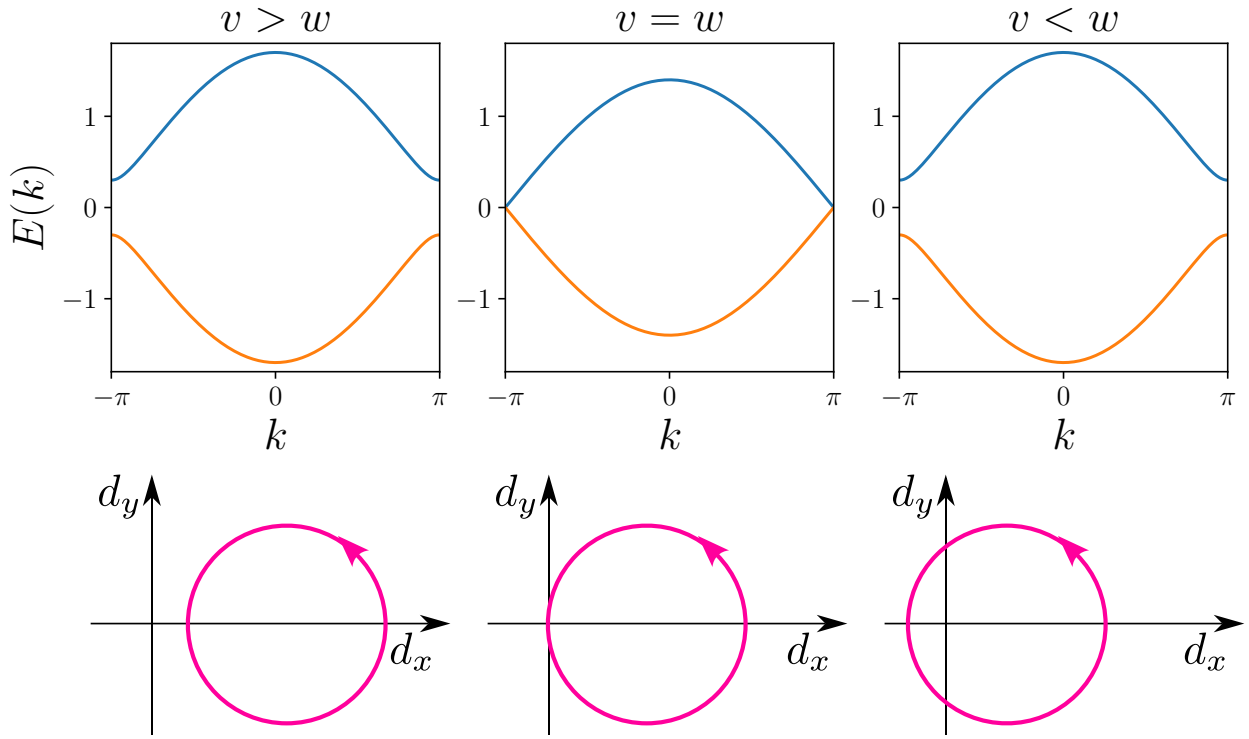

Fig. 1.5: *At the top, the figure shows the band diagram of the dispersion relation $E(k)$, for three different cases as indicated in each diagram. The color orange(light blue) represents the filled(empty) energy band. In the bottom, is shown the parameterization of the vector $\mathbf{d}$ in the d_x, d_y plane for the three cases of the energy band diagrams, where each parameterization corresponds to the case for the band diagram above the parameterization.*

In Fig. 1.5, the dispersion relation shows an energy band gap as long as $v \neq w$, which means that the system is an insulator, and becomes a conductor for $v = w$. Notice that in two chains, with $w > v$ and $w < v$, and equal $|v - w|$, the bands look identical, however, there is a relevant difference not distinguishable in $E(k)$, the topological facet present in this type of system that differentiates it from a regular insulator. This difference can be appreciated as we consider the vector $\boldsymbol{d}(k) = (v + w\cos k, w\sin k, 0)$, which arises from the expansion of $H(k) = \boldsymbol{d}(k) \cdot \boldsymbol{\sigma}$, where $\boldsymbol{\sigma} = \hat{\sigma}_x + \hat{\sigma}_y + \hat{\sigma}_z$ and $\{\hat{\sigma}_i\}$ is the Pauli matrices basis[4]. The parameterization of $\boldsymbol{d}(k)$ as k runs through the first Brillouin zone $k : 0 \to 2\pi$, draws a

[4]Where the factor of $\hat{\sigma}_0 = \mathbb{1}$ is zero

closed circle in the d_x, d_y plane, which can be topologically classified according to depending on this circle enclose or not the coordinates origin. This classification is encoded in the *winding number*:

$$\nu = \frac{1}{2\pi i}\int_{-\pi}^{\pi} dk \frac{d}{dk} \ln h(k) \tag{1.1}$$

The winding number is the characteristic topological invariant present in one-dimensional systems, in difference from the Chern number that characterizes the topology in two-dimensional systems, such as the mentioned QHE. The computation of ν for different hopping pairs results in $\nu = 1(\nu = 0)$ when the chain hoppings comply with $w > v(v < w)$, and becomes undefined when the energy band gap closes at $w = v$(see Fig. 1.5). Beyond the information obtained from the bulk, there is physical relevance of these topological features in addition to the difference for the $v < w$ and $v > w$ cases. Despite that the two gapped systems in Fig. 1.5 share their electronic bands, these systems are topologically different according to ν, because two PBC systems of $v < w$ and $v > w$ that latter we ''cut", results in two finite chains that exhibit an elemental difference. The chain where $\nu = 1(w > v)$, also known as the topological case, will support *zero energy* states in the thermodynamic limit[5], as long as the energy band gap remains open, but in contrast, the topologically trivial case ($\nu = 0$), will behave as an ordinary insulator. Remarkably these zero-energy modes will be exponentially localized in the edges because the zero energy level lies in the energy band gap, and consequently these modes cannot propagate through the bulk. Furthermore, these states are topologically protected states and will remain in the chain as long as the system preserves its non-trivial topology. This close relation between the bulk topology and the edge states is the aforementioned bulk-boundary correspondence.

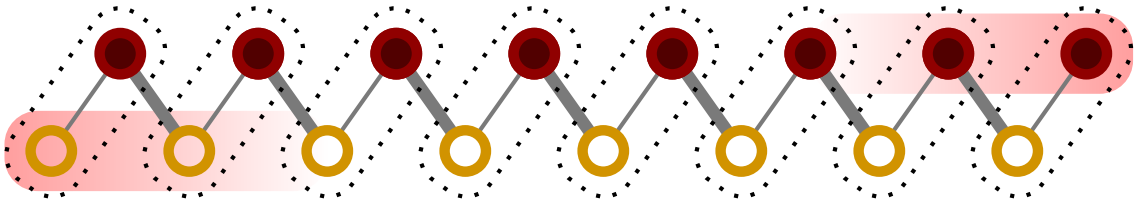

Fig. 1.6: *Finite SSH model chain for $w > v$, where zero energy modes appear at the boundaries. The highlight gradient under the sites represents the exponentially localized nature of these modes, which is supported only in the sub-lattice A(B) in the left(right).*

If the winding number represents a topological signature in the system, it should be invariant under continuous deformations. Here they are called *adiabatic transformations* and must meet the following conditions: In a Hamiltonian, this transformation can only produce continuous variations that keep open the bulk energy band gap, but also the transformation must preserve the relevant symmetries of the system[4]. In quantum mechanics, a symmetry represents

[5]In a finite case, only when $v = 0$ there are completely localized zero energy states, and out of this limit are exponentially localized almost-zero energy states, but in the thermodynamic limit is a good approximation call them as zero energy states.

a transformation where the Hamiltonian remains unchanged and can be represented by a unitary operator $\hat{U}$, as

$$[\hat{H}, \hat{U}] = 0$$
$$\Leftrightarrow \hat{U}\hat{H}\hat{U}^{\dagger} = \hat{H}$$

This system in contrast exhibits a more specific type of symmetry, a *chiral symmetry* $\hat{U}_s$, which involves a transformation that changes the Hamiltonian into its "mirror image'',

$$\hat{U}_s\hat{H}\hat{U}_s^{\dagger} = -\hat{H}$$

The presence of $\hat{U}_s$ in a system implies a symmetric energy spectrum(but not the inverse statement), as we observe in the SSH model, where each eigenstate $|\psi\rangle$ of energy E has their chiral symmetric partner $\hat{U}_S|\psi\rangle$ of energy $-E$. Additionally, a chiral symmetric system can be described by two subsystems with no interaction between the sites from the same subsystem. This feature is also present in the SSH model since there are no diagonal terms in $H(k)$ that couple sites that share sub-lattice index A or B, and implies that necessary $d_z = 0$ in $\boldsymbol{d}(k)$, which guarantees that this parameterized loop, is restricted to the d_x, d_y plane. Therefore the preservation of the symmetry by an adiabatic transformation can only shift the parameterization $d(\boldsymbol{k})$ in the d_x, d_y plane, and cannot change ν without passing through $d(\boldsymbol{k}) = 0$ which would close the gap where ν it is not well-defined.

In a chiral symmetric system, each zero energy state, in difference from the ordinary states, is supported exclusively in one of the two sub-systems. For instance, in the SSH model, a finite topological chain supports a zero energy state at the left edge, described only by states of sublattice index A, and a second zero energy state at the right edge, described only by states of sublattice index B (see Fig. 1.6). In addition to the finite chain, it is also possible to obtain these modes at the interface of two topologically distinct systems, as shown in Fig. 1.7 where there are three domains of fully dimerized chains, i.e. where $v = 0$ or $w = 0$, and there are two different types of completely localized zero energy states in the system.

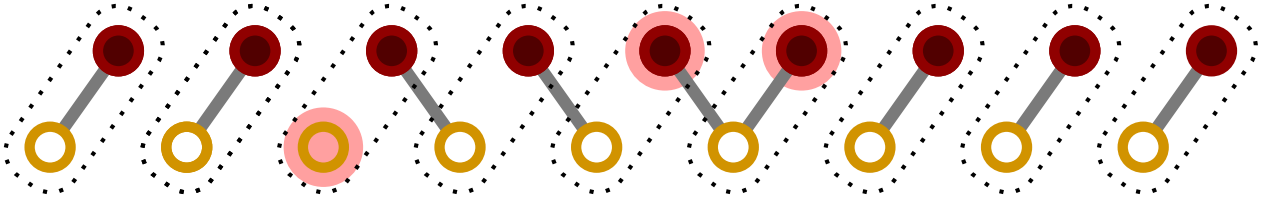

Fig. 1.7: *Three domains of dimerization in the SSH model. The figure shows a localized zero mode shared between two sites in the sub-lattice B, and another zero mode located only in a single site of sub-lattice A.*

In the previous system, there is an essential relation between the chiral symmetry and the

system's topological properties, but more symmetries can be present in quantum mechanical systems. Indeed, based on three prominent symmetries: *time reversal symmetry*, *particle hole symmetry* and chiral symmetry there is an extended classification scheme for topological insulators[6] called the *tenfold way*[25]. According to the Hamiltonian symmetries, this scheme developed a topological classification with respect to the homotopy groups of the Hamiltonian topological space. For instance, because of the chiral symmetry present in the SSH model, this model can be classified by this scheme, and the predictions are in concordance with the values obtained by its winding number. This systematic way of categorizing topological phases of matter provides powerful tools for characterizing the topological properties of these materials, and because of this advantage, a similar methodology will be recurrent in the following chapter's discussions.

Up to this point, we have talked about two systems that exhibit topological properties due to different causes, the QHE and a one-dimensional topological insulator, the SSS model. Even though these systems represent a promising class of materials with distinct topological features, their practical realizations have several drawbacks that restrict their applicability or utility. For instance, the first QHE realizations require highly specialized experimental setups, such as low-temperature control and high magnetic fields[21] which could make it difficult to study these systems. Also, topological insulators usually require a strong spin-orbit coupling or finely tuned fermi energy level[26]. Despite that there have been notable advances in recent years[27, 28], the implementation of analog systems has emerged as an alternative. In the recent years, several of these analogs have been developed in photonic crystals [29–31], phononics [32–57], mechanics [14–18, 32–84] and beyond, and despite is not possible to capture all the physics displayed in the quantum cases, many of it has been found an analogous. In particular, we are interested in the mechanical cases, and in the next section we discuss their advantages and why they are good candidates to display these topological phenomena.

1.3 Mechanical Metamaterials

According to one of the most extended and comprehensive definitions, metamaterials are artificial and ordered composites that exhibit exceptional macroscopic properties, that arise as a collective manifestation of a structure[85, 86]. This structure is built of several intended components usually arranged in regular patterns, acting as meta-atoms, where the distinctive features are obtained chiefly from this structure, rather than the chemical and physical properties of the material composition at the microscopic level[13]. This wide definition allows the development of metamaterials in several science fields, classifying them according to the nature of their functionality[10]. When a fashioned mechanical response is obtained, they are called mechanical metamaterials [87]. Such a general classification can include wide types of mechanical systems, including even some systems as old as those of Newton[88], but in modern times has become a trending research topic.

Among some of the modern examples of metamaterials, there are ones with unusual quasi-

[6]More precisely, it classifies topological insulators and superconductors, but the latter is beyond the scope of this discussion for the time being.

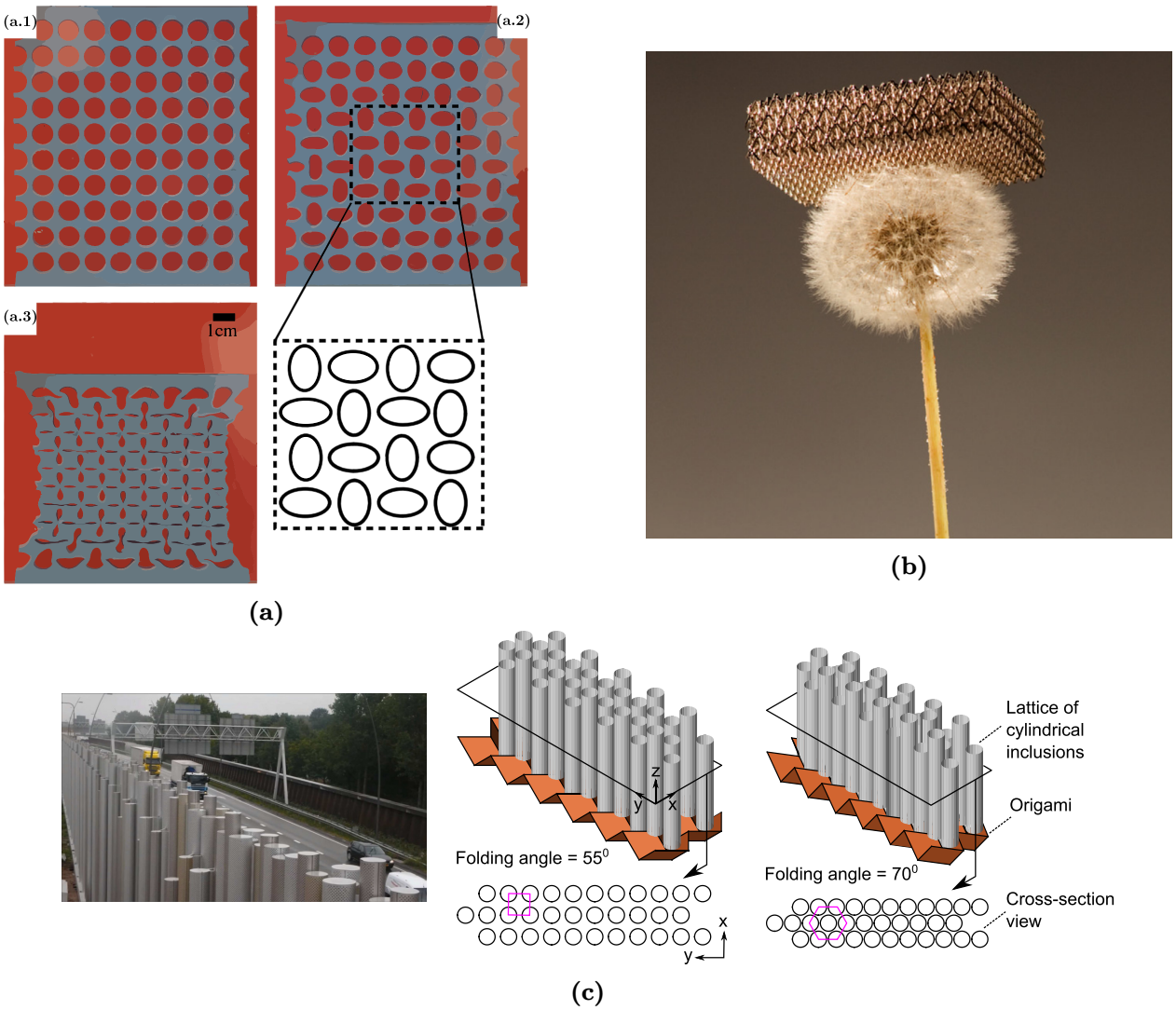

Fig. 1.8: *Metamaterials Examples. In* ***(a)*** *is shown a metamaterial of negative Poisson ratio, where* ***(a.1)****,* ***(a.2)*** *and* ***(a.3)*** *are different levels of compression and the zoom highlight the patter which takes the holes in the material when compressed. Reproduced from ref. [89]. In* ***(b)*** *is shown an ultralightweight mechanical metamaterial made by stereolithography and electroplating with copper where its voids have approximately the same mass as the surrounding elastic structure. Reproduced from ref. [90]. In* ***(c)*** *is shown an origami sonic barrier and its corresponding cross-section view, as well as the implementation at the side of a road. Reproduced from ref. [91]*

static responses such as a negative Poisson's ratio(i.e. auxetic)[92–94](see Fig. 1.8a), negative compressibility [95] or ultra-lightweight properties[90, 96](see Fig. 1.8b). In addition, some remarkable dynamical responses also can be found in mechanical metamaterials, such as acoustic wave guiding[97–99], acoustic cloaking[100, 101], or vibration isolation[48, 102–104](see Fig. 1.8c). Indeed many of the aforementioned dynamical examples can be considered also as a *phononic crystals*, where a periodic structure is designed to control the propagation of acoustic or elastic waves[11, 88](see Fig. 1.8c). These materials are particularly important in our discussion since the periodic structure is a fundamental feature in

condensed matter systems(e.g. the SSH model previously treated). Most of the mentioned examples work only in linear mechanics, but beyond this, there are fascinating ways that take benefits from the intrinsic non-linearities of these materials. In this context, there is a wide type of non-linearities that can be considered, which can lead to an even richer variety of mechanical responses[105]. For instance, some non-linear responses can arise from geometrically nonlinear deformation or structural instabilities, as some metamaterials design the mechanical response by making use of the buckling instability[89, 106], or the propagation of non-linear waves[66, 84, 105, 107]. In this thesis, we study a mechanical metamaterial, in both linear and the nonlinear regime, but the former being the major part of our study. This is because we are interested in the topological part of these systems, which is treated in the linear regime of oscillations.

1.4 Topological Mechanics

There are several rich phenomena restricted to the atomic scale, or that do not seem replicable at other scales. Some of these were the topological phases of matter such as the QHE or the topological insulators discussed in this chapter, which were for years a phenomena restricted to the electronic case, but in the present time some analogs of thse phenomena have been found even in classical mechanics systems [14, 17, 62, 64]. These systems can be more intuitive than quantum systems, and aspects as a wide range of materials and fabrication techniques allow for a precise design of structures geometries and properties [10]. The scalability of theses systems can also be beneficiated by this versability, which facilitates the production of metamaterials in a wide variety of sizes, from macroscale structures to microscale devices [13, 86]. Furthermore, the macroscopic scale of mechanical systems allows for direct observation and manipulation of their properties, and the required equipment for these experimental realizations is notably more accessible than in the quantum case. Overall, all these advantages allow us to state that mechanical systems are an excellent candidate for these analogies.

Topological mechanics is the branch of mechanical metamaterials that deals with topological aspects inspired by the topological phases of matter in condensed matter physics [14, 16]. As in condensed matter systems, the mechanical modes in topological mechanics systems are protected by the non-trivial bulk topology, and therefore the study of this topology is a central study of these systems. At first sight, the mechanical and quantum problem looks very different, starting from the fact that Newton's equation of classical mechanics is a second-order differential equation in time. In contrast, the Schrödinger equation which governs the quantum mechanics is only a first-order time differential equation. Similarly, the frequency of the normal modes in a mechanical system can only take non-negative eigenvalues; in contrast, in an electronic Hamiltonian, it is possible to have negative eigenvalues too. Depending on the mechanical system, this first problem can be solved in different ways, as we will explain in the next chapter.

Probably the first approach of a classical system in the line of topological insulators physics was done by Prodan and Prodan [78] where the concentration of energy at the edges of microtubules in live cells was explained using topological band theory including a non-trivial

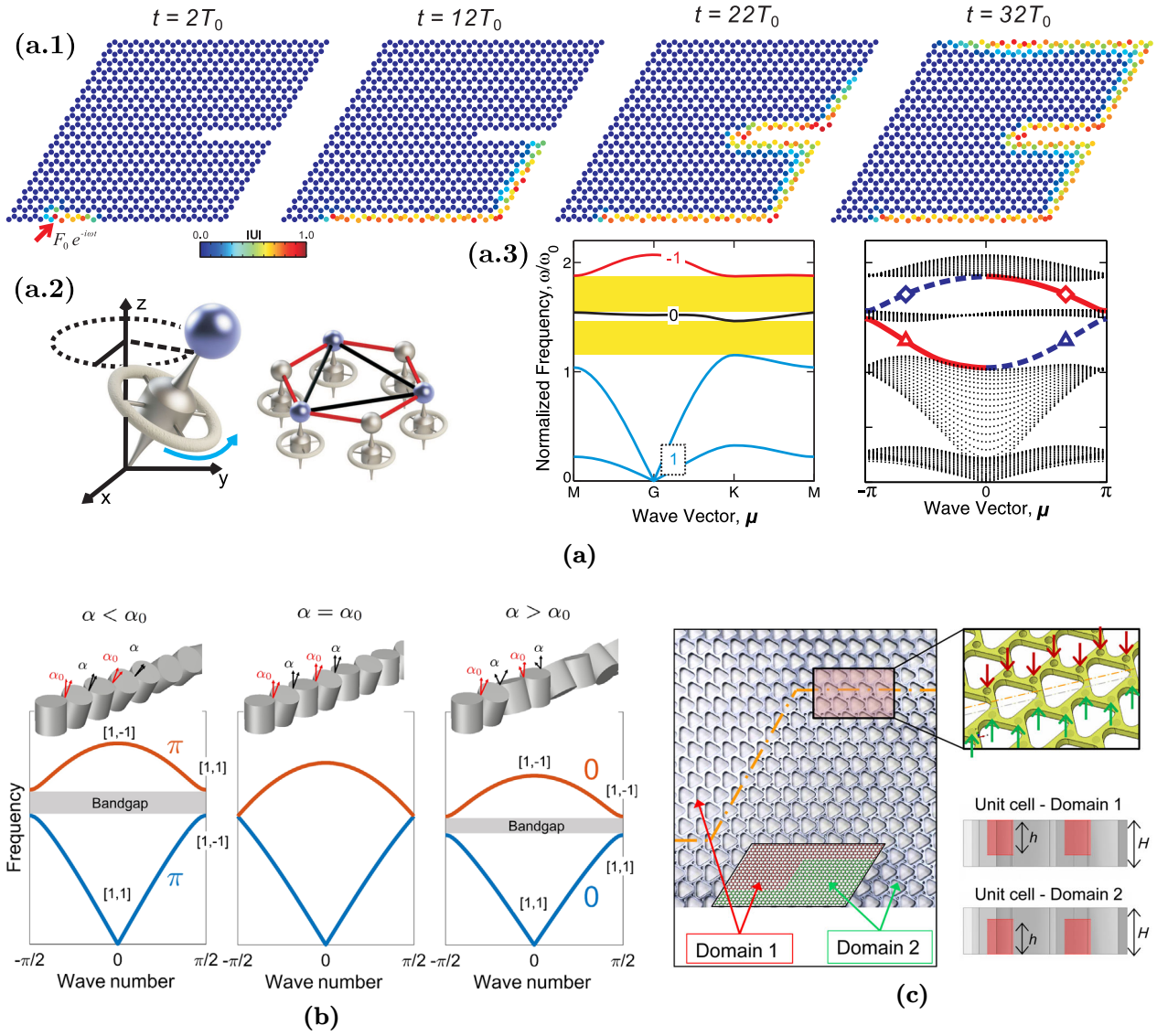

Fig. 1.9: *Topological mechanics metamaterials. In* ***(a)*** *is a mechanical analogous for the quantum anomalous Hall effect, where a hexagonal lattice of gyroscopes and springs with a mass attached at the top, is arranged in an hexagonal lattice as shown in* ***(a.2)****. The "Chern number" of each frequency band is shown in the left of* ***(a.3)****, where the right figure shown the edges modes that appear in the frequency band-gaps in a finite lattice. These modes are robust and propagate along the edge as shown in* ***(a.1)****. Reproduced from [48]. In* ***(b)*** *is shown the experimental realization of the SSH model in a highly tunable mechanical system made of cylindrical granular particles. By tuning the contact angles between the cylinders, the system can manifest boundary modes in a finite system. Reproduced from [108]. In* ***(c)*** *is shown the experimental realization of patterned elastic plates with reversed blind holes(zoom inset) that support topological boundary modes as shown in the interface between two domains. Reproduced from [109].*

Chern number. However, it was after Kane and Lubensky's work[72] that the subject became much more popular. They showed that the existence of certain topologically protected zero-frequency modes in spring-mass systems can be understood as the sum of a local boundary

contribution and a bulk topological contribution that relies on the system symmetry. In the next years, the topological mechanics study have been expanded to diverse new topological mechanics systems [14–18, 32–84], where we highlight numerous SSH model analogs [37, 43, 56, 57, 67, 72, 108, 110–113], or the mechanical analogs of some quantum Hall effect variants, such as the analog for the quantum anomalous Hall effect [48, 59](see Fig. 1.9a) and the analogs for the quantum spin Hall effect [42, 46, 109].

Along the line of the topological-zero frequency modes, the framework introduced by Kane and Lubensky [72] serves as the inspiration for various new problems, but also many of these problems inherited a fundamental characteristic of these systems, the balance between degrees of freedom(DOF) and constraints, which we call *isostatic*. In contrast in this thesis, the motivation is to study the existence of these modes in systems where the constraint number is higher than the DOF number, and where the aforementioned scheme is not valid. We refer to these types of systems as *hyperstatic* or *overconstrained*.

1.5 Outline and Thesis Contribution

Since our problems are still highly related to the topological zero-frequency modes introduced by Kane and Lubensky, in Chapter 2 we widely discuss this scheme and after this, in Chapter 3, we introduce a hyperstatic mechanical system that exhibits topological modes, introduced recently by Kedia et.al.[73]. In Chapter 4 we generalize the hyperstatic topological modes to even further constrained systems under certain symmetry conditions. Later, in Chapter 5, we take the previously mentioned system and describe the response of the system under non-linear deformations, where we show the existence of non-linear waves, previously described in an isostatic system[66]. In this thesis, we studied whether topological zero-frequency modes, which were previously restricted to isostatic systems, may be extended to hyperstatic systems in some way. We uncovered the limitations of a recent model that describes topologicalmodes in a hyperstatic system, but we were also able to expand this scheme outside of this domain, leading to numerous additional promising problems.

Chapter 2

Topological Mechanics of Zero Modes

The study of topological mechanics depends on mainly three factors, the mechanical system, the eventual topological properties and how to characterize these topological properties. In this chapter, we will set the approach of this thesis to these points. Our study focus is the mass-springs systems, a prototypical example of a physical systems that can be used to model a wide range of phenomena in physics and various science fields. We will review that these systems can exhibit a specific type of zero-frequency modes which can be topologically described by the inherited tools of topological insulators. In the first part, we review the physical formalism which facilitates the study of these modes and their physical meaning and after this, we discuss its topological properties.

2.1 Zero Frequency Modes in Mechanical Lattices

In mass-spring systems, the systems are composed of ideal springs and punctual masses, which allow for a basic but versatile description. Our interest is specific zero-frequency modes that are intimately related to the structural stability of the system in the linear regime. In the following section, a review of a specific formalism is shown, which leads directly to the aforementioned modes and their consequences.

2.1.1 Equilibrium and Compatibility Matrices

Under small perturbations over the equilibrium positions of masses in an ideal mass-spring system, the dynamics can be completely described by two structural matrices, Q and $R := Q^T$, called the *equilibrium* and *compatibility* matrix respectively. To discuss the physical meaning of both matrices, consider a system compose of N total punctual equal masses in d dimensions connected by a total of N_b springs or bonds(see Fig. 2.1), where these springs can rotate freely around each site. The matrix that maps the N_b-dimensional space of tensions in springs to the dN-dimensional space of forces on masses is the $dN \times N_b$ dimensional equilibrium matrix Q

$$Q\,\boldsymbol{t} = -\boldsymbol{f}\ , \tag{2.1}$$

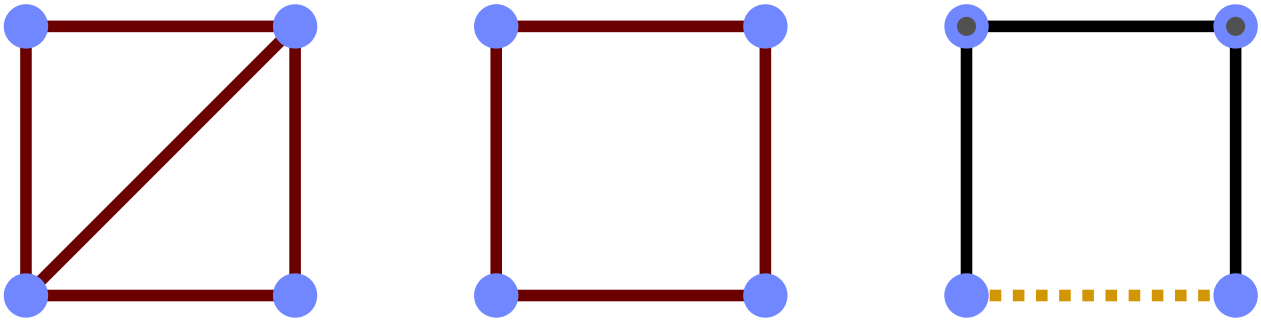

(a) **(b)** **(c)**

Fig. 2.1: *Three mass-spring systems. The solid circles represent identical punctual masses, connected by bonds or springs represented by solid or dotted lines. The frame in* ***(a)*** *and* ***(b)*** *frame only differs in the middle spring, while the frame* ***(c)*** *represents the center frame under different constraints and elastic constant limits. In* ***(c)****, the two top masses of the central frame are fixed to the plane, denoted with a gray center solid circle, while three of the springs become rigid bars(solid lines), and the remaining spring is denoted with a dotted line, remains as a normal spring, resulting in a system of two coupled pendulums.*

in which the vector $\boldsymbol{t}$ is composed of the tension in springs and $\boldsymbol{f}$ is the vector of the forces exerted on the masses. On the other hand, the equilibrium displacement of the connected masses determines the elongation of each spring. The N_b-dimensional tensions space is mapped to the dN-dimensional displacement space in the linear regime by the $N_b \times dN$-dimensional compatibility matrix R:

$$R\,\boldsymbol{u} = \boldsymbol{e}\ , \tag{2.2}$$

where $\boldsymbol{u}$ is the vector of the mass displacements and $\boldsymbol{e}$ the vector of spring elongations. Notice that (2.1) and (2.2) serve to argue why equilibrium and compatibility matrix are transposes of each other. To understand this consider an infinitesimal work produced by an external force f and the resulting displacements. This work would be the same as the one produced by tensions and their correspondent spring extensions, which shows the relation:

$$W_f = f_i^T u_i = (Q_{ij} t_j)^T u_i = t_j^T Q_{ji} u_i \qquad W_t = t_j^T e_j = t_j^T R_{ji} u_i$$

The computations of Q or R can be obtained by analyzing the tension-force or extension-displacement geometrical relations, respectively. For instance, in Fig. 2.1 there are three simple frames differing in the number of springs, where the compatibility matrix for the

frame of Fig. 2.1a is given by

$$R = \begin{pmatrix} -1 & 0 & 1 & 0 & 0 & 0 & 0 & 0 \\ 0 & 0 & 0 & 1 & 0 & -1 & 0 & 0 \\ 0 & 0 & 0 & 0 & 1 & 0 & -1 & 0 \\ 0 & 1 & 0 & 0 & 0 & 0 & 0 & -1 \\ 0 & 0 & \frac{1}{\sqrt{2}} & \frac{1}{\sqrt{2}} & 0 & 0 & -\frac{1}{\sqrt{2}} & -\frac{1}{\sqrt{2}} \end{pmatrix},$$

which can be obtained by displacing the masses in an infinitesimal quantity and expressing the spring extension due to this displacement. Notice that by removing the last row in the above matrix we also obtain R for the frame in Fig. 2.1b. In principle, this general framework allows us to describe wide types of mechanical systems, from this simple cases to larger or disordered systems[114–116]. Simple mass-spring systems can also reach additional systems by introducing some additional constraints or limits. For instance, the system in Fig. 2.1b composed of four masses system of eight DOFs and four springs, can be converted in the system to the system in Fig. 2.1c, if we restrict the movement of two masses and where the all the springs become rigid except the spring between these masses. This system could be a (zero-gravity) double-coupled pendulum where there is one spring and two DOFs. Indeed, similar pendulum systems are the principal study object in this thesis.

As an ideal system, the above framework assumes that the spring is described by ideal Hookean springs of constant κ, summarized in the $N_b \times N_b$ diagonal elastic constant matrix $\mathcal{K}$. According to this, the elastic energy V_e of the system can be written as

$$\begin{aligned} V_e &= \frac{1}{2}\kappa_{jj} e_j^2 \\ &= \frac{1}{2}\kappa_{jj}(R_{ji}u_i)^2 \\ &= \frac{1}{2}\kappa_{jj}(R_{ji}u_i)^T R_{ji}u_i \\ &= \frac{1}{2}\kappa_{jj}u_i R_{ij} R_{ji}u_i \\ &= \frac{1}{2}u_i R_{ij}\kappa_{jj} R_{ji}u_i \\ &= \frac{1}{2}\boldsymbol{u}^T Q\kappa R\,\boldsymbol{u} \end{aligned}$$

In addition to this energy, the kinetic energy of the punctual masses can be written also in function of a mass-matrix, but for our purposes, all the masses are equal to m. With a similar procedure can be shown that the kinetic energy E_k is given by

$$E_k = \frac{1}{2}m\dot{\boldsymbol{u}}^T\dot{\boldsymbol{u}}$$

Therefore, given the Lagrangian $L = E_k - V_e$, the equation of motion of the system is obtained from the Euler-Lagrange equation,

$$\begin{aligned} m\ddot{u}_i &= -\frac{\partial V_{el}}{\partial u_i} \\ \Leftrightarrow \ddot{u}_i &= -D_{ij}\ \boldsymbol{u}_i \end{aligned} \tag{2.3}$$

where $D = \frac{1}{m} Q\ \kappa\ R$ it is called the *dynamical matrix.* From the above equation, raise the characteristic eigenvalue problem under the usual harmonic decomposition $\boldsymbol{u}(\boldsymbol{x}) = u_n(\boldsymbol{x}) e^{-i\omega t}$:

$$\omega^2 \boldsymbol{u_n} = D\boldsymbol{u_n} \tag{2.4}$$

for some frequency ω. In Section 2.2, we will widely discuss eq.(2.3) and eq. (2.4) and how to link these equations to the quantum mechanical problem, to make use of its topological tools.

2.1.2 Zero Frequency Modes

The vectorial spaces described by Q and R encode relevant physical modes on their null spaces, as the ones shown in Fig. 2.2. The null space of R corresponds to the set of displacements that result in neither elongation nor compression of any spring, often known as *zero-energy modes*(ZM). These states usually include the lattice translation and rotation, but also some non-trivial ZM(see Fig. 2.2), sometimes called *floppy modes* or mechanism[115]. The ZM represents the inherent mobility of the structure or the instability of some parts, which is why one says that the structure is *kinematically determined* if the only nontrivial ZMs are uniform displacements or rotations[117]. In contrast, the null space of Q is the set of tensions that produce zero forces at each point, called *states of self-stress*(SSS), that is a SSS implies a spring tension distribution different from zero, that is balanced to reach equilibrium. The SSS produces that external loads or other disturbances do not deform the structure and maintain its shape. Similarly, if there are no SSSs, the structure is *statically determined* since is it always possible to know the force distribution in the system[117]. According to these two definitions, in Fig. 2.2, only the central frame is kinematically and statically determined.

There is also a close relation between ZMs and SSSs, which can be viewed by considering the rank-nullity theorem from linear algebra[118]. If some system supports N_s SSSs and N_0 ZMs, two relations arise from the vectorial spaces of Q and R:

$$\begin{aligned} \operatorname{Rank} Q + \operatorname{Null} Q &= N_b & \qquad \operatorname{Rank} R + \operatorname{Null} R &= dN \\ \Rightarrow \operatorname{Rank} Q + N_s &= N_b & \qquad \Rightarrow \operatorname{Rank} R + N_0 &= dN \end{aligned}$$

Because the matrix and its transpose range are the same, these two last equations provide the following significant result

$$N_0 - N_s = dN - N_b \tag{2.5}$$

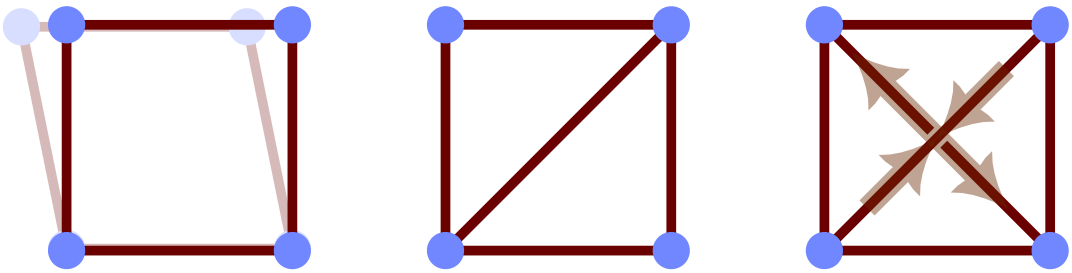

Fig. 2.2: *Three mass-spring systems that differ in their zero-frequency modes. The left frame shows one of the four ZMs supported in this system, represented as the blurred bond and masses, while the rest three modes are analogs but along the remaining bonds. The right frame supports one SSS represented by the arrows over the bonds, which in this case correspond to compression and extension of some springs according to the arrow directions. The central system, in difference from the others, does not support any SSS, and only trivial ZMs(displacement and rotations) and therefore is statically and kinematically determined.*

which relates the ZMs and SSSs numbers by simply counting the springs and masses in the system, known as the Maxwell rule, or Maxwell-Calladine theorem, due to their establishment of this rule at different times[119, 120]. According to the Maxwell-Calladine theorem, we can distinguish three different regimes, *isostatic*, floppy, and the one that we are interested in, *hyperstatic*. These regimes refer to the stability in the structure, where Maxwell described the following[119], which is equivalent to eq. (2.5).

A d-dimensional frame of N sites, is stable only if $z > dN - d(d+1)/2$, where z is the average coordination number related to the number of springs $N_b = zN/2$. For large N the stability critical point is then $z_c = 2d$, where we found the *isostatic* system. When $z > z_c$ the system will be hyperstatic or overconstrained, where the SSSs predominates over the ZMs, and in contrast, the system is floppy for $z < z_c$, where are more ZMs than SSSs. This classification says nothing about the geometry or order in the system. Thinking on the typical systems in condensed matter physics, we will treat only spatially periodic lattices. Concerning this, the most extended criteria to call a periodic system isostatic is that under PBC $z = z_c$[15, 115], and for a hyperstatic system under PBC $z > z_c$, which will be the criteria in this thesis.

2.1.3 Periodic Lattices

The lattices that we are interested in are spatially periodic for sites and connections, and therefore each site and spring can be represented in a Bravais lattice[115, 121]. Consider a *unit cell* of the lattice, that is, a region that can reproduce the Bravais lattice by tiling this cell. If every unit cell has n sites and n_b springs, then in the equilibrium, any site or spring in the lattice can be written as the position of certain unit cell of index s, $\mathfrak{R}_s$, plus the position $\boldsymbol{r}_\mu(\boldsymbol{r}_\sigma)$ of any site(spring) within the cell:

$$\mathfrak{R}_{s,\mu(\sigma)} = \mathfrak{R}_s + \boldsymbol{r}_{\mu(\sigma)} \qquad \begin{matrix} \mu = 1, \cdots, n \\ \sigma = 1, \cdots, n_b \end{matrix}$$

When the lattice is distorted, the sites in the lattice are displaced from the equilibrium to a new position $\mathfrak{R}_{s,\mu}+\boldsymbol{u}_\mu(s)$, then the vector $\boldsymbol{u}$ is composed by $\boldsymbol{u}_\mu(s)$, for every μ in a unit cell, and for every cell s. Similarly, it can be understood how the vectors $\boldsymbol{f}, \boldsymbol{e}$ and $\boldsymbol{t}$ are composed. Because of the cell periodicity, a spatial discrete Fourier transform(FT) over the unit cells can be obtained for all these vectors:

$$\boldsymbol{u}_\mu(\boldsymbol{k}) = \sum_s \boldsymbol{u}_\mu(s)\exp(-i\boldsymbol{k}\cdot(\mathfrak{R}_s+\boldsymbol{r}_\mu)) \qquad \boldsymbol{f}_\mu(\boldsymbol{k}) = \sum_s \boldsymbol{f}_\mu(s)\exp(-i\boldsymbol{k}\cdot(\mathfrak{R}_s+\boldsymbol{r}_\mu))$$
$$\boldsymbol{e}_\sigma(\boldsymbol{k}) = \sum_s \boldsymbol{e}_\sigma(s)\exp(-i\boldsymbol{k}\cdot(\mathfrak{R}_s+\boldsymbol{r}_\sigma)) \qquad \boldsymbol{t}_\sigma(\boldsymbol{k}) = \sum_s \boldsymbol{t}_\sigma(s)\exp(-i\boldsymbol{k}\cdot(\mathfrak{R}_s+\boldsymbol{r}_\sigma))$$

for the wavenumber $\boldsymbol{k}$, which is an scalar in one-dimensional system. By computing the FT for each μ and σ, it is possible to write the vectors $\boldsymbol{u}, \boldsymbol{t}, \boldsymbol{f}$ and $\boldsymbol{e}$ from these computations

$$\begin{aligned} \boldsymbol{u}(\boldsymbol{k}) &= (\boldsymbol{u}_1(\boldsymbol{k}), ..., \boldsymbol{u}_n(\boldsymbol{k})) & \boldsymbol{f}(\boldsymbol{k}) &= (\boldsymbol{f}_1(\boldsymbol{k}), ..., \boldsymbol{f}_n(\boldsymbol{k})) \\ \boldsymbol{e}(\boldsymbol{k}) &= (\boldsymbol{e}_1(\boldsymbol{k}), ..., \boldsymbol{e}_{n_b}(\boldsymbol{k})) & \boldsymbol{t}(\boldsymbol{k}) &= (\boldsymbol{t}_1(\boldsymbol{k}), ..., \boldsymbol{t}_{n_b}(\boldsymbol{k})) \end{aligned} \tag{2.6}$$

On the other hand, in a periodic lattice, the equilibrium and compatibility matrices are composed of sub-matrices associated with each unit cell:

$$Q_{ij}(\boldsymbol{k}) = \sum_s e^{-i\boldsymbol{k}\cdot(\mathfrak{R}_s-\mathfrak{R}_{s'})}Q_{ij}(s,s') \qquad R_{ij}(\boldsymbol{k}) = \sum_s e^{-i\boldsymbol{k}\cdot(\mathfrak{R}_s-\mathfrak{R}_{s'})}R_{ij}(s,s') \tag{2.7}$$

where s and s' are the indexes of the sub-matrix that identify each unit cell, and according to the number of sites and springs in the unit cell, $Q(\boldsymbol{k})$ and $R(\boldsymbol{k})$, are matrices of dimensions $dn \times n_b$ and $n_b \times dn$ respectively. In addition notice that $R(\boldsymbol{k}) = Q^\dagger(\boldsymbol{k})$, because $R = Q^T$. Considering the expressions (2.6) and (2.7) it is possible to rewrite the expressions (2.1) and (2.2) in the Fourier space as,

$$Q(\boldsymbol{k})\boldsymbol{t}(\boldsymbol{k}) = \boldsymbol{f}(\boldsymbol{k}) \qquad R(\boldsymbol{k})\boldsymbol{u}(\boldsymbol{k}) = \boldsymbol{e}(\boldsymbol{k})$$

Likewise, the theorem exposed in the equation (2.5) apply over each wavenumber $\boldsymbol{k}$:

$$n_0(\boldsymbol{k}) - n_s(\boldsymbol{k}) = dn - n_b \tag{2.8}$$

where $n_0(\boldsymbol{k})$ and $n_s(\boldsymbol{k})$ are the null spaces of $C(\boldsymbol{k})$ and $Q(\boldsymbol{k})$. Usually, to compute any of these Fourier transforms, it is enough to consider a PBC lattice, where we have some number of possible $\boldsymbol{k}$, and as would be expected the total number of ZM of these systems should be $N_0 = \sum_k n_0(\boldsymbol{k})$, and analog for the SSSs, $N_S = \sum_k n_s(\boldsymbol{k})$. Usually, if there exists, some of these modes can be seen with the naked eye at $\boldsymbol{k} = 0$, that is, a collective mode, like an ordinary collective displacement.

2.2 Link Between Quantum and Classical problems

The topological mechanical approach of using tools from the topological insulators framework, at first sight, deals with many elemental problems, starting with the governing equations difference. In this section, our milestone is to derive a way to connect these equations in some manner. The generic equation in our systems is given by eq. (2.3), but is also possible to consider some extra terms to include some additional force contribution, for instance, velocity-dependent forces such as Lorentz or Coriolis forces, which can imply additional effects like symmetry breaking[14, 48, 59], which is not necessary for the specific systems treated in this thesis.

On the other hand, the time-dependent Schrodinger equation takes the form[1],

$$i\frac{d}{dt}\boldsymbol{\psi}(t) = H\boldsymbol{\psi}(t) \tag{2.9}$$

for some eigenstate $\hat{\psi}$ with a Hamiltonian matrix H in a quantum mechanics system. At first sight, the mechanical and quantum problems look very different, starting from the fact that eq. (2.3) is a second-order differential equation in time, while the Schrödinger equation is only a first-order time differential equation. Similarly, the resultant eigenvalues in eq. (2.3) can only be non-negative; in contrast, an electronic Hamiltonian can have negative eigenvalues. To relate both systems, our focus is to rewrite (2.3) as the Schrödinger equation. To achieve this we promote the displacements vector $\boldsymbol{u}$ to the matrix $\begin{pmatrix}\dot{\boldsymbol{u}} & \boldsymbol{u}\end{pmatrix}^T$, obtaining

$$\frac{d}{dt}\begin{pmatrix}\dot{\boldsymbol{u}} \\ \boldsymbol{u}\end{pmatrix} = \begin{pmatrix}0 & -D \\ \mathbb{1} & 0\end{pmatrix}\begin{pmatrix}\dot{\boldsymbol{u}} \\ \boldsymbol{u}\end{pmatrix} \tag{2.10}$$

where we gathered the time dependence notation for simplicity. To reach the form of eq. (2.9), in the above equation it is necessary to discompose D on two matrices where we consider the decomposition on Q and R because of the modes of our interest. However, as you can read in the remarkable work of Susstrunk and Huber [47], the decomposition of D is not unique. Moreover, since we deal with non-dissipative and reciprocal interactions, D should be a positive semi-definite matrix[2], which implies that $\sqrt{D}$ is well-defined, and therefore any square root decomposition can be taken into account, depending on the system, or the topological framework.

In our case, we are more specifically interested in the decomposition $D = QR$ when $Q \in \mathbb{R}^{N\times M}$ and $N \neq M$ in general. For the sake of rewriting eq.(2.10) as (2.9), consider the transformation matrix

$$\begin{pmatrix}i\mathbb{1} & 0 \\ 0 & R\end{pmatrix}$$

where we emphasize that $\mathbb{1}$ is the N-dimensional identity, which in addition to the dimensions

[1] Considering the Plank constant as one

[2] Symmetric or hermitian, of non-negative eigenvalues

of R, $M \times N$, leads in general to an a rectangular transformation matrix. Thus we obtain that (2.10) under this transformation takes the form,

$$i\frac{d}{dt}\begin{pmatrix} i\dot{\boldsymbol{u}} \\ R\boldsymbol{u} \end{pmatrix} = \begin{pmatrix} 0 & Q \\ R & 0 \end{pmatrix}\begin{pmatrix} i\dot{\boldsymbol{u}} \\ R\boldsymbol{u} \end{pmatrix}$$

or alternatively according to eq.(2.9), the above equation can be written as

$$i\frac{d}{dt}\boldsymbol{\psi} = H\boldsymbol{\psi} \qquad \boldsymbol{\psi} = \begin{pmatrix} i\dot{\boldsymbol{u}} \\ R\boldsymbol{u} \end{pmatrix}, \qquad H = \begin{pmatrix} 0 & Q \\ R & 0 \end{pmatrix}$$

where H is a $(M+N)$-dimensional square matrix. This formulation includes the entire spectrum of (2.3), and could be fruitful to write this formulation as the eigenvalue equation considering the expansion $\boldsymbol{u} = u_n(x)e^{-i\omega t}$

$$\omega\begin{pmatrix} \omega\boldsymbol{u_n} \\ R\boldsymbol{u_n} \end{pmatrix} = \begin{pmatrix} 0 & Q \\ R & 0 \end{pmatrix}\begin{pmatrix} \omega\boldsymbol{u_n} \\ R\boldsymbol{u_n} \end{pmatrix}$$

However, the above formulation does not include the ZM, since when $\omega = 0$ and $R\boldsymbol{u_n} = 0$, the structure of the eigenvector raises a trivial zero vector. In the general case, when there is no structure for the eigenvector, the above equation would include both the ZMs and SSSs, thus a solution to this problem can be to modify the formulation to modify the eigenvector space. This modification emerges naturally after considering the matrix H^2, which shares the eigenvectors of H and their eigenvalues are the square of the eigenvalues of H

$$H^2 = \begin{pmatrix} QR & 0 \\ 0 & RQ \end{pmatrix} = \begin{pmatrix} D & 0 \\ 0 & \tilde{D} \end{pmatrix}$$

where $\tilde{D} = RQ$, share the non-zero eigenvalues with D, but differs in their zero eigenvalues:

$$\begin{aligned} QR\ \boldsymbol{u}_n &= \omega^2\boldsymbol{u}_n & \qquad QR\ \boldsymbol{u} &= 0 \\ RQ(R\boldsymbol{u}_n) &= \omega^2(R\boldsymbol{u}_n) & \qquad RQ(R\boldsymbol{u}) &= RQ\ \boldsymbol{t} = 0 \end{aligned}$$

where the eigenvectors of $\tilde{D}$, $\boldsymbol{t} = R\boldsymbol{u}$, are the spring tensions. In addition, the zero modes of D correspond to the ZMs mentioned in the previous section, while the zero modes of $\tilde{D}$ correspond to the SSSs. Notice that the $\boldsymbol{u}$ at the SSS are not displacements, but are springs extensions required in the SSS. Therefore, the eigenvalue equation of H^2 which includes both

ZM and SSS is given by

$$\omega^2 \begin{pmatrix} \boldsymbol{u}_n \\ R\boldsymbol{u}_n \end{pmatrix} = \begin{pmatrix} D & 0 \\ 0 & \tilde{D} \end{pmatrix} \begin{pmatrix} \boldsymbol{u}_n \\ R\boldsymbol{u}_n \end{pmatrix}$$

where its square root can be easily written:

$$\pm\omega \begin{pmatrix} \boldsymbol{u}_n \\ R\boldsymbol{u}_n \end{pmatrix} = \begin{pmatrix} 0 & Q \\ R & 0 \end{pmatrix} \begin{pmatrix} \boldsymbol{u}_n \\ R\boldsymbol{u}_n \end{pmatrix}$$

which is nothing more that $\begin{pmatrix} \omega\boldsymbol{u}_n \\ R\boldsymbol{u}_n \end{pmatrix} \to \begin{pmatrix} \boldsymbol{u}_n \\ R\boldsymbol{u}_n \end{pmatrix}$ respect the previous formulation. Notice that this last equation takes the form of the time-independent Schrödinger equation

$$E\boldsymbol{\psi} = H\boldsymbol{\psi} \qquad\qquad H = \begin{pmatrix} 0 & Q \\ R & 0 \end{pmatrix} \quad \psi = \begin{pmatrix} \boldsymbol{u}_n \\ R\boldsymbol{u}_n \end{pmatrix} \quad E = \pm\omega \tag{2.11}$$

and also works their representation in the Fourier space $\boldsymbol{k}$ given by

$$H(\boldsymbol{k}) = \begin{pmatrix} 0 & Q(\boldsymbol{k}) \\ R(\boldsymbol{k}) & 0 \end{pmatrix} \quad \psi(\boldsymbol{k}) = \begin{pmatrix} \boldsymbol{u}(\boldsymbol{k}) \\ R(\boldsymbol{k})\boldsymbol{u}(\boldsymbol{k}) \end{pmatrix} \tag{2.12}$$

2.2.1 Symmetry Analysis

The matrix H can be topologically classified in the framework of topological insulators. In a similar form as treated by Susstrunk and Huber[47], we examine what would imply on the mechanical system a symmetries analysis on the $\boldsymbol{k}$-space matrix $H(\boldsymbol{k})$. We will not elaborate much further on the meaning of these symmetries beyond the examples in Section 1.2 since we are focused on what they imply on the mechanical system in this formulation. For additional details, you can refer to the many excellent reviews of the classification based on topological insulators symmetries at ref[5, 6, 8, 9, 25]

The three symmetries involved in this classification are the *time-reversal* symmetry $\mathcal{T}$ (TRS), the *particle-hole* symmetry $\mathcal{C}$ (PHS), and the chiral symmetry $\mathcal{S}$, discussed in the SSH model. Based on the aforementioned classification, we consider a TRS and PHS if the symmetry operators $\mathcal{T}$ and $\mathcal{C}$ act on $H(\boldsymbol{k})$ as

$$\begin{aligned} \mathcal{T}H(\boldsymbol{k}) &= H(-\boldsymbol{k})\mathcal{T} \\ \mathcal{C}H(\boldsymbol{k}) &= -H(-\boldsymbol{k})\mathcal{C} \end{aligned}$$

for some anti-unitary operator $\mathcal{T}^2, \mathcal{C}^2 = \pm\mathbb{1}$. In the case of TRS, since H is purely real, and therefore $H(k)$ complex, the generic operator $\mathcal{T} = \mathbb{1}K$, with K as the complex conjugation operator, allows to always guarantee this symmetry no matter the dimensions of Q and R. This means nothing else that the band structure is symmetric under $\boldsymbol{k} \to -\boldsymbol{k}$, as expected in these ideal systems. Thinking in quantum systems that require a TRS breaking, it is possible

to break this symmetry in multiple forms on some mechanical systems, for instance considering some additional forces, that lead to interesting topological mechanics phenomena[48, 59]. For PHS, the symmetry also can be achieved by considering $\mathcal{C} = U_{\mathcal{C}} K$, where $U_{\mathcal{C}}$ is the unitary operator

$$U_{\mathcal{C}} = \begin{pmatrix} \mathbb{1}_N & 0 \\ 0 & -\mathbb{1}_M \end{pmatrix}$$

where the dimension of the identity are picked considering that $Q(\boldsymbol{k}) \in \mathbb{C}^{N \times M}$. This symmetry implies that $H(\boldsymbol{k})$ has a symmetric spectrum that is, for every mode at $+\omega$ there is a symmetric partner at $-\omega$ (the negative frequency does not have any physical meaning, but we will back to this point at the end of this discussion). The combination of both symmetries operators, acts as a chiral symmetry U_s, in the same form as in the SSH model

$$(\mathcal{C}\mathcal{T})^{\dagger} H(\boldsymbol{k}) (\mathcal{C}\mathcal{T}) = U_{\mathcal{C}} H(\boldsymbol{k}) U_{\mathcal{C}} = -H$$

which implies that the chiral symmetry operator is $\mathcal{S} = U_s = U_{\mathcal{C}}$. As we mentioned in Section 1.2 a chiral symmetry implies some consequences in the band structure of $H(\boldsymbol{k})$. First, an eigenstate at wave-vector $\boldsymbol{k}$ and some eigenvalue E_n, their chiral partner is also at $\boldsymbol{k}$, but with $-E_n$, and these states can have contributions of both parts of the sub-lattices as long as $E \neq 0$, where each zero energy state is only supported in one sub-lattice simultaneously. The first point can be directly verified in this case when considering the aforementioned chiral operator $\mathcal{S} = U_s$ and the equation (2.12)

$$\begin{aligned} H\ U_s \psi(\boldsymbol{k}) = -U_s\ H\psi(\boldsymbol{k}) &= -\omega \begin{pmatrix} \mathbb{1}_N & 0 \\ 0 & -\mathbb{1}_M \end{pmatrix} \begin{pmatrix} \boldsymbol{u}(\boldsymbol{k}) \\ R(\boldsymbol{k})\boldsymbol{u}(\boldsymbol{k}) \end{pmatrix} \\ &= -\omega \begin{pmatrix} \boldsymbol{u}(\boldsymbol{k}) \\ -R(\boldsymbol{k})\boldsymbol{u}(\boldsymbol{k}) \end{pmatrix} \end{aligned}$$

which is effectively the chiral partner of ψ. However, the minus sign in the frequency does not have any physical meaning but is the consequence of the doubling of DOF in the formulation. The second point refers to the zero-energy states, which in the SSH model are only supported in one sub-lattice per state. This also can be verified by considering $\omega = 0$

$$H(\boldsymbol{k}) = \begin{pmatrix} 0 & Q(\boldsymbol{k}) \\ R(\boldsymbol{k}) & 0 \end{pmatrix} \begin{pmatrix} \boldsymbol{u}_n(\boldsymbol{k}) \\ R(\boldsymbol{k})\boldsymbol{u}_n(\boldsymbol{k}) \end{pmatrix} = 0$$

which implies

$$\begin{aligned} Q(\boldsymbol{k}) R(\boldsymbol{k}) \boldsymbol{u}_n(\boldsymbol{k}) &= 0 \\ R(\boldsymbol{k}) \boldsymbol{u}_n(\boldsymbol{k}) &= 0 \end{aligned}$$

where the first are the SSSs and the second the ZMs. If some ZM is associated with $\boldsymbol{u}_{\text{ZM}}(\boldsymbol{k})$, then $R(\boldsymbol{k})\boldsymbol{u}_{\text{ZM}}(\boldsymbol{k})$ cannot be in $\text{Null}\, Q$, since this space is composed only by non-zero vectors, and $R(\boldsymbol{k})\boldsymbol{u}_{\text{ZM}}(\boldsymbol{k}) = 0$ (this analysis equivalent to the Rank-Nullity theorem or the Maxwell-

Calladine theorem). Thus the zero-frequency modes in $H(\boldsymbol{k})$ looks like

$$\begin{pmatrix} \boldsymbol{u}_{\text{ZM}}(\boldsymbol{k}) \\ 0 \end{pmatrix} \quad \text{and} \quad \begin{pmatrix} 0 \\ R(\boldsymbol{k})\boldsymbol{u}_{\text{SSS}}(\boldsymbol{k}) \end{pmatrix}$$

for ZMs and SSSs respectively. So far, all the expected consequences of this symmetry are supported by $H(\boldsymbol{k})$, and therefore, thinking on the SSH model is natural to ask if also there are topological aspects within these systems, which will be treated in detail in the following chapter.

2.3 Isostatic Topological Mechanics

Among the several studies on topological mechanics in the past few years, a seminal paper by Kane and Lubensky [72] on a topological characterization in mechanical systems of these zero-frequency modes(ZMs and SSSs), marked one of the starting points of this trend. The authors showed that the Maxwell-Calladine theorem from eq. (2.5), which quantifies the difference between ZMs and SSSs, arises as a contribution of the topological properties of the system and local mismatch of springs and sites. We will start explaining their framework with the illustrative mechanical system that can be understood as an analog of the SSH model system, and later we review how this topological classification can be extended. However, the analysis of ref [72] was limited to the isostatic regime, where there is a balance of springs and DOFs, where the existence of ZMs or SSS is equiprobable, and as we will review at the end, is not possible to extrapolate their analysis directly out of this limit.

2.3.1 Isostatic Chain

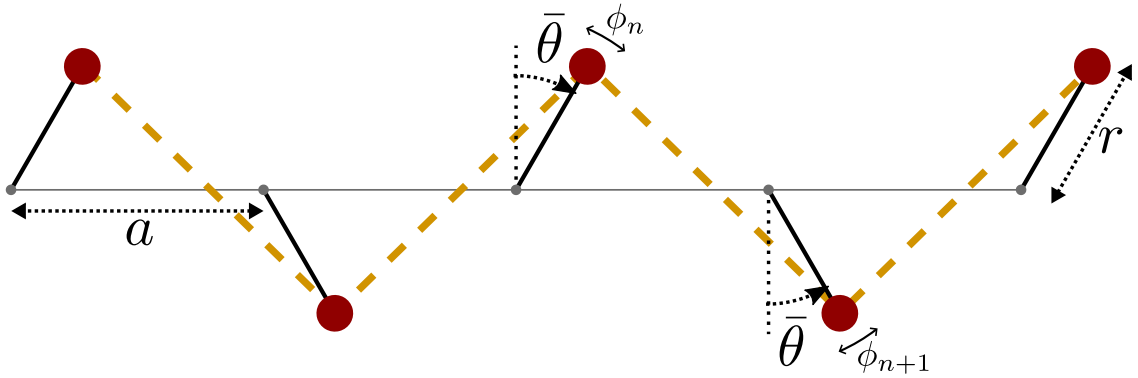

Fig. 2.3: *Isostatic Chain System. The chain is composed of identical mass-less rigid bars(black solid thick line) of radius r attached to a static horizontal line(gray solid thin line), and to which an identical punctual mass(red solid circle) is attached at the free end of each bar. Each bar rotation point is equally spaced from its neighbors a distance a, and an identical ideal spring(yellow dashed lines) is attached to the masses of every two adjacent bars, where the length of the springs is chosen in such a way that the bars are arranged in an alternating rest angle $\bar{\theta}$ or $\pi - \bar{\theta}$ with respect to the vertical. We take the convention of measuring the angles in an alternating direction so that all bars will have the same rest angle $\bar{\theta}$. For a small perturbation ϕ_n the n-th bar tilt around the rest angle.*

The *isostatic chain* emerges as a mechanical analog of the SSH model, which exhibits topological zero-energy state (see Section 1.2). In this section, we present the system and its analogy with the SSH model and use slightly different explanations than those already mentioned in the typical articles[15, 72]. The mechanical model of this chain, presented in Fig. 2.3 consists of a one-dimensional array of rigid bars of length r that rotates about a fixed point, separated by a distance a. At the end of each bar, there is the same punctual mass, which has attached an ideal spring that connects two adjacent bars. The natural length of these springs is chosen to that the bar array forms an alternating rest angle $\bar{\theta}$ with the upward or downward normal. This last detail implies that the orientation of the angle measurement also alternates from chain to chain. An unit cell in the chain is *right compatible* if is composed of a spring on the left and a bar on the right, or is *left compatible* in the opposite case. The former option will be used in this initial analysis, and later we will discuss the second case. This system is isostatic, since in periodic boundary conditions, there is exactly one DOF and one restriction per unit cell. Under small perturbations, the angle at each bar goes as $\theta_s = \bar{\theta} + \phi_s$, for $\phi_s \ll \bar{\theta}$. Thus the extension e of each spring is given by

$$e(\theta_n, \theta_{n+1}) = \ell(\theta_n, \theta_{n+1}) - \ell(\bar{\theta}, \bar{\theta})$$

where

$$\ell(\theta_n, \theta_{n+1}) = \sqrt{(a - r\sin\theta_n + r\sin\theta_{n+1})^2 + (r\cos\theta_n + r\cos\theta_{n+1})^2}$$

In the linear regime, this extension can be approximated as

$$\begin{aligned} e(\bar{\theta} + \phi_n, \bar{\theta} + \phi_{n+1}) &\approx e(\bar{\theta}, \bar{\theta}) + \phi_n \left.\frac{\partial e}{\partial \theta_n}\right|_{\theta_n = \theta_{n+1} = \bar{\theta}} + \phi_{n+1} \left.\frac{\partial e}{\partial \theta_{n+1}}\right|_{\theta_n = \theta_{n+1} = \bar{\theta}} \\ &\approx -v_1\phi_n + v_2\phi_{n+1} \end{aligned}$$

where

$$v_{1,2} = \frac{r\cos\bar{\theta}(a \pm 2r\sin\bar{\theta})}{\sqrt{a^2 + 4r^2\cos^2\bar{\theta}}}$$

The geometrical parameters $v_{1,2}$, are related to $\bar{\theta} > 0 (< 0)$ when $|v_1| > |v_2| (|v_1| < |v_2|)$, and $\bar{\theta} = 0$ when $|v_1| = |v_2|$. The expression for e is enough to write the compatibility and equilibrium matrix, where $R\boldsymbol{\phi} = \boldsymbol{e}$ relate the extension of the spring $\boldsymbol{e}$ and the angle perturbation $\boldsymbol{\phi}$ as expected, but $Q\boldsymbol{t} = -\boldsymbol{\tau}$ now relate the springs tensions with the torque τ on the bars. For instance in a chain under PBC composed of four unit cells, these relations take the form

$$\begin{pmatrix} v_2 & 0 & 0 & -v_1 \\ -v_1 & v_2 & 0 & 0 \\ 0 & -v_1 & v_2 & 0 \\ 0 & 0 & -v_1 & v_2 \end{pmatrix} \begin{pmatrix} \phi_1 \\ \phi_2 \\ \phi_3 \\ \phi_4 \end{pmatrix} = \begin{pmatrix} e_1 \\ e_2 \\ e_3 \\ e_4 \end{pmatrix} \qquad \begin{pmatrix} v_2 & -v_1 & 0 & 0 \\ 0 & v_2 & -v_1 & 0 \\ 0 & 0 & v_2 & -v_1 \\ -v_1 & 0 & 0 & v_2 \end{pmatrix} \begin{pmatrix} t_1 \\ t_2 \\ t_3 \\ t_4 \end{pmatrix} = - \begin{pmatrix} \tau_1 \\ \tau_2 \\ \tau_3 \\ \tau_4 \end{pmatrix}$$

Notice the expected delay in the index for R and Q, because the first refers to the springs and the second to the bars. The above results can be summarized in the matrix H

$$H = \begin{pmatrix} 0 & Q_{s,s'} \\ R_{s,s'} & 0 \end{pmatrix} = \begin{pmatrix} 0 & v_1\delta_{s,s'} - v_2\delta_{s,s'-1} \\ v_1\delta_{s,s'} - v_2\delta_{s,s'+1} & 0 \end{pmatrix}$$

On the other hand, the Fourier transform, $R(k)$ or $Q(k)$, can be easily obtained from eq. (2.7), which corresponds to scalars rather than matrices, due to the equal DOFs and constraints number per unit cell:

$$H(k) = \begin{pmatrix} 0 & Q(k) \\ R(k) & 0 \end{pmatrix} = \begin{pmatrix} 0 & v_2 - v_1 e^{-ika} \\ v_2 - v_1 e^{ika} & 0 \end{pmatrix} \tag{2.13}$$

thus the dispersion relation $\omega(k)$ is obtained from H, obtaining then[3]

$$\omega(k) = \pm\sqrt{v_1^2 + v_2^2 - 2v_1 v_2 \cos(k)}$$

For this mechanical system, there is a frequency band gap around $\omega = 0$, except when $|v_1| = |v_2|$, where it closes at $k = 0$ and where all the bars are in a vertical position. In the rest of the cases, the chain is orientated in one direction, depending on the relative magnitude of v_1 and v_2. According to the Maxwell-Calladine theorem (2.8), under PBC conditions, the chain has no ZMs or SSSs as long as $|v_1| \neq |v_2|$, but in contrast, when $|v_1| = |v_2|$, a ZM and a SSS appear at $k = 0$, that is, a uniform perturbation produce the ZM, and the uniform pre-stress in the springs is the SSS. On the other hand, in the finite chain case, the chain necessary has one spring less than the number of bars, and according to the Maxwell-Calladine theorem, it is necessary that $N_0 - N_S = 1$. We already said that the bulk does not support a ZM or SSS when $|v_1| \neq |v_2|$, then these modes should appear at the edges, but a SSS is not possible here because it requires two springs, and therefore the unique option is that in a finite case, there are one ZM and zero SSS. Depending on the orientation of the chain, this

[3]Considering the elastic constant, the inertia moment, and the lattice spacing as one

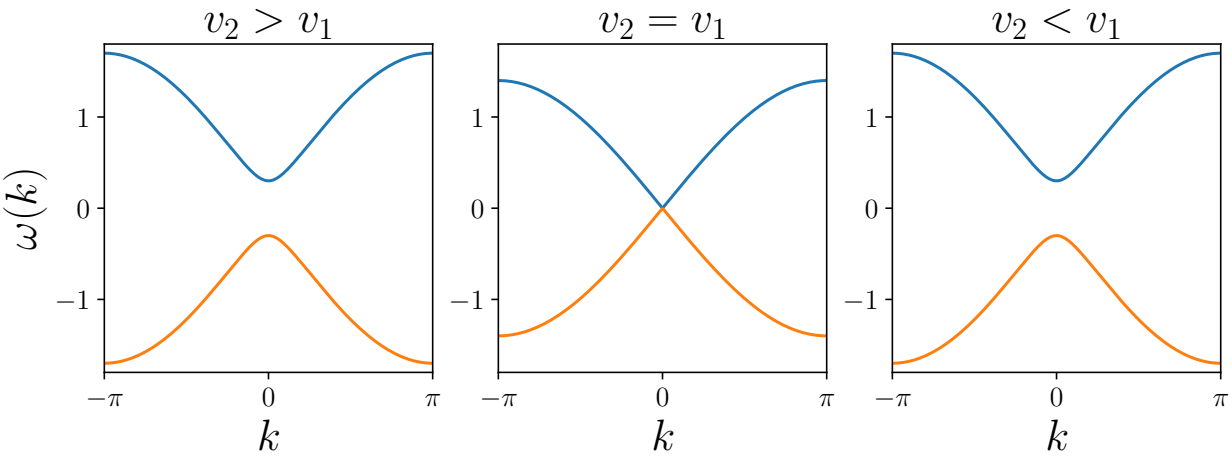

Fig. 2.4: *Isostatic chain dispersion relation. The figure shows the band diagram $\omega(k)$ for three different pairs of values (v_1, v_2), from left to right $(1, 0.7)$, $(0.7, 0.7)$ and $(0.7, 1)$, as also is labeled as a relative relation in the title of each diagram. The dispersion relation closes the gap in the middle figure, where the bars are in a vertical position, while in the remaining two cases the bands look identical because the absolute difference $v_1 - v_2$ is equal, even though they differ in v_1 and v_2.*

mode is located at the left or right edge, and its decay is obtained as

$$\begin{aligned} C_{s,s'} = v_2\phi_s - v_1\phi_{s-1} &= 0 \\ \phi_{s-1} &= \left(\frac{v_2}{v_1}\right)\phi_s \\ \Rightarrow \phi_{N-s} &= \left(\frac{v_2}{v_1}\right)^s \phi_N \end{aligned}$$

in a finite chain of N bars. This result only has physical meaning for $|v_1| > |v_2|$ where the ZM is exponentially located at the left edge and decaying to the right. It is direct to understand that in a chain with an opposite orientation, there is also a ZM located at the left side that decays to the right, and we will back to this case later. Notice that up to this point, we can identify many similarities with the SSH model.

First, the Hamiltonian bulk matrix of the SSH model is identical to $H(k)$ at eq. (2.13), while the eigenstates in the SSH model are composed of the sub-lattice coefficients, and here the eigenvector in eq.(2.12) is composed by the eigenstates of D and $\tilde{D}$, which correspond to angular displacements and tension respectively.

$$|\psi\rangle = \begin{pmatrix} a(k) \\ b(k) \end{pmatrix} \Leftrightarrow \boldsymbol{\psi} = \begin{pmatrix} u(k) \\ R(k)u(k) \end{pmatrix}$$

For this reason, there is a correspondence one-to-one between these systems, where the

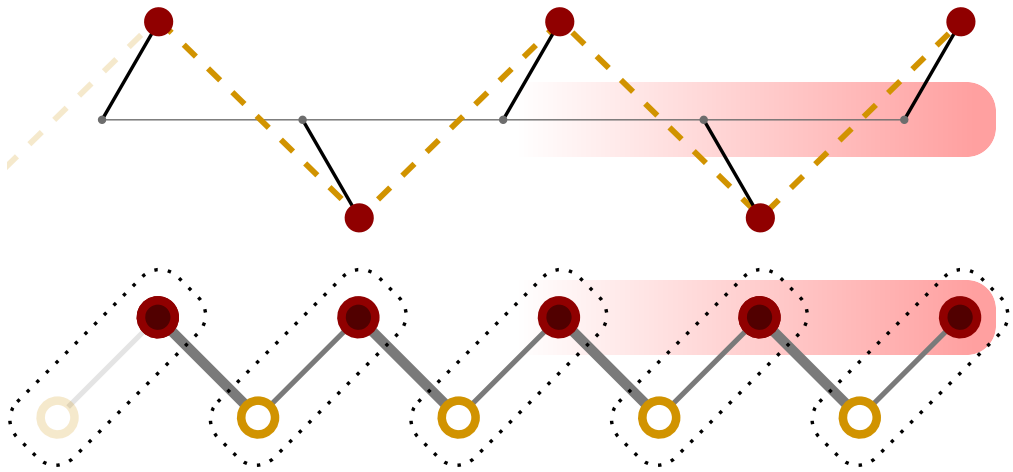

Fig. 2.5: *Zero energy mode in the isostatic chain and the analog in the SSH model. The right oriented isostatic chain(top), where $v_2 < v_1$, supports an exponentially localized ZM in the right edge, which is analog to electronic zero energy mode in the SSH model(bottom) when the intra-cell coupling is smaller than the inter-cell coupling. This analogy is between the bar perturbation(spring tension) and the B(A) site in the SSH model(see Fig. 1.4). The highlight gradient under the figure represents the amplitude decaying of the mode. On the left side of the figure is shown the eventual next unit cell, wherein the SSH model is only necessary to include an additional site A, while the analog in the isostatic chain implies the inclusion of a spring(which does not have mechanical relevance due the unit cell choice).*

springs can be identified with the A-sites in the SSH model and the B-sites with the masses when considering a right compatible chain. However, there are two relevant points in this analogy, that can lead to confusion. First, in contrast to the SSH model where a zero-energy mode appears only when the intercell coupling is bigger than the intracell coupling, in this mechanical case the ZM appears to be in the chain no matter the relation between v_1 and v_2, and also can cause confusion that in the mechanical case, the ZM only appear at one edge, but in the opposite does not appear to be a ZM. These two apparent discordance however have a physical meaning in the isostatic chain where we have an alternative explanation.

Consider the right compatible finite chain, where the ZM appears at the bar on the right edge. In the SSH model, the right ZM analog(the zero energy state) is on B site, and according to this same analogy also an analog should appear at the left side, but in the sub-lattice A. In the isostatic chain, the sub-lattice A is analog to a spring, and therefore that mode should be a SSS, but this mode is not possible if we do not add a new pendulum to left the and therefore another unit cell. According to this conclusion, it is not possible to have an isolated finite SSH, but we can build an interface that "disconnect" two finite chains. If we consider the analog the SSH model, the coupling would fulfill that the interaction for both sides of the interface would vanish(see Fig. 2.7), however in principle, we do not know what is the relation between the couplings at both sides of the interface, to be physically realizable in the mechanical case.

If we consider that the right compatible finite chain has an equilibrium angle $\bar{\theta}_R > 0$, we can obtain the new coefficients for the interface, and impose the condition of vanishing coupling,

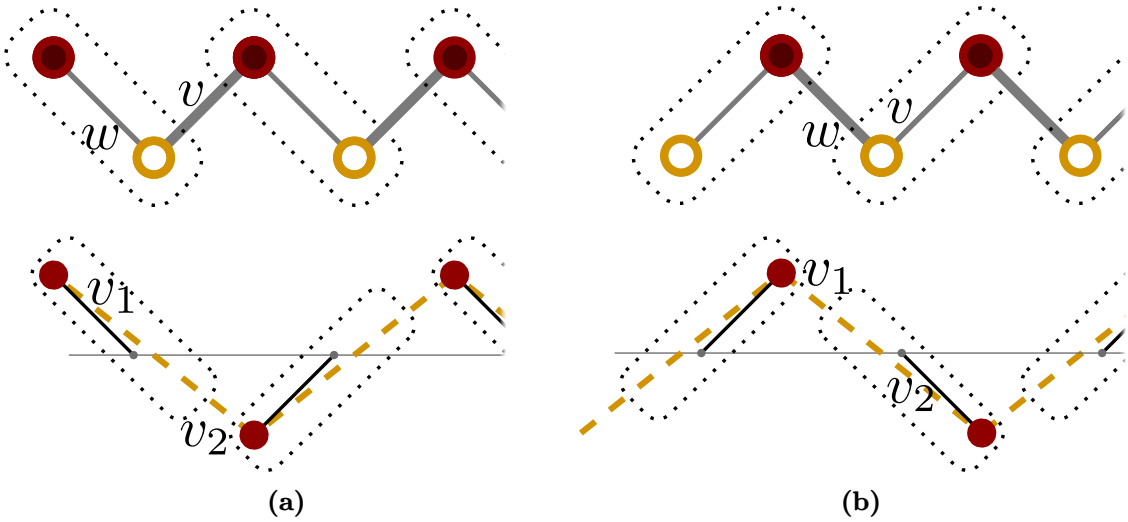

Fig. 2.6: *Unit-cell dependence of the mechanical-electronic analogy. When the isostatic chain in Fig. 2.5 takes the opposite orientation, the ZM also appears but on the opposite edge. However, to explicitly obtain this analogy the isostatic chain unit cell has to be in concordance with the unit cell choice in the SSH model. In the case shown in Fig. 2.5 the unit cell choice is right-compatible, shown here in* ***(b)****, where the dotted line encloses the unit cell choice, and where there is a direct correspondence between the couplings* $v_1 \leftrightarrow w$ *and* $v_2 \leftrightarrow v$*, in concordance for the existence of the ZMs in the mechanical and electronic case. We the left-compatible unit-cell* ***(a)*** *is chosen in the isostatic chain the same ZM is obtained in the left edge, and now the analog SSH model also has a different unit cell.*

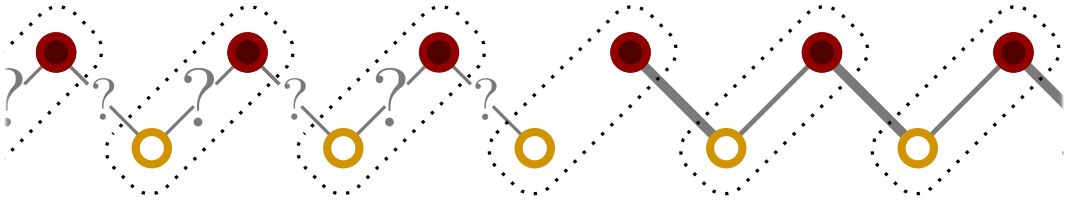

Fig. 2.7: *The figure shows the left edge of a finite topological chain in the SSH model. An isostatic chain, which may be the analog of a finite chain in the SSH model, should decouple somehow at the left edge (for a rigth-compatible chain), that is* $v_1 = 0$*, as in the SSH model where the intracell coupling vanish. In principle, we do not know what this condition may imply for the mechanical case on the left side of the decoupled interface.*

but the unique realizable solution for the mechanical case is that the bar at the interface follows $\bar{\theta} = 0$ and that the chain at the left side of the interface must have an equilibrium angle $\bar{\theta}_L = -\bar{\theta}_R$(see Fig. 2.8). With this solution, the analogy is complete, in Fig. 2.8 a right-compatible isostatic chain supports a ZM in the bar angle(sub-lattice B), and in the opposite edge, at the interface, there is a SSS. The left side of the system will also have a ZM, and share the SSS with the right side of the chain, but the choice of the unit cell as right compatible produce that the analogy is not valid on this side, however, if we consider a left compatible unit cell(see Fig. 2.6), now the analogy with the SSH model is with this side. The ZM in the left compatible chain is given by

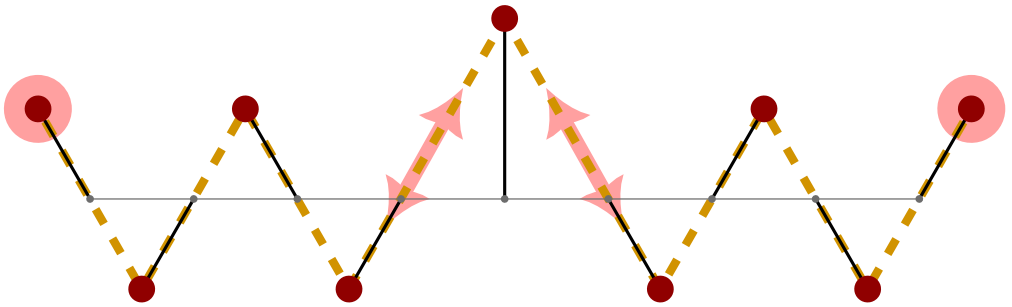

(a)

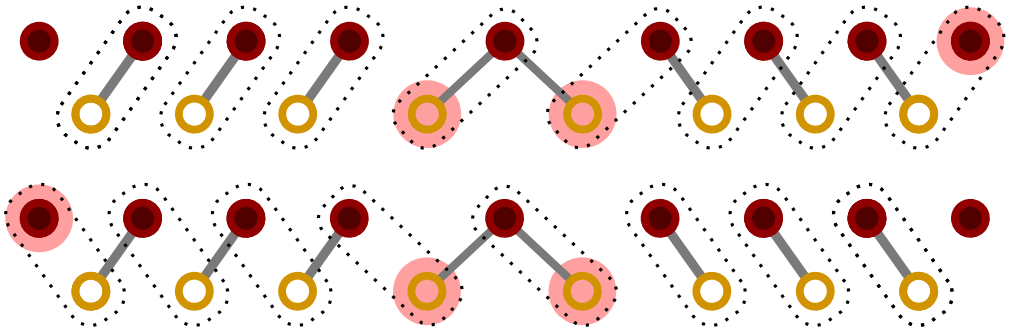

(b)

Fig. 2.8: *Zero modes and self-stress modes in the isostatic chain. In* ***(a)*** *the figure shows an interface between two isostatic chains where a localized ZM is supported at each edge. The chains have an opposite orientation and an equilibrium angle* $\bar{\theta} = \pm \sin^{-1}(a/2r)$*, where each spring is aligned with the bar. At the interface, there is a vertical bar that guarantees the decoupling condition, and a localized SSS mode is supported in the adjacent springs to this bar. This system is also analog to an interface in the SSH model between two fully dimerized chains, as shown in* ***(b)****, where the analogy for a right-compatible chain is shown at the top and the analogy with the left-compatible chain is shown at the bottom.*

$$
\begin{aligned}
C_{s,s'} = v_2\phi_{s+1} - v_1\phi_s = 0 \\
\phi_{s+1} = \left(\frac{v_1}{v_2}\right)\phi_s \\
\Rightarrow \phi_s = \left(\frac{v_1}{v_2}\right)^s \phi_0
\end{aligned}
$$

where $|v_1| < |v_2|$ is the physical case, as expected, where the mode is located at the left edge and exponentially decays to the right, while the matrix $R(Q)$ is equal to the matrix $Q(R)$ in the right compatible chain.

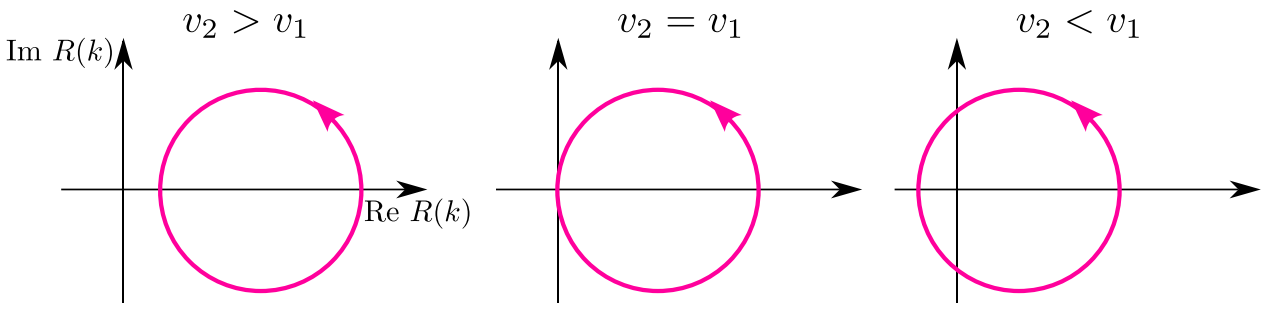

Fig. 2.9: *Parameterization in the complex plane of $R(k)$, for the three cases showed in Fig. 2.4. When $v_2 > v_1 (v_2 < v_1)$ the winding number of this parameterization is zero(one), in concordance with the number of ZM at the right edge(for a right-compatible unit cell). As in the SSH model, the winding number is not well-defined when $v_1 = v_2$.*

2.3.2 Topological Classification

So far, all these analogies also reach the winding number in the SSH model. In Section 1.2 we mentioned that based on the Hamiltonian symmetries, it is possible to classify the quantum system concerning homotopy groups. Since H in this case follows the same symmetries as the SSH model, also shares its topological properties. More specifically, according to this classification, the fundamental homotopy group of the corresponding space in one-dimensional systems is $\pi_1(H(k)) = \mathbb{Z}$, which similarly to the SSH model, a winding number can describe this invariant:

$$n = \frac{1}{2\pi i} \int_{-\pi/a}^{\pi/a} dk \frac{d}{dk} \ln(|R(k)|)$$

where "$|R(k)|$" denotes the determinant of $R(k)$, and a is the lattice spacing. This formulation is equivalent to the one in eq.(1.1), and returns $n = 1$ or $n = 0$ when the parameterization of $R(k)$ in the complex plane winds or not the origin. The winding number also can be computed by using Q, but here the parameterization wind clockwise and therefore the possible values are $n = -1$ and $n = 0$. As in the SSH model, where this invariant is related to the zero energy states, here it is related to the zero frequency states. The isostatic chain supports a ZM in the right(left) boundary and will be zero when the mode is not supported in this boundary. Similarly, this winding number also distinguishes the trivial and topological phases in the mechanical chain, but for a topologically non-trivial chain which is non-trivial for certain uni-cell choice, the same chain will be trivial for the opposite unit-cell choice(see Fig. 2.6).

The fact that unit cell matters in the winding number result, implies that this winding number is not gauge invariant. However, this problem can be fixed by including the unit cell choice, summarized in a different number which counts the ZM depending on the unit cell choice [15].

2.3.3 Extension and Limitations

The preceding review on the topological characterization of H, can be widely applied to periodic lattices, as long as the equation of motion can be described via eq. (2.11), which

guarantees the symmetry features on $H(\boldsymbol{k})$. The usual extension of the problem is to consider two-dimensional(2D) isostatic systems, where $R(\boldsymbol{k})$ and $Q(\boldsymbol{k})$ depends on a vector wavenumber rather than a scalar. The bulk topological properties in these cases depend on the winding number

$$n_{i=0,1} = \frac{1}{2\pi i} \oint_{C_i} d\boldsymbol{k} \cdot \mathrm{Tr}\left[Q^{-1}(\boldsymbol{k}) \nabla_{\boldsymbol{k}} Q(\boldsymbol{k})\right]$$

for certain closed paths C_i in the first Brillouin zone. In this thesis we are not interested in going too deeply into this counting for 2D systems, instead, we will focus on the fundamental limitations it presents, but a detailed explanation can be found in the references[72, 115]. The above topological index depends on the fundamental assumption that the lattices are isostatic, and therefore $R(\boldsymbol{k})$ and $Q(\boldsymbol{k})$ are square matrices, where the topological numbers n are well-defined. In contrast, for rectangular matrices, the above expression for the winding number is not valid anymore, as in the case of hyperstatic systems. The Maxwell-Calladine theorem and the zero-frequency modes can also be present in these systems, but their topological characterization and how they are related to these modes is still unknown. Nevertheless, the symmetry aspects on H do not depend on the dimension of Q and R, and then there are no reasons to think that there are topological properties beyond the isostatic regime, and that are not been taken into account in the topological scheme.

Chapter 3

Hyperstatic Topological Mechanics

As we mentioned in the past chapters, the Maxwell-Calladine theorem tells us that in systems that are in the hyperstatic regime, i.e. when the coordination number is larger than the degrees of freedom, self-stress modes are predominant over the zero energy modes in the system. However, this does not imply that such a rigid system cannot host rich static or dynamic behavior due to its topology. The same methodology applied to isostatic systems may not be useful in rigid ones to study or characterize the topologically protected modes. Over and above, there are recent studies that show the topological existence of these modes, in free boundaries and interfaces[73]. Our work in this chapter is mainly focused on this last case, where we will review an hyperstatic system that presents topologically protected low-frequency modes.

3.1 Hyperstatic Chain

The system we will study in this section is a hyperstatic generalization of the previous chapter's system. It was introduced recently as an example of topologically protected modes in the interface of a hyperstatic system[73], and in this section, we will give a brief report of the main result that concerns our purpose. The system is made up of two isostatic chains(shown in Chapter 2) with opposite signs for the equilibrium angle $\bar{\theta}$. These chains are joined in their rotation point, obtaining a straight bar that can rotate around their middle point, and that has an alternating angle equilibrium angle with respect to the vertical(see Fig. 3.1). This mechanical configuration then has two constraints(springs) and one DOF(rotation angle θ) at each unit cell n, being then an over-constrained or hyperstatic system. The rotation angle of the nth-bar is given by $\theta_n(t) = \bar{\theta} + \phi_n$ for a small perturbation $\phi_n \ll \bar{\theta}$, measuring the angles in an alternating form just as in the isostatic chain. This last consideration also makes it possible to distinguish between chains with $\bar{\theta} < 0$ and $\bar{\theta} > 0$. In the linear regime, the geometrical parameters $v_{1,2}$ that arise from the linear expansion of the spring extension are the same that in the isostatic chain, but here there is an additional spring per cell which implies that in a N-bars system under PBC, R is exactly a $(2N \times N)$-dimensional matrix. For instance, if the system in Fig. 3.1 is a four-bars chain under PBC, R is given by,

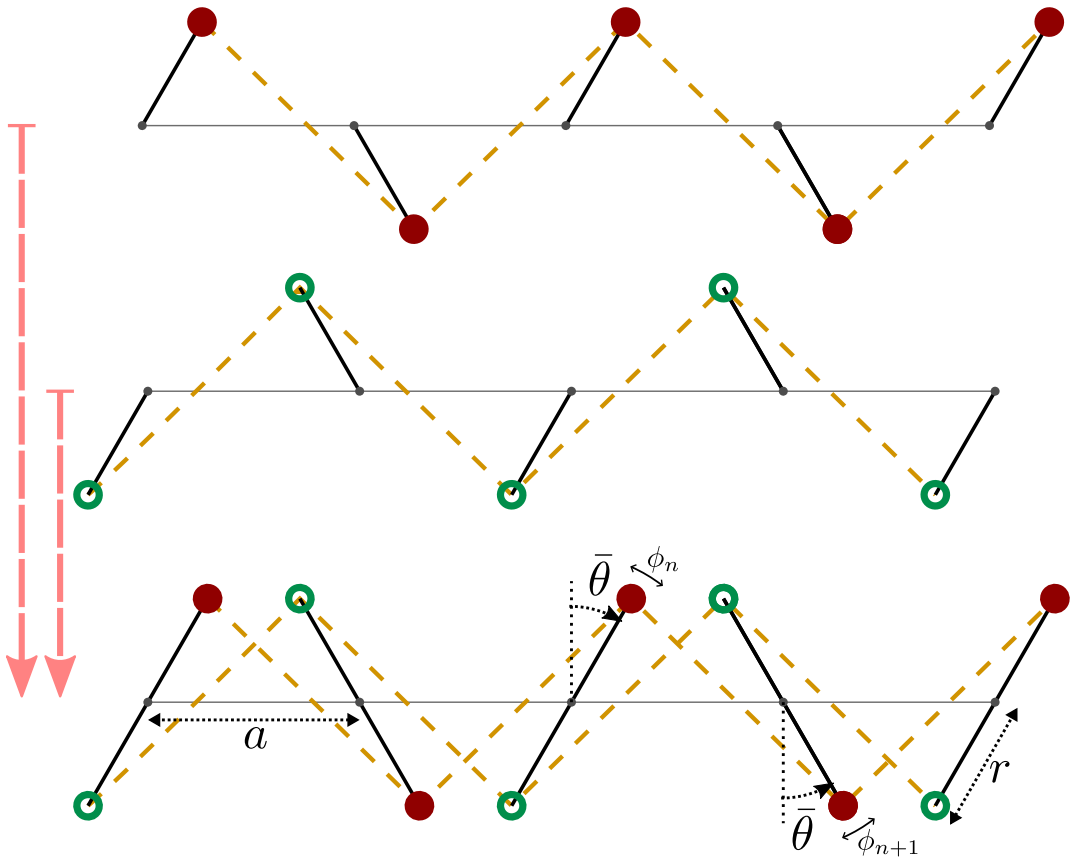

Fig. 3.1: *Hyperstatic chain system. The system is built by coupling two isostatic chains with opposite signs for the equilibrium angle. The resultant system is composed of straight bars of length $2r$ that rotate around their middle point, where each unit cell has two springs and one DOF. As in the isostatic chain, the rotations points are separated by a distance a, and the n-th bar tilt ϕ_n around the rest angle.*

$$R = \frac{1}{\sqrt{2}} \begin{pmatrix} v_1 & -v_2 & 0 & 0 \\ -v_2 & v_1 & 0 & 0 \\ 0 & v_1 & -v_2 & 0 \\ 0 & -v_2 & v_1 & 0 \\ 0 & 0 & v_1 & -v_2 \\ 0 & 0 & -v_2 & v_1 \\ -v_2 & 0 & 0 & v_1 \\ v_1 & 0 & 0 & -v_2 \end{pmatrix} \tag{3.1}$$

Also in the above equation, the geometrical parameters $v_{1,2}$ can be reduced to one dimensionless parameter [1] $c = \frac{v_1}{v_2} = \frac{a+2r\sin\bar{\theta}}{a-2r\sin\bar{\theta}}$, where $c < 1 (c > 1)$ when $\bar{\theta} < 0 (\bar{\theta} > 0)$, and $c = 1$ for

[1] With the appropriated normalization

$\bar{\theta} = 0$(see Fig. 3.2). Therefore the above compatibility matrix can be written as

$$R = \frac{1}{\sqrt{2}} \begin{pmatrix} c & -1 & 0 & 0 \\ -1 & c & 0 & 0 \\ 0 & c & -1 & 0 \\ 0 & -1 & c & 0 \\ 0 & 0 & c & -1 \\ 0 & 0 & -1 & c \\ -1 & 0 & 0 & c \\ c & 0 & 0 & -1 \end{pmatrix} \tag{3.2}$$

Therefore, in a generic system, R can be written in a compressed form

$$R = \begin{pmatrix} R_{2p-1,q} \\ R_{2p,q} \end{pmatrix} = \frac{1}{\sqrt{2}} \begin{pmatrix} c\delta_{p,q} - \delta_{p,q+1} \\ c\delta_{p,q} - \delta_{p,q-1} \end{pmatrix}$$

In the previous chapter, we assert that in this thesis the criteria to refer to a system as "hyperstatic", is that given a periodical configuration of the system the bulk k-space compatibility matrix $R(k)$ is a rectangular matrix, where the number of rows(related to the coordination number), is strictly greater than the columns(related to the DOFs number). This condition can be verified in this system by computing $R(k)$ according to (2.7), that is

$$R(k) = \frac{1}{\sqrt{2}} \begin{pmatrix} c - e^{ik} \\ c - e^{-ik} \end{pmatrix} \tag{3.3}$$

Up to this point in this system, the matrix dimension is the only main difference with the isostatic chain, but due to this extra spring, the Maxwell-Calladine theorem also reveals some effects on the ZMs and SSSs in the system. To analyze this consider the k-space version of this theorem (see eq. (2.8)) which in this case leads to $N_0(k) - N_s(k) = -1$, that is, there is always one SSS more than ZM at each k. More specifically, when $c \neq 1$, there are no zero modes since $\text{Null}\, R(k) = 0$ for all k, while $\text{Null}\, Q(k) = 1$, which means that in a PBC system, for each bar, there is one SSS(see Fig. 3.2c). In contrast, just as in the isostatic chain when the bars are in a vertical position, or equivalently $c = 1$, is possible to obtain that $\text{Null}\, R(k = 0) = 1$, that is, a uniform ZM(see Fig. 3.2b), which will be relevant in the discussion of the topological properties of the system.

There is one last important difference between these chains when we consider a finite system. In the isostatic case, the finite chain directly implies the existence of ZM at the edges, which depending on the orientation $\bar{\theta}$ can be located at the left or right edge. However in a finite hyperstatic chain, even though the inversion $+\bar{\theta} \to -\bar{\theta}$ flips the chain, this makes no difference for the bars located at the edge because this chain is the superposition of a $+\bar{\theta}$ and $-\bar{\theta}$ chain, where at each edge one of these chains would be compatible for the ZM and one would not be. Nonetheless, this does not imply something specific to a chain interface, which is the focus of study in this system.

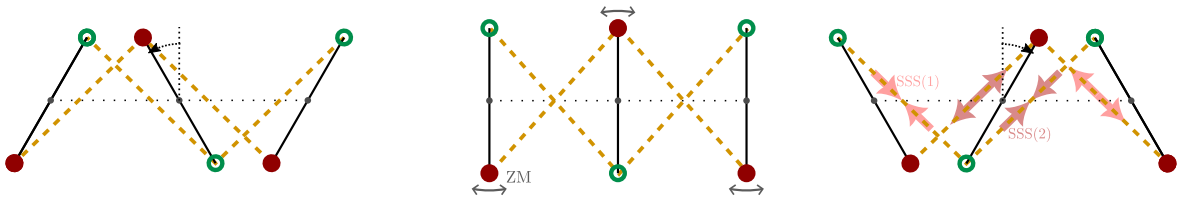

(a) $\bar{\theta} < 0$ **(b)** $\bar{\theta} = 0$ **(c)** $\bar{\theta} > 0$

Fig. 3.2: *The three possible equilibrium configurations in the hyperstatic chain, for* $\bar{\theta} < 0$, $\bar{\theta} = 0$ *and* $\bar{\theta} > 0$ *in* ***(a)***, ***(b)***, *and* ***(c)*** *respectively. Additionally, under PBC, that is, when the first and third bar represents the same bar, in* ***(b)*** *and* ***(c)*** *is shown the ZM and a SSS that the chain support respectively.*

3.2 Topological Characterization of Non-Square Matrices

Let us remember how the topological classification arises in isostatic lattices. The classification and their topological invariant are obtained from a specific type of quantum mechanical system that shares their symmetries with H (see eq. (2.11)) and results that the topological properties can be described by mean a winding number that depends on the bulk space matrix $Q(\boldsymbol{k})$ or $R(\boldsymbol{k})$. The extension of this winding number is possible since these two matrices are square in the isostatic regime, but the extension would not be possible to do it if this condition is not met. Up to this point, independently if it has a physical meaning, in a hyperstatic system $Q(\boldsymbol{k})$ and $R(\boldsymbol{k})$ are rectangular, and therefore it is not possible to use of this method. However, if we look back at $H(k)$, its symmetries do not depend on the dimensions of R and Q, and the chiral symmetry in $H(k)$ is nothing but the manifestation of classical mechanics' time-reversal symmetry. The problem emerges in the topological characterization and the topological invariant formulation, where the isostatic framework recurs to the tenfold way explained in Chapter 1, so in the hyperstatic case arises the question, is it possible to topologically classify these spaces? That eventual topological classification should work on non-square matrices, which is the focus of this section. Fortunately for this purpose, there are some topological studies about this problem, where a "tenfold way inspired"[25] topological characterization on non-square matrices can be a good option following the isostatic methodology[79]. In the following section, we will discuss this classification and later what implies in the hyperstatic chain.

3.2.1 Classification

To discuss the topological characterization used, consider a general case where $R \in \mathbb{R}^{M\times N}$, which will be useful for the thesis work. Inspired by the eigenvalues topological analysis in the topological insulators tenfold-way classification, in this classification, it is considered a *singular value decomposition*(SVD) for $R(k)$(since), namely $R(k) = U\Lambda_R V^\dagger$, where Λ_R is the $M \times N$-dimensional singular values matrix with non-zero values only in the main diagonal called *singular values*, and U, V are the SVD transformation matrices. Following the analogy with the tenfold-way characterization, in the SVD decomposition, a *flattening* of the singular

values is applied $\Lambda_R \to \tilde{\Lambda}_R$, where each non-zero value is replaced by 1. This process lead to two $\tilde{\Lambda}_R$ types, depending on the bigger dimension of R, where these matrices take the form

$$\tilde{\Lambda}_R = \begin{pmatrix} 1 & 0 & \cdots & 0 \\ 0 & 1 & \cdots & 0 \\ \vdots & \vdots & \vdots & \vdots \\ 0 & 0 & \cdots & 1 \\ 0 & 0 & \cdots & 0 \\ \vdots & \vdots & \vdots & \vdots \\ 0 & 0 & \cdots & 0 \end{pmatrix} = \begin{pmatrix} \mathbb{1}_N \\ 0_{N,(M-N)} \end{pmatrix} \qquad \text{when} \quad M > N$$

$$\tilde{\Lambda}_R = \begin{pmatrix} 1 & 0 & \cdots & 0 & 0 & \cdots & 0 \\ 0 & 1 & \cdots & 0 & 0 & \cdots & 0 \\ \vdots & \vdots & \vdots & \vdots & \vdots & \vdots & \vdots \\ 0 & 0 & \cdots & 1 & 0 & \cdots & 0 \end{pmatrix} = \begin{pmatrix} \mathbb{1}_M & 0_{M,(N-M)} \end{pmatrix} \qquad \text{when} \quad M < N$$

With the above matrix, it is possible to obtain a R flattened version from the SVD transformation matrix U, V, that is

$$\tilde{R} = U\tilde{\Lambda}_R V^\dagger \ ,$$

where this matrix is topologically classified by its homotopy groups. For further details, the extended analysis of the classification can be read in ref. [122], while the topological analysis where rectangular matrices as $\tilde{R}$ belongs can be read in ref. [3]. In this thesis, we will treat only two cases, when R is a real or complex rectangular matrix. When R is complex, the homotopy groups of $\tilde{R}$ are high-order non-trivial groups[122] where is not clear how to write the invariant. In contrast for real R, the space $\tilde{R}$ is isomorphic to well-know spaces from which the first non-trivial homotopy groups of $\tilde{R}$ are obtained[3]

$$\pi_\Delta(\tilde{R} \in \mathbb{R}^{M\times N}) \cong \begin{cases} \mathbb{Z} & \text{for } N = 1 \text{ or } \Delta \text{ even} \\ \mathbb{Z}_2 & \text{for } N \geq 2 \text{ and } \Delta \text{ odd} \end{cases} \qquad \Delta := |M - N| \ , \tag{3.4}$$

where π_Δ is the Δ-st order homotopy group with Δ the dimension difference in R. In general, is not clear what this invariant is, but $\tilde{R}$ could suggest it.

3.2.2 Topological Invariant

Returning to the hyperstatic chain, the topological problem is not completely solved, because the invariant formulation is unknown up to this point. The approach of use the above classification is not the best candidate, because $R(k)$ is complex in this case. However, in ref. [73] they argue the existence of symmetry as a solution. They postulate that a generic system of any dimensions has a *generalized inversion symmetry* (GIS) if there is a unitary

transformation for the compatibility matrix $R(\boldsymbol{k})$, namely

$$\mathcal{R}(\boldsymbol{k}) = UR(\boldsymbol{k})W^{\dagger}\ , \tag{3.5}$$

where U, W are unitary matrices such that $\mathcal{R}(\boldsymbol{k})$ is real for a real wavenumber $\boldsymbol{k}$. Notice that this symmetry could be present even if the number of degrees of freedom is different from the number of restrictions, as in the hyperstatic chain. This case is precisely an example of this symmetry because for $R(k)$ in equation (3.3), the desired unitary transformation is given by

$$\begin{aligned} \mathcal{R}(k) &= \frac{1}{\sqrt{2}}\begin{pmatrix} 1 & 1 \\ i & -i \end{pmatrix} \cdot \frac{1}{\sqrt{2}}\begin{pmatrix} c - e^{ik} \\ c - e^{-ik} \end{pmatrix} \cdot \begin{pmatrix} 1 \end{pmatrix} \\ \Rightarrow \mathcal{R}(k) &= \begin{pmatrix} c - \cos k \\ \sin k \end{pmatrix} \end{aligned} \tag{3.6}$$

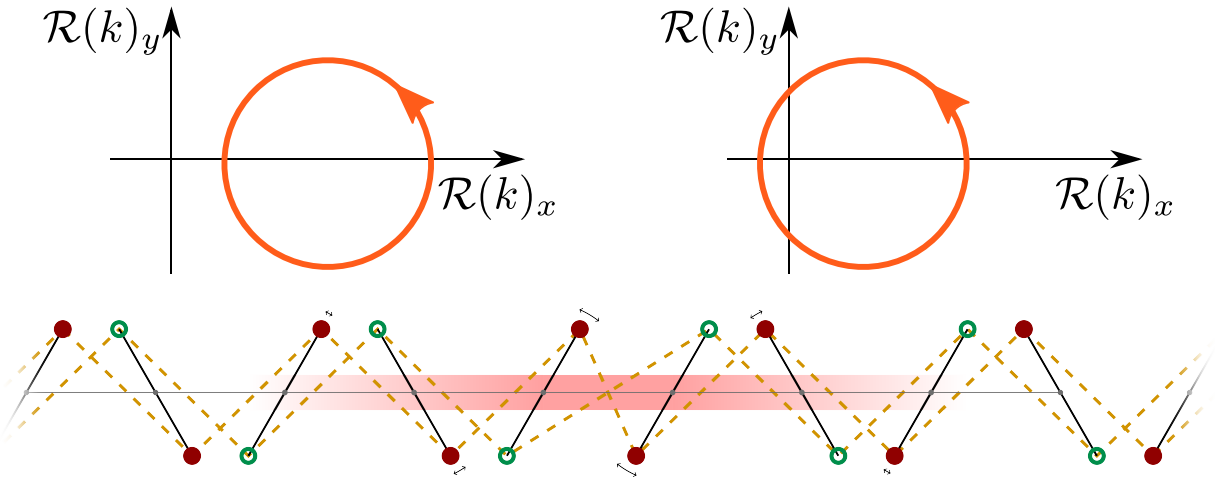

Fig. 3.3: *The parameterization of the components of $\mathcal{R}(k)$ is a circle that can enclose or not the origin when $c > 1$(top left) or $c < 1$(top left) respectively. When an interface between these two different topological phases is built(bottom), the system supports an exponentially localized state around the interface(represented by the highlight at the interface), which has a finite frequency and lies in the frequency band gap.*

According to the topological characterization discussed in the previous section, for $\mathcal{R}(k)$, its flattened version is given by

$$\tilde{\mathcal{R}}(k) = \frac{1}{\sqrt{(c - \cos k)^2 + \sin^2(k)}}\begin{pmatrix} c - \cos k \\ \sin k \end{pmatrix}$$

According to (3.4), here $\Delta = 1$ and therefore the fundamental homotopy group is $\pi_1(\tilde{\mathcal{R}}(k)) \cong \mathbb{Z}$, for which here the topological invariant is a winding number ν of the curve parametrized

by the components of $\mathcal{R}(k)$ when k run through the first Brillouin zone, according to (3.6). Notice that this clearly could be viewed directly on $\mathcal{R}(k)$, but the above classification is a formal scheme to argue this. Beyond the topological properties of this space, the question is if all of this has some kind of physical meaning in the physical system, and it is possible to realize that this invariant distinguishes two (topological) chain phases for $c > 1$ or $c < 1$ with a winding number zero or one respectively(see Fig. 3.3.a). In the following section, we will expose what relevance has in the chain's dynamics and compare it with the isostatic chain.

3.3 Soft Interface Modes

Up to this point, this hyperstatic chain does not show significant differences with their isostatic version, rather than be stiffer. But as we mentioned in the chapter preamble, the topological behavior here happens at low frequency, in contrast to the zero frequency modes(ZMs and SSSs) in the isostatic case. This statement could lead to thinking that these two problems are not related, but as we will review they have the same nature. First, the equation of motion for small perturbations can be obtained using the dynamical matrix. However, according to the previous section, the existence of two topological phases leads us to think about the possible effects of an interface between them. For the sake of this, if we allow for site-variations in c, i.e $c \to c_n$ the movement equation for the perturbation ϕ_n is given by

$$\begin{aligned}
\ddot{\phi}_n &= -Q\,R\,\phi_n \\
&= -\left(\phi_n(c_n^2+1) - \frac{1}{2}\phi_{n-1}(c_n + c_{n-1}) - \frac{1}{2}\phi_{n+1}(c_n + c_{n+1})\right) \\
\ddot{\phi}_n &= -(c_n-1)^2\phi_n + c_n(\phi_{n+1} - 2\phi_n + \phi_{n-1}) \\
&\quad + (c_{n+1} - c_n)\frac{\phi_{n+1}}{2} - (c_n - c_{n-1})\frac{\phi_{n-1}}{2}
\end{aligned} \tag{3.7}$$

in their non-dimensional version, which will be discussed at the end of the chapter. In an infinite system, a single change in c produces an interface for two different values for c, c_L and c_R for the left and right sides of the interface respectively. Most of these interfaces are physically trivial, except for the interface of two topologically different chains, which happen around $c = 1$, that is an interface $c_L < 1$ and $c_R > 1$(see Fig. 3.3). More specifically when the difference from $c = 1$ is symmetric at both sides, that is, when both chains have the same frequency gap or equivalently $c_L + cR = 2$, it is possible to analytically obtain a mode of finite-frequency given by

$$\omega^2 = \frac{4m_0^2 - 2m_0^4}{4 - m_0^2} \qquad \text{where } c_L = 1 + m_0 \text{ and } c_R = 1 - m_0$$

This mode is located within the frequency band gap(see Fig. 3.4), and therefore is exponentially localized at both sides of the interface. This mode is called a *soft mode* since it is located just under the lowest band.

In Fig. 3.4 a simulation over a long chain under PBC for $c_L = 1.3$ and $c_R = 0.7$ shows the existence of the vibration mode of frequency$\omega = 0.296$, where the units of ω had been

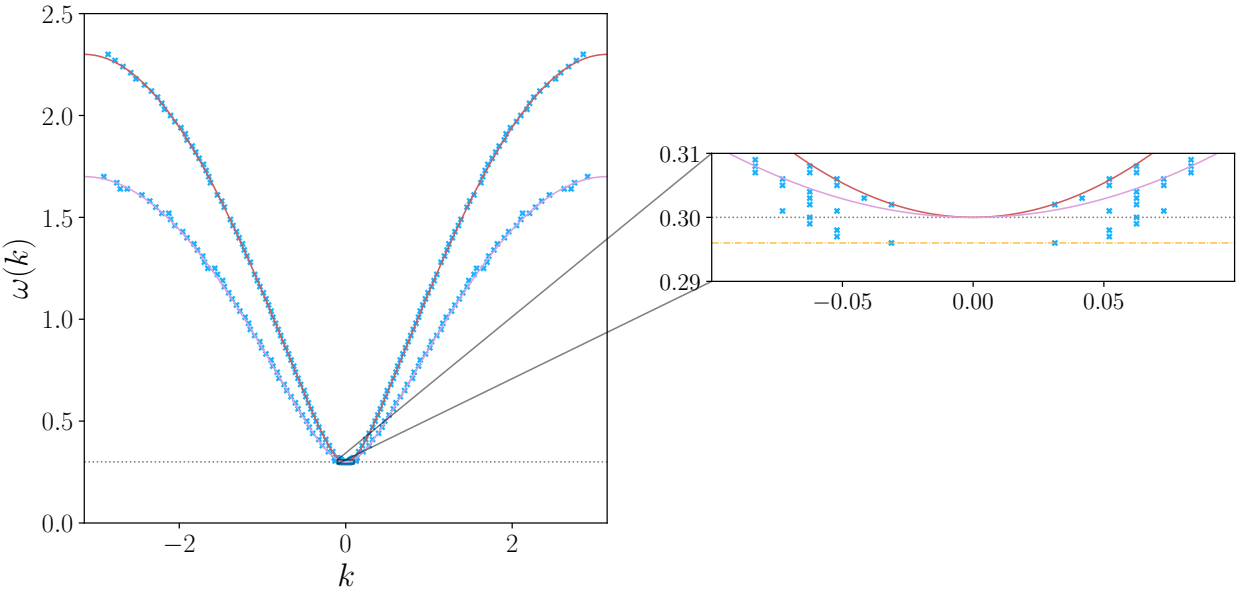

Fig. 3.4: *The figure shown the dispersion relation $\omega(k)$ for the interface system in Fig. 3.3. The solid line represents the frequency bands for the bulk of both sides of the interface, where the colors distinguish the left and right side bulk band. The points represent the results of a numerical simulation of an interface system under PBC and the horizontal dotted gray line in the main figure indicates the lowest bulk frequency. The zoomed part in the figure shows the modes at the interface which are located just below the bulk bands. An additional horizontal line(orange) passes through the lowest modes, which are modes of the interface's closest bars.*

dropped in the non-dimensionalization equation of motion, discussed in the next section. This frequency is within the band gap, and in the vicinity of $k = 0$, which corresponds to the interface mode of the two bars at the interface, with the wavelength equal to the system length. The modes arise as reminiscent of the zero modes at $c = 1$, which appear as a consequence of merging the topologically different chains from $c < 1$ to $c > 1$. The mode frequency and decaying length depend only on the difference from $c = 1$ at both sides of the interface (see Fig. 3.5a), but in addition, the interface supports the mode even when the frequency band gap is different at both sides of the interface, i.e. $c_L + c_R \neq 2$(see Fig. 3.5b) which shown the robustness of these modes.

3.4 Important Remarks

There are some relevant points, which are omitted in ref [73], but that we think are relevant to take into account. First, there is an implicit normalization in the equation of motion that will be important in the next chapter's discussion. The equation of motion with no treatment

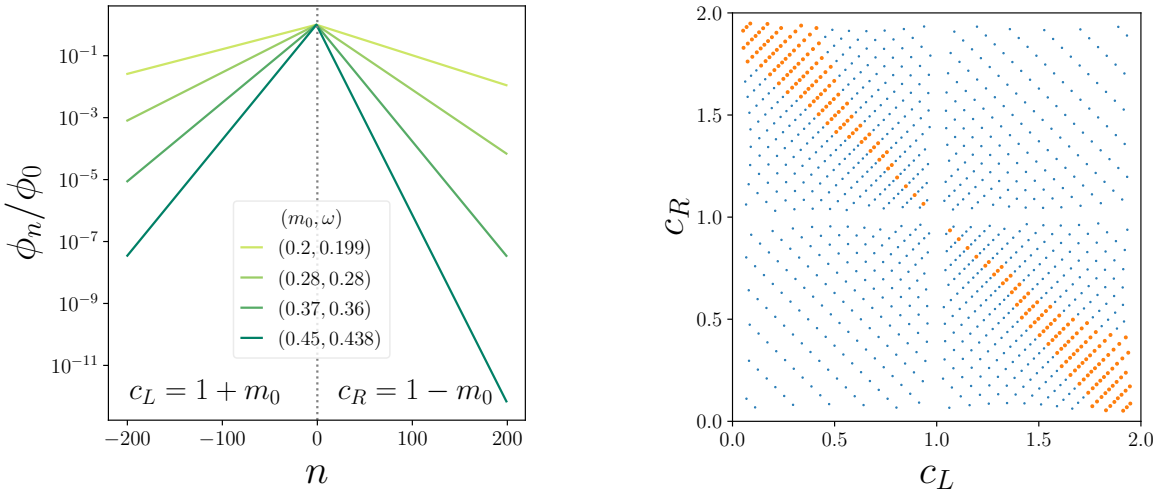

(a) **(b)**

Fig. 3.5: *In* ***(a)*** *is shown the decay of the soft-modes for different values of* $c_L = 1 + m_0$ *and* $c_R = 1 - m_0$ *and their corresponding frequency* ω*. In* ***(b)*** *is shown the pair* (cL, c_R) *for which these soft modes can be supported in the interface. The simulations were done for each point in the grid, and the cases that support the mode are the thick orange points(*$c = 1$ *where omitted since the frequency band gap closes).*

is given by eq. (2.3):

$$\begin{aligned}\ddot{\phi}(k) &= -D(k)\phi(k) \\ &= -\begin{pmatrix} c - e^{-ik} & c - e^{ik} \end{pmatrix} \left(\frac{\kappa v_2^2}{2J}\right) \begin{pmatrix} c - e^{ik} \\ c - e^{-ik} \end{pmatrix} \phi(k)\end{aligned}$$

for some inertia moment J. Consider the non-dimensional variable τ, related to the time as $t = \tau t_c$, for a time constant t_c. Then with the operator $\left(\frac{d}{dt}\right)^2 = \frac{1}{t_c^2}\frac{d^2}{d\tau^2}$ the above equation is rewritten as[2]

$$\frac{d^2\phi(k)}{d\tau^2} = -\frac{1}{\sqrt{2}}\begin{pmatrix} c - e^{-ik} & c - e^{ik} \end{pmatrix} \left(\frac{\kappa t_c^2 v_2^2}{J}\right) \frac{1}{\sqrt{2}} \begin{pmatrix} c - e^{ik} \\ c - e^{-ik} \end{pmatrix} \phi(k)$$

By setting $\frac{\kappa t_c^2 v_2^2}{J} = 1$, the frequency scale in the system is $\frac{1}{t_c} := \omega_0 = v_2\sqrt{\frac{\kappa}{J}}$. Notice that this scaling depends on the geometrical parameter v_2, and therefore two chains with different c also differ in this scaling. By setting the geometry of the system for two sides with $c_L \neq c_R$, this will imply that both sides of the chain will have a different elasticity if we want to use the same time scale.

Also, it is important to remark that to merge two chains of different c, it is necessary to choose two springs in the interface that guarantee the chain's mechanical equilibrium, as we did for the interface modes in the isostatic chain in Chapter 2. These springs are different

[2]The trivial non-dimensionalization for the spatial variable is the lattice spacing a

from the ones in the bulk of the chains, and therefore the bars at the interface are coupled by different factors than c_L and c_R which are neglected in the equation of motion (3.7). Considering this, the equation of motion is given by

$$\begin{aligned}
\ddot{\phi}_n &= -\left(-c_{L(R)}\phi_{n-1} + \phi_n(c_{L(R)}^2 + 1) - c_{L(R)}\phi_{n+1}\right) \quad \text{for } n < 0 (n > 1) \\
\ddot{\phi}_0 &= -\left(\frac{1}{2}\phi_0\left(2 + c_I^2 + c_L^2\right) - \phi_{-1}c_L - \phi_1 c_I\right) \\
\ddot{\phi}_1 &= -\left(\frac{1}{2}\phi_1\left(2 + c_I^2 + c_R^2\right) - \phi_2 c_R - \phi_0 c_I\right)
\end{aligned} \tag{3.8}$$

for an interface between $n = 0$ and $n = 1$m where $c_I = \frac{v_{1I}}{v_{2I}}$, and $v_{1I,2I}$ are the corresponding linear terms for the interface springs extension, where $c_L \neq c_I \neq c_R$ which is the assumption used in ref. [73] for the bars at the interface, but is not true in general. We assert that to deal with the soft modes shown in the previous sections, at the interface c_L, c_R should be near one and $c_L + c_R = 2$. By considering this, the equation of motion (3.7) remains a good approximation of eq. (3.8). Notice that this implies that the results of Fig. 3.5b that are far from $c \sim 1$ could have a different nature than the modes $c \sim 1$. This question is still open in our analysis.

Chapter 4

Hyperstatic Chain Generalization

The topological soft modes showed in the previous chapter were a direct consequence of the zero modes at $c = 1$, but as we mentioned in the previous chapter when the number of constraints in the system increases, the system becomes stiffer until there is a point where the system does not support any ZM. However, that assumption is only valid considering only one bond between two sites. In the hyperstatic chain, at each angle, two springs are connected, which allows for the existence of zero modes, even when the DOFs have been increased. This increase in the number of constraints was done by adding more restrictions to bars that already have one constraint per unit cell in the isostatic case. In this thesis, we ask, what if we similarly increase the stiffness in the system? In this section, we show that in stiffer chains, under specific fulfilled requirements, the topological characterization from the previous section can be generalized, and where the soft modes encountered in the regular hyperstatic chain also can be supported.

4.1 Multiple Chain System

The following scheme can build a stiffer hyperstatic chain, and keep the simplicity to explain the topological aspect of the problem. The approach to generalize the problem, similar to the one used in Chapter 3, is to include more constraints without breaking the symmetry of the system (which should sound logical for the topological problem), while holding the characteristic physics at $c = 1$. To build a system that supports these requirements, consider n different and independent infinite hyperstatic chains, where $\bar{\theta}$ and r are free parameters at each chain(see Fig. 4.1), but the periodicity a between bars is the same at each chain. Now, we place all these chains on the same line, so that the rotation points coincide, and additionally we couple the n chains at each site so that now all these chains rotate with the same angle. The resultant system has one DOF and $2n$ constraints per unit cell, which we call a *multiple chain* system. The compatibility matrix R of this system can be written by a direct extension of the single hyperstatic chain but for multiple geometrical parameters $v_{1,2}$(one pair per chain). This mean that in this case, R, can be written exactly as in (3.1), but with a promotion of $v_{1,2}$ into vectors that is

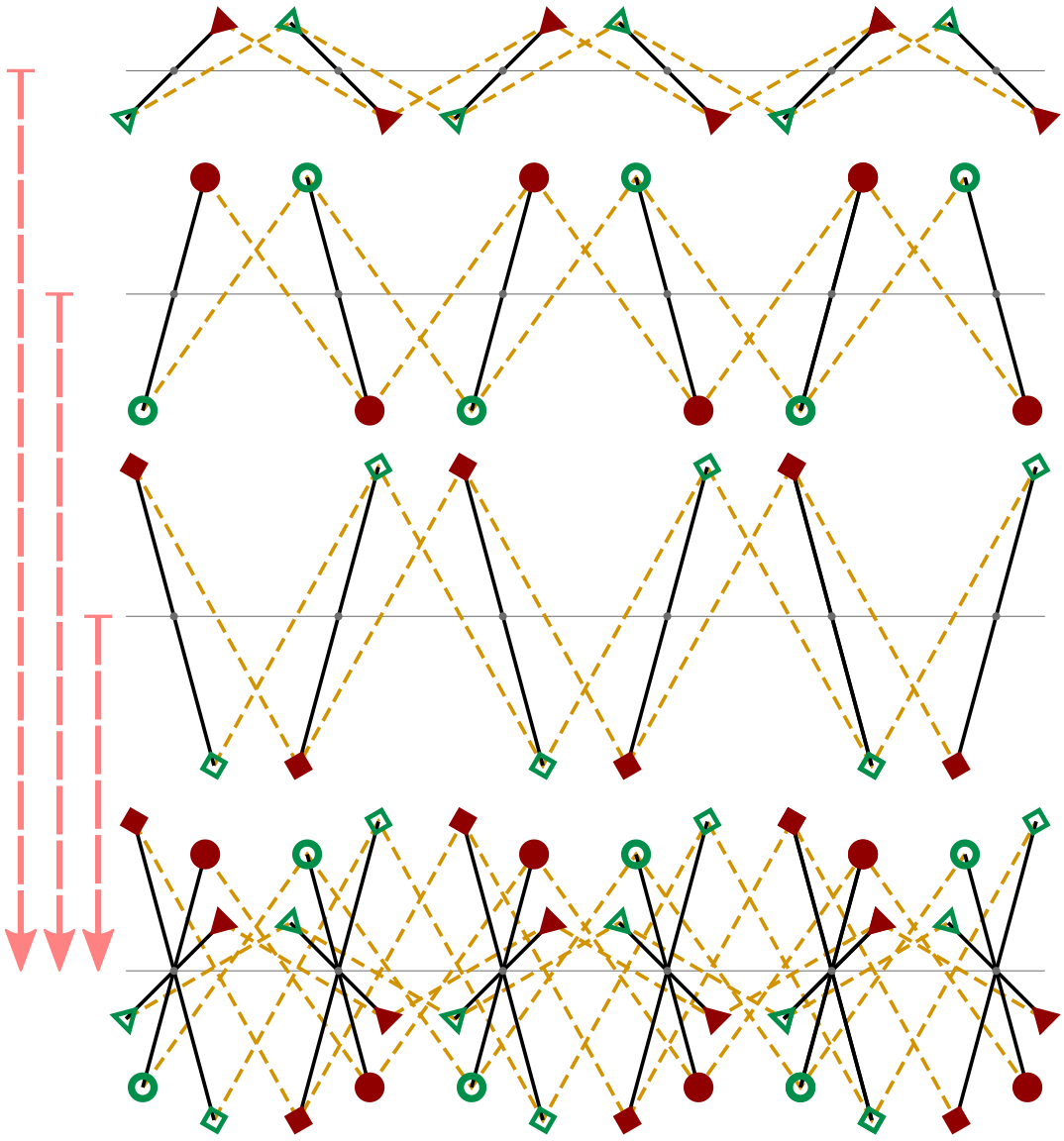

Fig. 4.1: *Multiple Hyperstatic Chain. The chain is composed of multiple hyperstatic chains in the same line, where all the bars in the same site are "glued", and rotates collectively. Each chain only shares its periodicity and attached masses, but the equilibrium angle $\bar{\theta}$ and the bar radius r may differ. The shape of the masses does not have a physical meaning and is only for better chain differentiation.*

$$v_{1,2} \to \boldsymbol{v}_{1,2} = \begin{pmatrix} v_{1,2(0)} \\ v_{1,2,(1)} \\ \vdots \\ v_{1,2,(n-1)} \end{pmatrix} \quad \text{where } v_{1,2(i)} = \frac{r_i \cos\bar{\theta}_i (1 \pm 2 r_i \sin\bar{\theta}_i)}{\sqrt{1 + 4 r_i^2 \cos^2\bar{\theta}_i}}$$

It is more comprehensible to reorder the rows in the k-space compatibility matrix $R(k)$, and

similarly to the hyperstatic chain, write it in terms of multiple values for cm one for each chain in the composition. Thus for n coupled chains, $R(k)$ takes the form

$$R(k) = \frac{1}{\sqrt{2n}} \begin{pmatrix} v_{2(0)}(c_0 - e^{ik}) \\ v_{2(0)}(c_0 - e^{-ik}) \\ \vdots \\ v_{2(n-1)}(c_{n-1} - e^{ik}) \\ v_{2(n-1)}(c_{n-1} - e^{-ik}) \end{pmatrix} \tag{4.1}$$

where $c_i = v_{1(i)}/v_{2(i)}$ is defined exactly as in the previous section, however now it can be different for each chain. In eq. (4.1), as we discuss in the final part of Chapter 3, the authors did not discuss its normalization of the factor $v_{2(i)}$ by inertia moment and the elastic constant. However, this assumption has an implicit detail that now would be relevant, which is that there is a dependence between the inertia moment, the elastic constant and c. In the single hyperstatic chain, this implies not other than scaling the energy of the system, but in the case of the multiple chain system, it is not possible to ensure normalization in every chain. Nonetheless, it is possible to get rid of every $v_{2(i)}$ if we re-scale by choosing different elastic constants in each chain, although now there will be an energy difference between the chains. By doing so for n coupled chains $R(k)$ takes the form

$$R(k) = \frac{1}{\sqrt{2n}} \begin{pmatrix} c_0 - e^{ik} \\ c_0 - e^{-ik} \\ \vdots \\ c_{n-1} - e^{ik} \\ c_{n-1} - e^{-ik} \end{pmatrix}. \tag{4.2}$$

For the moment, we assert without proof that under some conditions, this scaling does not have a significant influence on topological properties. This scaling and how is applied to multiple chain system will be discussed later in this chapter, to quantify these effects in the system with a known topology.

4.2 Topological Characterization

We already reach the target of increasing the constraint number and not the number of DOFs, and the next step is to analyze the topological properties of the multiple chain system, how it can be related to an eventual topological non-trivial behavior and also what conditions would to be met in that case. This last detail in the hyperstatic chain was closely related to the symmetry in the system, which allows for a topological classification according to the discussion of Chapter 3. To keep this symmetry in our system would be a priority, which requires the existence of some unitary transformation to be present, according to equation (3.5). Given the $R(k)$ shape in (4.2), we notice that in this case the transformation can be obtained by a direct generalization of the transformation U used in (3.6). That is, a block

diagonal matrix with the (2×2)-dimensional unitary transformation used in that case at each block(which is also unitary), since each block acts independently on each $R(k)$ subsystem

$$\begin{aligned}
\mathcal{R}(k) &= UR(k)W^{\dagger} \\
&= \frac{1}{\sqrt{2}}\begin{pmatrix} 1 & 1 & & & \\ i & -i & & & \\ & & 1 & 1 & \\ & & i & -i & \\ & & & & \ddots \end{pmatrix} \frac{1}{\sqrt{2n}}\begin{pmatrix} c_0 - e^{ik} \\ c_0 - e^{-ik} \\ c_1 - e^{ik} \\ c_1 - e^{-ik} \\ \vdots \end{pmatrix} \\
\Rightarrow \mathcal{R}(k) &= \frac{1}{\sqrt{n}}\begin{pmatrix} c_0 - \cos k \\ \sin k \\ c_1 - \cos k \\ \sin k \\ \vdots \end{pmatrix} .
\end{aligned} \tag{4.3}$$

Here $\mathcal{R}(k)$ is simply the result of the concatenation of each $\mathcal{R}(k)$ obtained as an independent system. The above results in the desired symmetry requirement, but also according to the discussion in Chapter 3, it is easier to get into a topological classification of $\mathcal{R}(k)$ rather than their complex form. According to the homotopy group presented in eq. (3.4), here the first nontrivial homotopy group is always $\mathbb{Z}$, no matter the number of chains in the composition, and the order of this group is the difference between the DOFs and constraints, that is, for a multiple chain system of n-chains, $\pi_{\Delta=2n-1} \cong \mathbb{Z}$. As we mentioned in Chapter 1, these high-order topological groups are out of discussion in this work, and for this reason, we looked for additional details that would simplify the problem. As a starting point, we can consider a multiple chain system composed of only two hyperstatic chains superposed, where $\mathcal{R}(k)$ represents the parameterization in $\mathbb{R}^4$ dependent on c_0 and c_1. However, if we select any set of four different vectors $\{\mathcal{R}(k_i)\}$ in this parameterization, we can prove that using the cross product[1], this is a set of orthogonal vectors,

$$\mathcal{R}(k_1) \cdot [\mathcal{R}(k_2) \times \mathcal{R}(k_3) \times \mathcal{R}(k_4)] = 0 \ ,$$

for any set $\{k_i\}$ of different wave vector $k \in [\,0, 2\pi)$. The result implies that the parameterization lies in a $(4-1)$-hyperplane, but if we would like to use a topological characterization like the winding number, seems reasonable to ask under what conditions this hyperplane encloses the origin, following the idea from Chapter 3. If the origin belongs to this hyperplane, it is necessary that

$$[c_0 - c_1][\sin(k_1 - k_2) - \sin(k_1 - k_3) + \sin(k_2 - k_3)] = 0 \tag{4.4}$$

[1] In the context of multi-linear algebra

where $\{k_i\}$ are a set of different wave vector in $[0, 2\pi)$. Because the right term is not zero in general, the origin lies on the hyperplane only if $c_0 = c_1$. With this hint in mind, we can apply this idea to several chains in equation (4.2). Suppose n coupled chains our system, where $\mathcal{R}(k)$ is a $(2n)$-dimensional column vector as in (4.3), which can be expanded as

$$\begin{aligned}\mathcal{R}(k) = c_0\boldsymbol{v}_0 + \cdots + c_m\boldsymbol{v}_{2m-2} - \cos k(\boldsymbol{v}_0 + \cdots + \boldsymbol{v}_{2m-2}) \\ + \sin k(\boldsymbol{v}_1 + \cdots + \boldsymbol{v}_{2m-1}) \ . \end{aligned} \tag{4.5}$$

Here $\{\boldsymbol{v_j}\}$ is the basis column vector set in the transformed space. In addition to the previous equation, we notice that due to the unitary transformation $\boldsymbol{v}_j = (\boldsymbol{v}_{j-1})^*$, which implies that this parameterization will always lie in an $(n+1)$-dimensional effective space, no matter the c values. The topological description of the previous section only takes into account the number of constraints and the symmetry aspects of the space, instead, this last result considers particular aspects of this system which could lead to a more specific characterization. By considering this effective dimension, in a n multiple chain system, the first non-trivial homotopy group is still $\mathbb{Z}$[3] but instead being the group π_{2m-1} is now π_{m+1}. As explained above, we are not interested in trying to find topological invariants in high-homotopy groups but does not appear to be additional ways to simplify such a generic problem. In this context, the result obtained in (4.4) arises as the obvious hint. Only when we have the same value for c in every chain the effective dimension decreases to 2, whereby formalizing the entire previous analysis, we can write $\mathcal{R}$ from equation (4.5) as

$$\mathcal{R}(k) = (c - \cos k)\,\boldsymbol{v}_0' + \sin k\,(\boldsymbol{v}_0')^* \ .$$

Here $\{\boldsymbol{v}_0, (\boldsymbol{v}_0')^*\}$ span a 2-dimensional plane, that shares the same homotopy group [3] as the single hyperstatic case. Consequently, we can use the same topological characterization used in the single chain case as long as chains have the same c value.

Despite the above simple requirement, as we mentioned before in this chapter, c_i is a function of r_i and $\bar{\theta}$ at each bar, which allows to built of chains with the same c-value, but this does not imply that the chains are the same(see Fig. 4.2): It only implies that $\bar{\theta}$ has the same sign in every chain in the composition, but may differ in magnitude as well as the bar radius, as shown in Fig. 4.2. More specifically, starting from a *reference chain* of parameters $\bar{\theta}_0, r_0$, to couple additional chains of equal c the radius in each new chain goes as $r_i(\bar{\theta}_i) = r_0(\sin\bar{\theta}_0/\sin\bar{\theta}_i)$, which implies that for $r_i < r_0 (r_i > r_0)$ require that $|\bar{\theta}_i| < |\bar{\theta}_0| (|\bar{\theta}_i| > |\bar{\theta}_0|)$. Nonetheless, as we will review in the following section there are also some additional requirements.

4.3 Normalization Consideration

As we indicate in the section beginning, the assumption of normalization over every chain has no topological consequences under determined conditions, which we will discuss in the following analysis. Consider two coupled chains system with equal c, for some different values

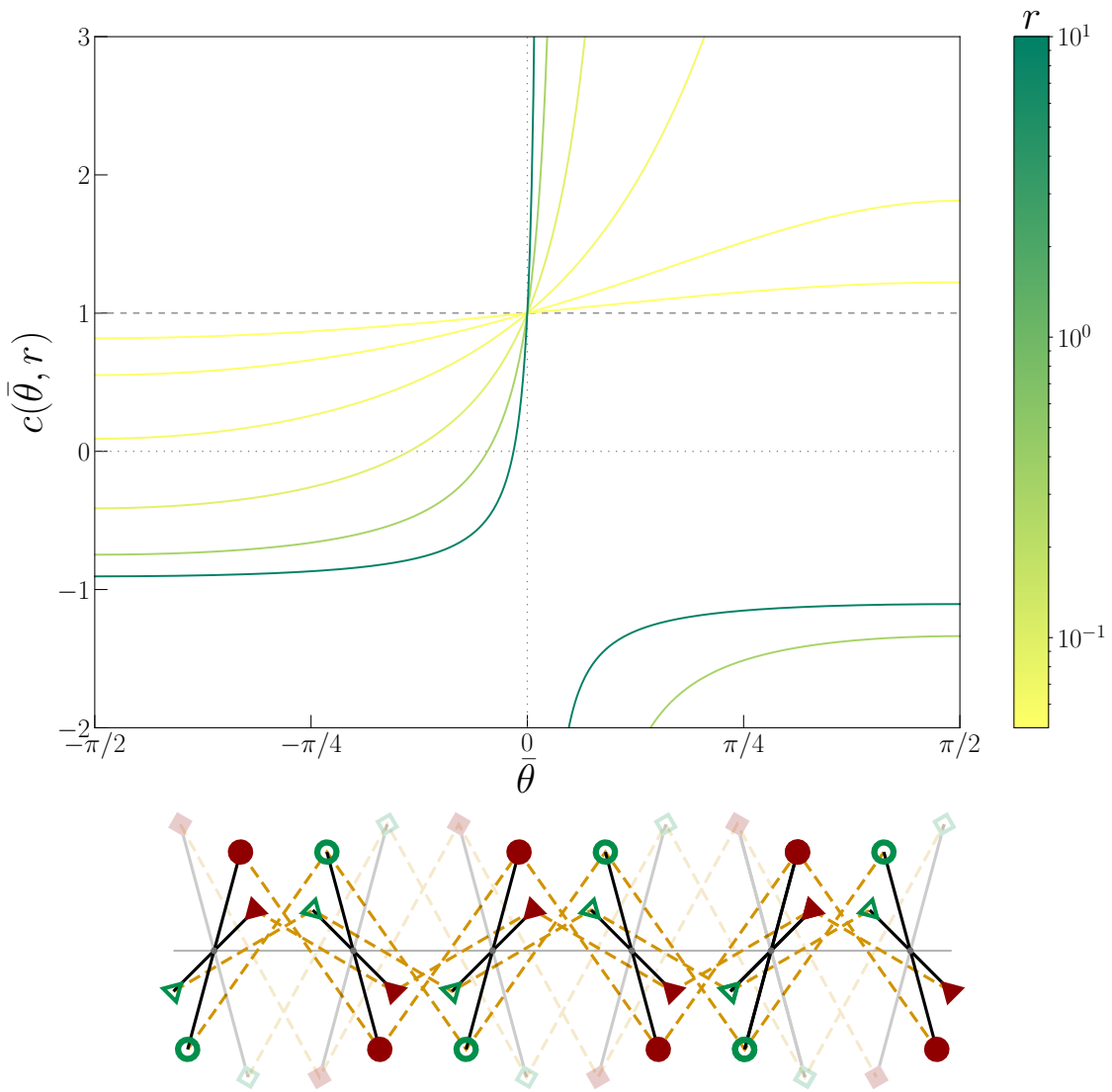

Fig. 4.2: *The parameter $c(\bar{\theta}, r)$ (top) is plotted as a function of $\bar{\theta}$ for multiple radius r, where its value follows the color bar at the right. Notice that for a specific c value, it can be achieved by multiple values of r and $\bar{\theta}$, where the unique requirement for two chains that share c is that $\bar{\theta}$ in both chains has the same sign, as shown the bottom figure, where the blurred chain of $\bar{\theta} < 0$ is not compatible with the remaining two highlighted chains with $\bar{\theta} > 0$.*

$\kappa_{0,1}, \bar{\theta}_{0,1}, r_{0,1}$. In this case, the equation of motion in the Fourier space is

$$\begin{aligned}\ddot{\phi}(k) &= -D(k)\phi(k) \\ &= -R(k)^\dagger \begin{pmatrix} v_{2(0)} & 0 \\ 0 & v_{2(1)} \end{pmatrix} \begin{pmatrix} \frac{\kappa_0}{J} & 0 \\ 0 & \frac{\kappa_1}{J} \end{pmatrix} \begin{pmatrix} v_{2(0)} & 0 \\ 0 & v_{2(1)} \end{pmatrix} R(k)\phi(k)\end{aligned}$$

for some total inertia moment J and where the three matrices between $R(k)^\dagger$ and $R(k)$ should be equal to the identity. As the chains share c, the variables are related according to $r_0 \sin\bar{\theta}_1 = r_1 \sin\bar{\theta}_0$. Then by setting $\frac{v_{2(0)}^2}{J} = 1$, $\kappa_0 = 1$ and the non-dimentionalization

explained in Section 3.4, the remaining normalizing elastic constants can be written as

$$\kappa_i(r_i, r, \bar{\theta}) = \frac{(r\cos\bar{\theta}(1-2r^2\sin\bar{\theta}))^2(1+4r_i^2-4r^2\sin^2\bar{\theta})}{(1-2rr_i\sin\bar{\theta})^2(1+4r^2\cos^2\bar{\theta})(r_i^2-r^2\sin^2\bar{\theta})}$$

where we have changed $r_0 \to r, \bar{\theta}_0 \to \bar{\theta}$. The above expression can be applied to an undetermined number of additional chains, but there are some limit values for which this scaling is not well-defined, and depend on the geometric configuration of the system. For instance, the function is approximated to first order as

$$\kappa_i(r_i, r, \bar{\theta}) \approx \frac{\cos^2\bar{\theta}}{(r_i/r)^2 - \sin^2\bar{\theta}} \qquad \text{when } r \ll 1$$

$$\kappa_i(r_i, r, \bar{\theta}) \approx \frac{[1+4r^2(r_i/r)^2]\left[1+4r^2((r_i/r)-1)\bar{\theta}\right]}{(1+4r^2)(r_i/r)^2} \qquad \text{when } |\bar{\theta}| \ll 1$$

In the limit $r \ll 1 (c \sim 1)$ the function has a divergence at a critical radius $r_{min} = r\sin\bar{\theta}$, where κ_i is only well-defined for $r_{min} < r_i$ because a chain with smaller radius requires a negative κ_i(see Fig. 4.3). In the regular cases, κ_i is bigger(smaller)than one, when $r_i < r (r_i > r)$. In difference when $\bar{\theta} \ll 1$, and $r \sim a = 1$ the function has a minimum value typically at $r_i/r \sim 1$, but most of the possible chains will have $\kappa_i > 1$. Additionally, a divergence appears at $r_i \to 0$, which corresponds to the bars approaching the horizontal position, where the divergence point is at the equilibrium angle $\pm\pi/2$. Also, there is an upper radius limit(see inset Fig. 4.3b) where a divergence appears, because when r_i is big enough to "touch" the bar in the neighbor sites, then c becomes negative, which produces some consequences that we will discuss in the next section, but for now we are restricted to c values out of these divergence points. We assert that under the previous conditions, we can keep the topological analysis from the previous section and the topological properties of the multiple chains system are not altered. Under a continuous change c, we can also continuously change the system to preserve the shape of $R(k)$ as in eq.(4.2), however, this does not imply that this energetic difference between chains has no other consequences in the dynamics of the chain's soft-modes.

4.4 Soft Modes in Multiple Chain System

The soft modes presented in the single chain can be understood as the reminiscence of the zero mode at $c = 1$, thus sounds reasonable to ask if is it possible to replicate them in the multiple chain case. Because of the effective dimension of R in the multiple chain system when the c values are equal, the equation of motion takes the same form as eq. (3.7) and therefore at the interface of two topologically distinct chains with $c_L + c_R = 2$ there is also a soft mode, that in principle has the same frequency and decay length as the hyperstatic single chain.

As shown in Fig. 4.4, it is possible to couple from two up to an undetermined number of chains, restricted only by the limiting values for the equilibrium angles and the elastic

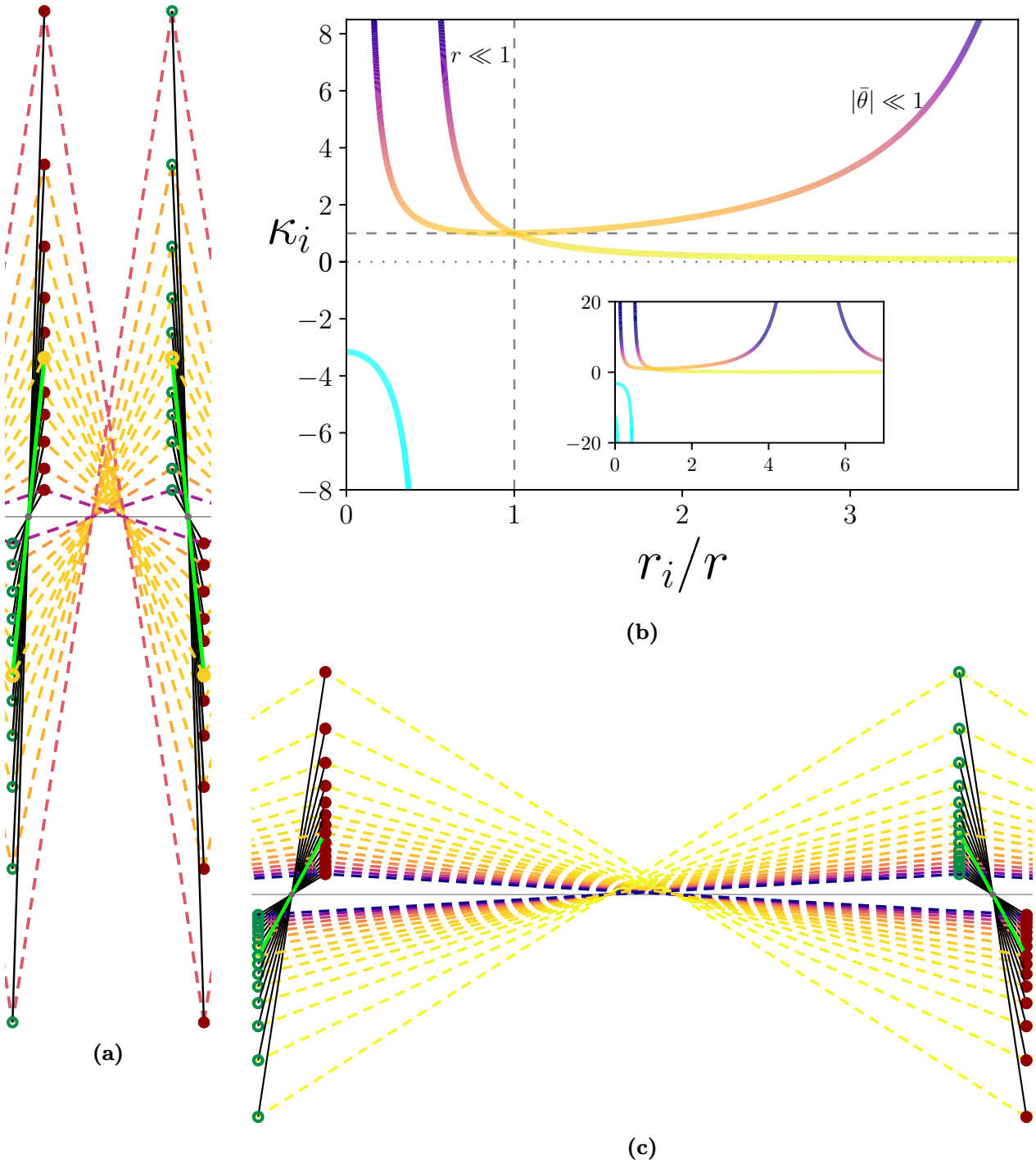

Fig. 4.3: *Normalization in the multiple chain system. In* ***(b)*** *is shown the plot of* $\kappa_i(r_i/r, \bar{\theta})$ *in the two limits mentioned in the main text, including the negative part(light blue) in the limit* $r \ll 1$*, and an inset that shows the second divergence in the limit case of* $|\bar{\theta}| \ll 1$*. The line color in* ***(b)*** *represents the values of* κ_i *in the diagrams* ***(a)*** *and* ***(c)****, which are systems in the limit cases* $|\bar{\theta}| \ll 1$ *and* $r \ll 1$ *respectively. The site spacing in* ***(a)*** *and* ***(c)*** *are equal, and the thick green bar represent the reference bar* $r_i/r = 1$*.*

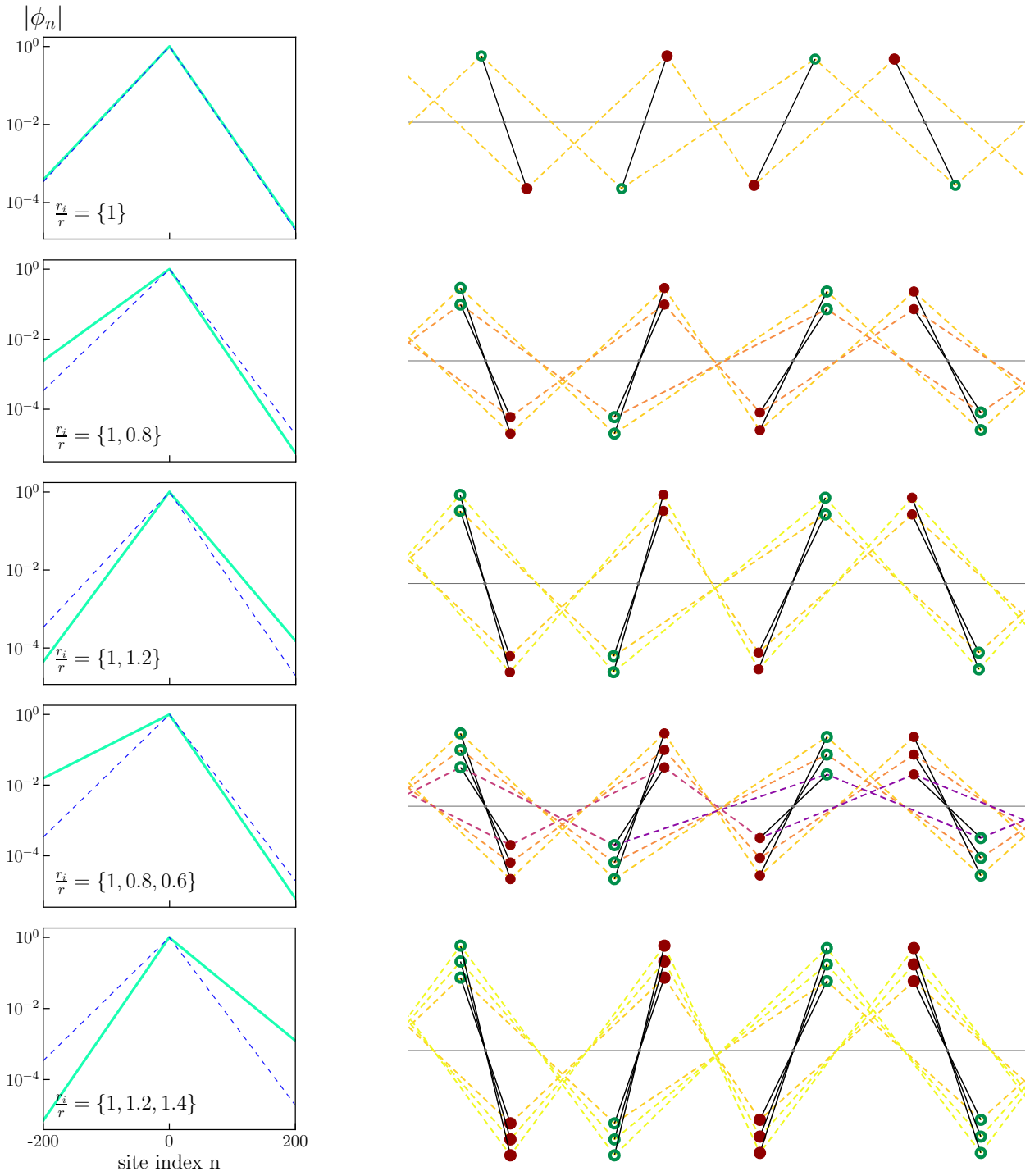

Fig. 4.4: *Topological soft modes in the interface between two different topological chains for* $c_L = 1.3$ *and* $cR = 0.7$ *for several multiple chain systems. The left row shows the n-th site amplitude* $|\phi_n|$ *in a logarithmic scale for the topological soft mode in the chain, where the dashed line represents the theoretical prediction in the single chain case, and the solid line represents the numerical result in a multiple chain system with radius according to the legend that indicates the* r_i/r *ratio of the composition, and where the reference chain is the one of* $r_i/r = 1$*. On the right side of each plot is shown the interface of the corresponding system(the chain is infinite in both directions) and where the spring color represents the spring elastic constant according to the colors of Fig. 4.3 and where the size scale of all the bars was readjusted by a factor of* $x2.5$ *for better visualization.*

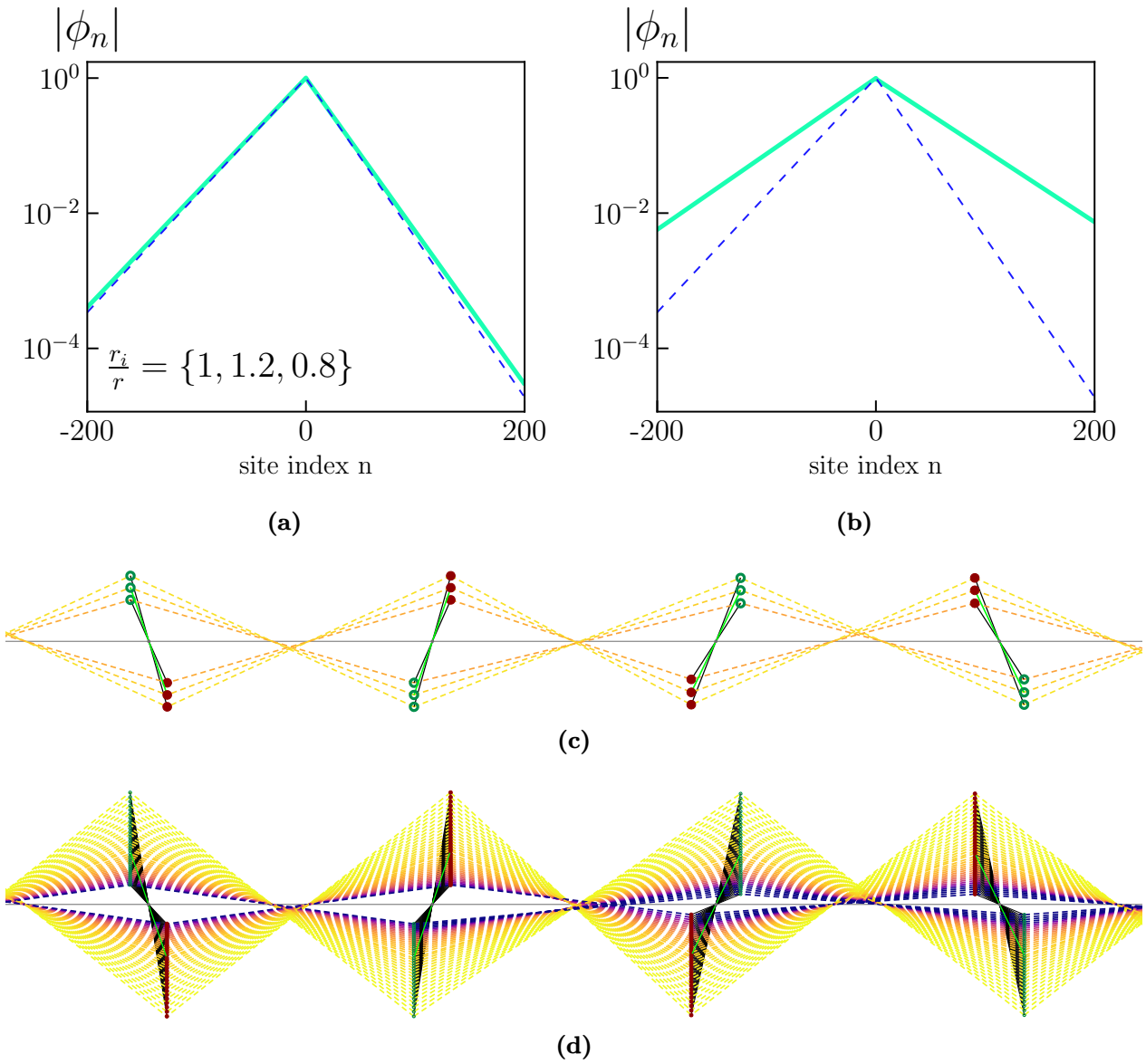

Fig. 4.5: *By coupling some particular chains, the decay length can be adjusted to follow the expected one, as shown in* ***(a)****, where the corresponding system is shown in* ***(c)****. The decay length* ***(b)*** *corresponds to the system shown in* ***(d)****, composed of thirty-seven, where eighteen chains equally angular-spaced with a bigger and smaller radius than the reference chain have been coupled. Both figures,* ***(c)*** *and* ***(d)*** *show the system with the same values of* $r, \bar{\theta}, a$ *than the system in Fig. 4.4 and also the lines represent the same, but here the bar sizes are shown in the real scale. The spring color represents the spring elastic constant according to the colors of Fig. 4.3*

Fig. 4.6: *The unit cell used before includes one spring at each side of the bar(left), now we will take a chain that includes both springs at right-side(right).*

constants. Notice that depending on the additional coupled chains, the decaying length appears to be slightly different from the one predicted theoretically, depending on which additional chains are coupled. When the system has two chains, the decaying length differs on the left(right) side when the additional chain has a bar radius bigger(smaller) than the radius of the reference chain, but when combining chains with bigger and smaller radii the effect appears to be compensated in some manner(see Fig. 4.5). This is in general hard to reach and is not related only to the number of chains with smaller and bigger radii than the reference chain, as shown in Fig. 4.5b.d, however, rather than a disadvantage, this scheme provides a method to tune the decaying length of the mode by controlling the number of chains and their equilibrium angle or radius. The difference between the predicted and the obtained decay length confirms that the energy scale is also a relevant factor to take into account in this interface state, which is protected by the topological nature of the system, even when the system has an undetermined number of constraints.

4.5 Localized Modes in Variable Stiffness Chain

Inspired by the vacuum-boundary edge states that can appear on topological insulators, we look for something similar in the regular hyperstatic chain. However, our first calculations raise that in a semi-infinite hyperstatic chain, the system does not show relevant phenomena in principle. This is a consequence of the symmetry of the chain, which is only appreciable when comparing two chains in an interface, in contrast to the boundary of a finite chain where both chain phases are equivalent. Because of this, we look again at the interface system where we test a different type of interface. This interface consists of an infinite and geometrically uniform where an elastic constant interface is possible. Particularly, we are interested in the case where the energy scale difference between both sides of this interface is large.

For this purpose, it is convenient to redefine the unit cell as we have been treating it. Consider the R from eq. (3.2), now we consider the unit cell as shown in Fig. 4.6, where the new unit cell includes the elastic constant value at both sides of the interface. By doing this R can be written as,

$$\begin{pmatrix} R_{2j-1,j'} \\ R_{2j,j'} \end{pmatrix} = \sqrt{\frac{\kappa_j}{2}} \begin{pmatrix} c_j\delta_{j,j'} - \delta_{j,j'-1} \\ c_{j+1}\delta_{j,j'-1} - \delta_{j,j'} \end{pmatrix}$$

where κ_j is the j-th unit cell elastic constant. From R, we can obtain the equation of motion

from $\ddot{\boldsymbol{u}} = -D\boldsymbol{u}$

$$
\begin{aligned}
\ddot{u}_n &= -\sum_{j,l} R^T_{n,j} R_{j,l}\ u_l \\
&= -\sum_{j,l} R_{j,n} R_{j,l}\ u_l \\
&= -\sum_{k,l} (R_{2j-1,n} R_{2j-1,l} + R_{2j,n} R_{2j,l})\ u_l \\
&= -\frac{1}{2}\sum_{j,l} [(c_j\delta_{j,n} - \delta_{j,n-1})(c_j\delta_{j,l} - \delta_{j,l-1})\kappa_j + (c_{j+1}\delta_{j,n-1} - \delta_{j,n})(c_{j+1}\delta_{j,l-1} - \delta_{j,l})\kappa_j] u_l \\
&= -\frac{1}{2}\sum_{j,l} [c_j\delta_{j,n} c_j\delta_{j,l} - c_j\delta_{j,n}\delta_{j,l-1} - c_j\delta_{j,n-1}\delta_{j,l} + \delta_{j,n-1}\delta_{j,l-1} \\
&\qquad + c_{j+1}\delta_{j,n-1} c_{j+1}\delta_{j,l-1} - c_{j+1}\delta_{j,n-1}\delta_{j,l} - \delta_{j,n} c_{j+1}\delta_{j,l-1} + \delta_{j,n}\delta_{j,l}] u_l \kappa_j \\
\Rightarrow 2\ddot{u}_n &= -u_n(c_n^2 + 1)(\kappa_n + \kappa_{n-1}) + u_{n+1}\kappa_n(c_n + c_{n+1}) + u_{n-1}\kappa_{n-1}(c_n + c_{n-1})
\end{aligned}
$$

which can be rewritten as

$$
\begin{aligned}
2\ddot{u} = &-(c_n^2 - 1)^2(\kappa_n + \kappa_{n-1})u_n + c_n(u_{n+1}\kappa_n - 2u_n(\kappa_n + \kappa_{n-1}) + u_{n-1}\kappa_{n-1}) \\
&+ u_{n+1}\kappa_n c_{n+1} + u_{n-1}\kappa_{n-1}c_{n-1}
\end{aligned}
$$

which is equal to equation (3.7) when $\kappa = 1$. Consider an interface for two values of κ, namely κ_L and κ_R for the left and right sides respectively, where c is constant in the chain. If $u_n = u_0 z^n e^{-i\omega t}$, the equation of motion in the system for the left and right side is given by

$$
\begin{aligned}
\omega^2 &= \kappa_L(c-1)^2 - c\kappa_L(z_L + z_L^{-1} - 2) \\
\omega^2 &= \kappa_R(c-1)^2 - c\kappa_R(z_R + z_R^{-1} - 2)
\end{aligned}
$$

By solving the equation system, for $\kappa_R = 1$ it is possible to obtain an interface localized mode that is in the energy band gap, for certain values of c given by,

$$
\omega^2(c) = \frac{(c^2-1)^2(1+\kappa_L)}{2(c^2+1)}
$$

The possible values of c where the mode is supported increase as $\kappa_L \to 0$, where the mode exists for any $c \neq \{0, 1\}$, but the $\kappa_L \ll 1$ is enough to have considerable possible values for

c as shown in Fig. 4.7. The mode is localized when c is in the set

$$(-\infty, -c_0) \cup \left(\frac{1}{-c_0}, 0\right) \cup \left(0, \frac{1}{c_0}\right) \cup (c_0, \infty) \qquad \text{where } c_0 = \frac{1+\sqrt{\kappa_L}}{1-\sqrt{\kappa_L}}$$

There is also an analytic expression for the decay z_L, z_R, but we preferred to show the plot in Fig. 4.7, where is visible that the decay on the right side is very slow to compare with the right side. In difference from the previous mode, rather than for topological reasons, here the mode is explained by the energy difference between both chains.

In this problem, we came across a detail that we had not taken into account so far. Notice that the mode does not appear to be restricted to the typical values of c, because there is no geometrical dependence for c as we treat in previous sections. This allows us to take negative values of c, where the bars intersect each other(see Fig. 4.8). In the limit case when $c = -1$, implies that $a = 0$, i.e. all the bars are located at the same point. For negative values of c, the band gap closes at $\pm\pi/a$, for $c = -1$, that is, the oscillation has a wavelength of $2a$ instead of zero for the $c > 1$ case. This led to thinking if the interface modes could exist near $c = -1$ instead of $c = 1$, which is our current focus in the topological part of the problem.

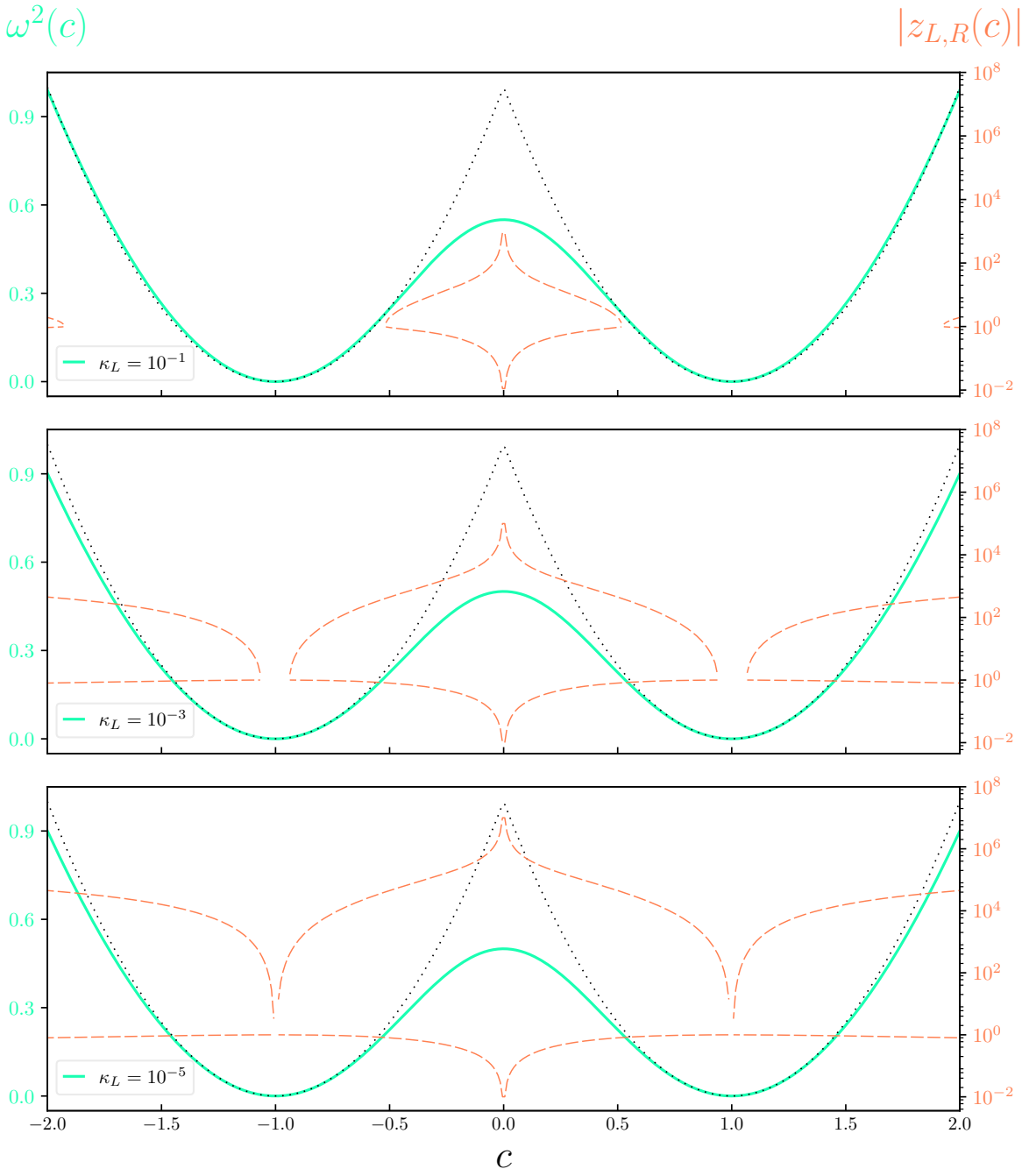

Fig. 4.7: *The figure shows $\omega^2(c)$ (solid line) for three different values of κ_L, which can be compared with the lowest propagative frequency for the variable stiffness chain (dotted line). There are values of c for which the state is localized, which can be distinguished by looking at the decay, where the dashed line below one is the decay $|z_R(c)|$ and the dashed line bigger than one is $|z_L(c)|$*

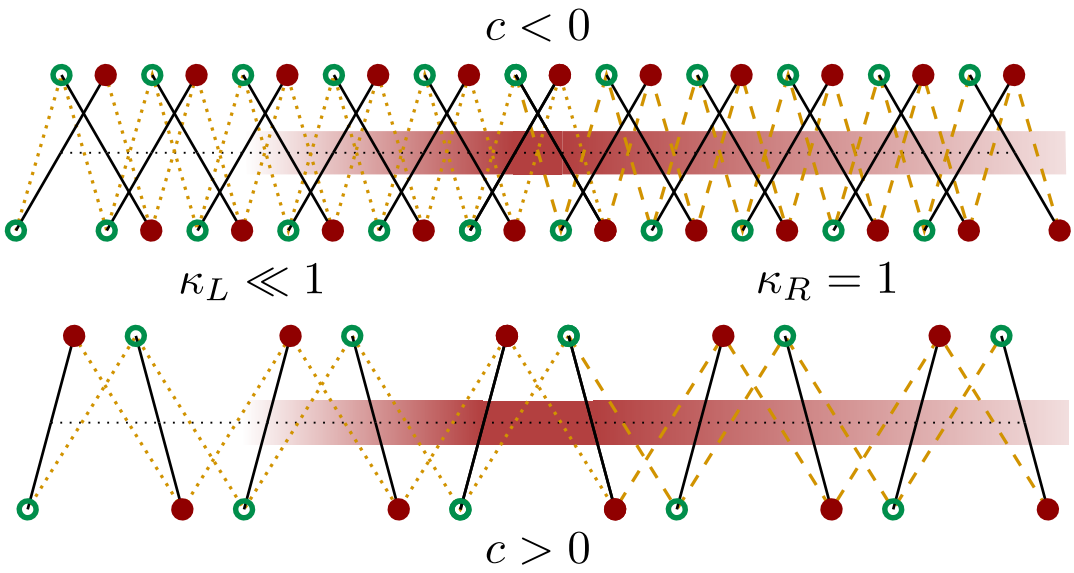

Fig. 4.8: *The figure shows a schematic view of the interface in the variable stiffness chain, for* $c < 0$ *(top) and* $c > 0$ *(bottom). The chain is infinite in both directions and the dashed lines represent the normal springs from the right side* $\kappa_R = 1$ *and the dotted line represents the springs of vanishing elasticity* κ_L*. The red highlighted zone represents the decay amplitude of the mode*

Chapter 5

Non-Linear Waves in Hyperstatic Chain

The isostatic chain reviewed in Chapter 2, presents a band gap as long as the bars are not in a vertical position($c = 1$), and in the finite case also can present ZM and SSS depending on the configuration. In the most simple case, a topological ZM is located in the compatible side of the chain that is exponentially localized at the edge, as we explained in Chapter 2. These consequences are only valid in the linear regime where infinitesimal oscillations are considered. Instead, a finite amplitude implies non-linear dynamics which is far from the effects discussed in this chapter. In particular, this finite movement can be well explained in the limit when the springs become rigid bars that we call *linkage isostatic chain*, where the chain describes non-linear solitary waves called solitons[66]. Inspired by this effect on the linkage isostatic chain, we explored what would imply a similar limit on the hyperstatic chain. In this chapter, we explore these effects and compare them with the results obtained in the isostatic version.

5.1 Brief Review of the Linkage Isostatic Chain

In difference from the linear elasticity approach, when the isostatic topological chain springs become rigid, the system becomes a rigid-bars chain which we call *linkage isostatic chain*, which can behave in rich manners different from their regular case. In principle, the compatible edge of the chain supports a similar floppy mode, but in addition to big amplitudes, the system also propagates a non-linear wave along the chain(see Fig. 5.1). It had been proved that the propagation of this mechanical mode is described as a *soliton*[66] that remarkably can propagate with zero energy, in difference from a linear oscillation in the regular chain, and where the unique zero mode is the floppy mode that does not propagate. Depending on the relation of the geometrical parameters, it is possible to distinguish two phases, *flipper* and *spinner* phases, for $r \sin^2 \bar{\theta} < a$ or $r \sin^2 \bar{\theta} > a$ respectively. We will discuss only the flipper case in this chapter, where we start reviewing the results of ref [66], for the sake of understanding the consequences in the hyperstatic case.

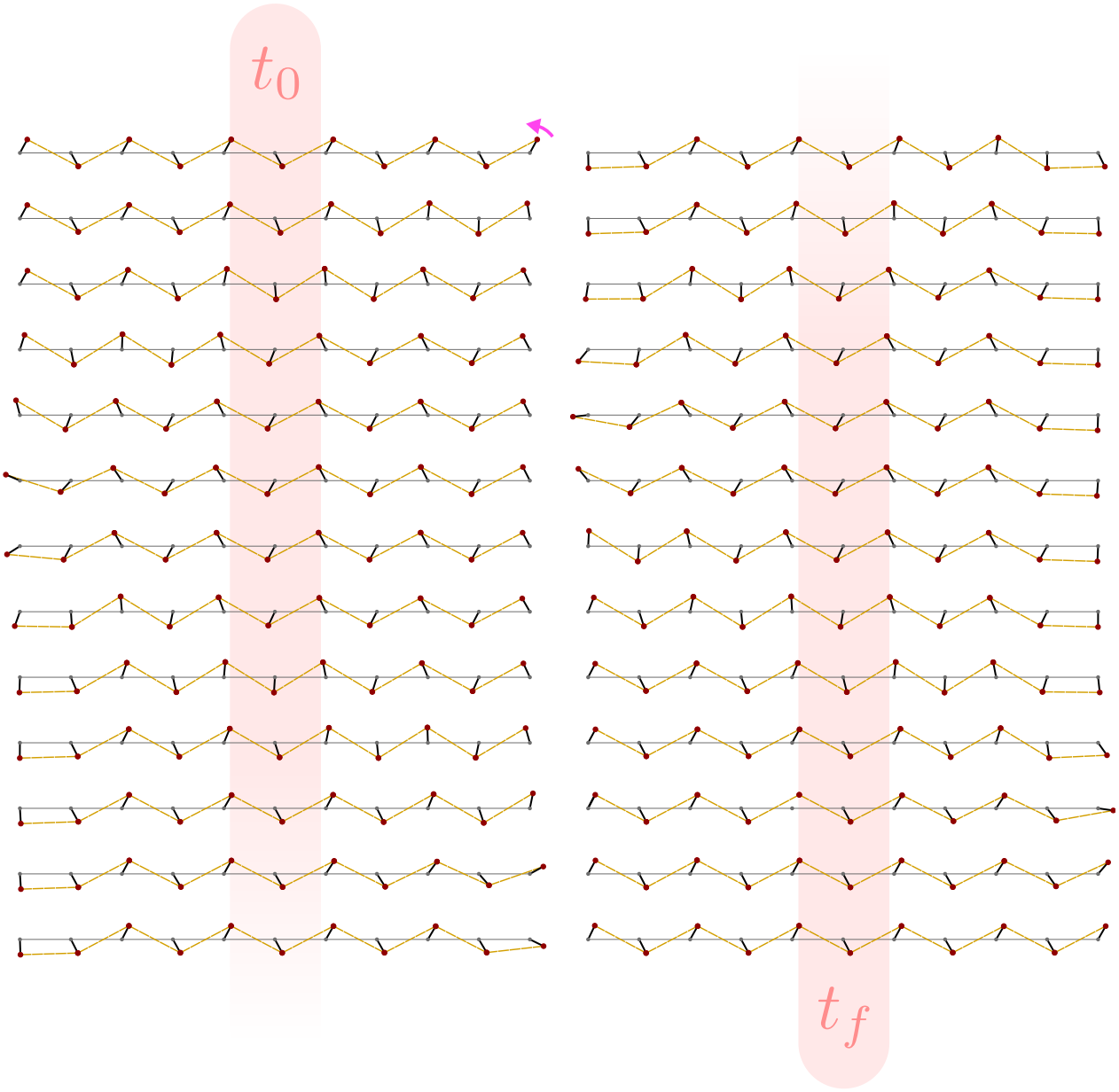

Fig. 5.1: *The figure shows the temporal evolution of the non-linear wave propagation in the isostatic chain, starting from the frame just under t_0 and ending at the frame just over t_f, following the highlight in the middle of the columns, where the left column continues at right column. The dashed lines represent the springs that become rigid bars.*

At the starting point, to understand how it is described this movement, consider the discrete Lagrangian of the regular isostatic chain:

$$L = \sum_{i=1}^{n} \frac{Mr^2}{2} \left(\frac{d\theta_i}{dt}\right)^2 - \sum_{i=1}^{n-1} \frac{1}{2}\kappa \left[\ell(\theta_i, \theta_{i+1}) - \bar{\ell}\right]^2 \tag{5.1}$$

where $\bar{\ell} = \ell(\bar{\theta}, \bar{\theta})$ and $\ell(\theta, \theta')$ is the length of the spring as defined in Chapter 2.

In the non-linear regime, the spring length does not change ostensibly, that is $[\ell_{i,i+1}-\bar{\ell}]^2 \approx 0$, thus we discard all the higher terms than quadratic for this length change. In addition to the limit of small $\bar{\theta}$, the approximation $[\ell(\theta_n,\theta_{n+1})+\bar{\ell}]^2 \approx 4\bar{\ell}^2$, capture these conditions. By taking this it is possible to write the potential energy term in (5.1) as

$$\begin{aligned}\frac{1}{2}\kappa[\ell(\theta_i,\theta_{i+1})-\bar{\ell}]^2 &= \frac{1}{2}\kappa[\ell(\theta_i,\theta_{i+1})-\bar{\ell}]^2\frac{[\ell(\theta_i,\theta_{i+1})+\bar{\ell}]^2}{[\ell(\theta_i,\theta_{i+1})+\bar{\ell}]^2} \\ &\approx \frac{\kappa}{8\bar{l}^2}[\ell(\theta_i,\theta_{i+1})^2-\bar{\ell}^2]^2\end{aligned}$$

When $\bar{\ell}$ and $\ell(\theta_n,\theta_{n+1})$ are replaced in the above equation, the potential in the spring is

$$V_{i,i+1} = \frac{\kappa}{2\bar{\ell}^2}[ar(\sin\theta_{i+1}-\sin\theta_i)-r^2\cos 2\bar{\theta}+r^2\cos(\theta_i+\theta_{i+1})]^2 \tag{5.2}$$

Next, a continuum limit a can be taken over the chain in the potential term, which describes the dynamics for $a\to 0$, and where the discrete variable θ_i can be promoted to the continuum field $\theta(x)$, where x is the spatial variable. To apply this limit consider the expansion of the spatial variable centered at the inter-space between two bars $x = a(i+1/2)$, where the two angular discrete variables θ_i and θ_{i+1} are expanded to first order as,

$$\begin{aligned}\theta_i \to \theta\left(x-\frac{a}{2}\right) &\approx \theta(x)-\frac{a}{2}\left(\frac{\partial\theta}{\partial x}\right) \\ \theta_{i+1} \to \theta\left(x+\frac{a}{2}\right) &\approx \theta(x)+\frac{a}{2}\left(\frac{\partial\theta}{\partial x}\right)\end{aligned}$$

Considering these expansions and the equation (5.2), the potential energy density can be written as

$$\begin{aligned}aV(\theta) &= \frac{\kappa}{2\bar{\ell}^2}\left(ar\left[\sin\left(\theta\left(x+\frac{a}{2}\right)\right)-\sin\left(\theta\left(x-\frac{a}{2}\right)\right)\right]-r^2\cos 2\bar{\theta}+r^2\cos 2\theta(x)\right)^2 \qquad (5.3)\\ &= \frac{\kappa}{2\bar{\ell}^2}\left(a^2 r\cos\theta(x)\frac{\partial\theta}{\partial x}+r^2\sin^2\bar{\theta}-r^2\sin^2\theta(x)-r^2\cos^2\bar{\theta}+r^2\cos^2\theta(x)\right)^2 \\ &= \frac{2\kappa}{\bar{\ell}^2}\left(\frac{a^2}{2}\frac{du}{dx}+\bar{u}^2-u^2\right)^2\end{aligned}$$

where $u = r\sin\theta$ and $\bar{u} = r\sin\bar{\theta}$. Similarly, the kinetic energy term in eq. (5.1), in the continuum limit under the approximation $\dot{\theta}_i(t)\approx\dot{\theta}(x,t)$, become the kinetic energy density

is given by

$$\begin{aligned} aT(\dot{\theta}) &= \frac{1}{2}Mr^2\dot{\theta}(x,t)^2\frac{[r^2\cos^2\theta(x,t)]}{[r^2\cos^2\theta(x,t)]} \\ &= \frac{1}{2}\frac{Mr^2}{(r^2-r^2\sin^2\theta(x,t))}(r^2\cos^2\theta(x,t)\dot{\theta}(x,t))^2 \\ &= \frac{1}{2}\frac{Mr^2}{(r^2-u^2)}\left(\frac{du}{dt}\right)^2 \end{aligned}$$

Therefore, given both energy densities, we can write the Lagrangian in the continuum limit as

$$\begin{aligned} \mathcal{L} &= \int dx\,[T(\dot{u})-V(u)] \\ \mathcal{L} &= \int dx\left[\frac{M}{2a}\left(\frac{\partial u}{\partial t}\right)^2-\frac{\kappa a^3}{2\bar{\ell}^2}\left(\frac{\partial u}{\partial x}\right)^2-\frac{2\kappa}{a\bar{\ell}^2}(\bar{u}^2-u^2)^2-\frac{\kappa a}{\bar{\ell}^2}\frac{\partial u}{\partial x}(\bar{u}^2-u^2)\right] \\ \mathcal{L} &= \int dx\left[\frac{M}{2a}\left(\frac{\partial u}{\partial t}\right)^2-\frac{\kappa a^3}{2\bar{\ell}^2}\left(\frac{\partial u}{\partial x}\right)^2-\frac{2\kappa}{a\bar{\ell}^2}(\bar{u}^2-u^2)^2\right]-\int dx\left[\frac{\kappa a}{\bar{\ell}^2}\frac{\partial u}{\partial x}(\bar{u}^2-u^2)\right] \end{aligned}$$

where only the first term on the kinetic contribution was considered, which es is valid enough in the limit $\theta \ll 1$. Notice that every term in the integral scale consistently in the limit $a \to 0$ and $k \to \infty$, which in turn implies that M scale with a[1]. Given $\mathcal{L}$, the Euler-Lagrange equations lead to

$$\frac{M}{a}\frac{\partial^2 u}{\partial t^2}-\frac{\kappa a^3}{\bar{\ell}^2}\frac{\partial^2 u}{\partial x^2}-\frac{8\kappa}{a\bar{\ell}^2}\bar{u}^2u+\frac{8\kappa}{a\bar{\ell}^2}u^3=0 \tag{5.4}$$

The Lagrangian which supports the above equation of motion is usually written as

$$\mathcal{L}=\frac{1}{2}\left(\frac{\partial\varphi}{\partial t}\right)^2-\frac{1}{4}(1-\varphi^2)^2$$

which is called a φ^4 model [123] and support multiple solutions. Considering the solutions in the φ^4, the equation (5.4) supports the trivial solution $u=0$, which is an unstable solution where the bars are in a vertical position. Additionally, there are two ordinary solutions $u=\pm\bar{u}$, for the two stables and degenerated solution. On the other hand, the non-trivial solution is obtained by considering the field at $u(x\to\pm\infty,t)=\pm\bar{u}$ and $u(x\to\mp\infty,t)=\pm\bar{u}$,

[1]This analysis is more clear by non-dimensionalizing the equations first.

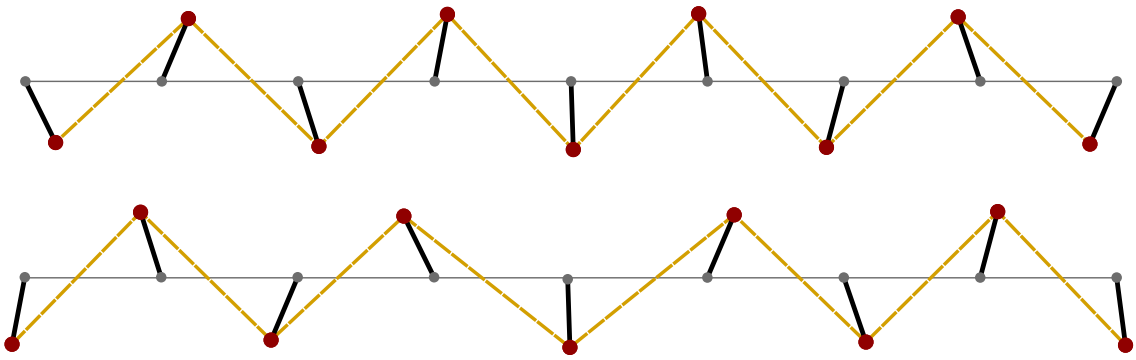

Fig. 5.2: *The figure shows the two solutions isostatic linkage chain non-linear wave, the kink solution(top) and the anti-kink solution(bottom)*

where the solutions are given by

$$u(x,t) = \pm\bar{u}\tanh\left[\frac{x - x_0 - vt}{\left(\frac{a^2}{2\bar{u}}\right)\sqrt{1-\frac{v^2}{c^2}}}\right]$$

which are called the *kink*(-) and *antikink*(+) solutions for the positive and negative sign(see Fig. 5.2), respectively, where $c = (a^2/\bar{\ell}\sqrt{\kappa/M})$ is the velocity of sound in the medium.

By introducing the kink solution in the potential energy density in eq. (5.3), a perfect square is obtained and therefore the kink solution propagates in the chain with zero energy. Remarkably, this solution propagates with smaller energy than the linear oscillations. In contrast, this does not apply to the antikink solution, which propagates with finite energy.

5.2 Hyperstatic Case

Knowing about the soliton in the isostatic chain, we wondered if it was possible to obtain a similar result in the hyperstatic one. However, here is not possible to take the rigid spring limit in all the springs, because the system will be completely static. Nonetheless, we can take this limit only in one spring per unit cell. Our first numerical simulations in this limit(see Fig. 5.3) showed a similar non-linear wave as in the linkage isostatic case. In this context, we did a similar theoretical analysis in the hyperstatic chain to understand the difference between both cases.

The discrete Lagrangian in a hyperstatic chain with two springs of elastic constant κ_1 and κ_2 is given by

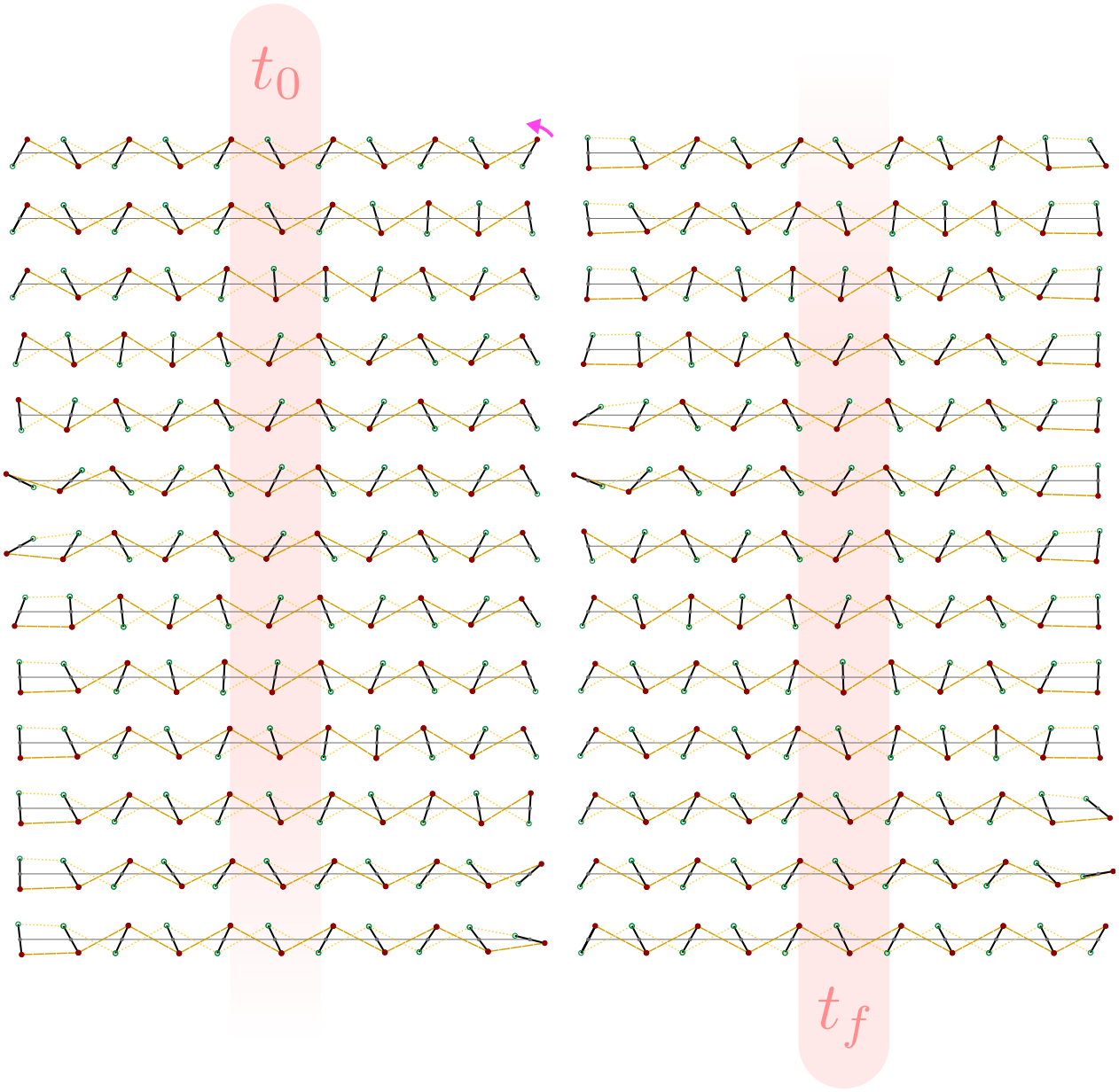

Fig. 5.3: *The figure shows the temporal evolution of the non-linear wave propagation in the hyperstatic chain, starting from the frame just under t_0 and ending at the frame just over t_f, following the highlight in the middle of the columns, where the left column continues at right column. The dashed thick lines represent the springs that become rigid bars, while the dashed thin lines represent the non-rigid springs.*

$$L = \sum_{i=1}^{n} \frac{Mr^2}{2} \left(\frac{d\theta_i}{dt}\right)^2 - \sum_{i=1}^{n-1} \frac{1}{2}\kappa_1 \left[\ell(\theta_i, \theta_{i+1}) - \bar{\ell}\right]^2 - \sum_{i=1}^{n-1} \frac{1}{2}\kappa_2 \left[\ell(\theta_{i+1}, \theta_i) - \bar{\ell}\right]^2$$
$$= L_{iso} - \sum_{i=1}^{n-1} \frac{1}{2}\kappa_2 \left[\ell(\theta_{i+1}, \theta_i) - \bar{\ell}\right]^2$$

Here the Lagrangian only differs from the isostatic one, L_{iso}, in the second potential energy term due to the extra spring. However, in this case, the rigid and the non-rigid spring are related geometrically. More specifically if κ_1 is the elastic constant of the rigid spring, in the limit $[\ell_{i,i+1} - \bar{\ell}]^2 \approx 0$, the extension in the remaining spring, $[\ell(\theta_{i+1}, \theta_i) - \bar{\ell}]^2$, can be written as

$$\frac{1}{2}\kappa_2(\ell(\theta_{i+1},\theta_i) - \bar{\ell})^2 = \frac{\kappa_2}{2}\left(-\bar{\ell} + \sqrt{\bar{\ell}^2 - (a - r\sin\theta_i + r\sin\theta_{i+1})^2 + (a - r\sin\theta_{i+1} + r\sin\theta_i)^2}\right)^2$$

$$= \frac{\kappa_2\bar{\ell}^2}{2}\left(-1 + \sqrt{1 - \frac{4ar(\sin\theta_{i+1} - \sin\theta_i)}{\bar{\ell}^2}}\right)^2$$
$$\approx 2\kappa_2\left(\frac{ar(\sin\theta_{i+1} - \sin\theta_i)}{\bar{\ell}}\right)^2$$

In this point, we can proceed similarly than in the isostatic case, where we consider $\theta_i \to \theta\left(x - \frac{a}{2}\right)$ y $\theta_{i+1} \to \theta\left(x + \frac{a}{2}\right)$, that implies that the contribution to potential energy density due to this new spring is given by

$$\begin{aligned} aV_2(\theta) &= \frac{2\kappa_2}{\bar{\ell}^2}\left(ar\left[\sin\theta\left(x + \frac{a}{2}\right) - \sin\theta\left(x - \frac{a}{2}\right)\right]\right)^2 \\ &= \frac{2\kappa_2}{\bar{\ell}^2}\left(a^2 r\cos\theta(x)\frac{\partial\theta}{\partial x}\right)^2 \\ &= \frac{2\kappa_2}{\bar{\ell}^2}\left(a^2\frac{du}{dx}\right)^2 \end{aligned}$$

Considering this contribution, in this case, the Lagrangian in the continuous limit would be similar to the one shown in the isostatic case but considering the contribution to the potential energy density of both springs, that is,

$$\begin{aligned} \mathcal{L} &= \int dx\,[T(\dot{u}) - V_1(u) - V_2(u)] \\ \mathcal{L} &= \int dx\left[\frac{M}{2a}\left(\frac{\partial u}{\partial t}\right)^2 - \frac{\tilde{\kappa}a^3}{2\bar{\ell}^2}\left(\frac{\partial u}{\partial x}\right)^2 - \frac{2\kappa_1}{a\bar{\ell}^2}(\bar{u}^2 - u^2)^2 - \frac{a\kappa_1}{\bar{\ell}^2}\frac{\partial u}{\partial x}(\bar{u}^2 - u^2)\right] \\ &= \int dx\left[\frac{M}{2a}\left(\frac{\partial u}{\partial t}\right)^2 - \frac{\tilde{\kappa}a^3}{2\bar{\ell}^2}\left(\frac{\partial u}{\partial x}\right)^2 - \frac{2\kappa_1}{a\bar{\ell}^2}(\bar{u}^2 - u^2)^2\right] - \int dx\left[\frac{a\kappa_1}{\bar{\ell}^2}\frac{\partial u}{\partial x}(\bar{u}^2 - u^2)\right] \end{aligned}$$

where $\tilde{\kappa} = \kappa_1 + 4\kappa_2$. From the above Lagrangian, the equation of motion is obtained

$$\frac{M}{a}\frac{\partial^2 u}{\partial t^2} - \frac{\tilde{\kappa} a^3}{\bar{\ell}^2}\frac{\partial^2 u}{\partial x^2} - \frac{8\kappa_1}{a\bar{\ell}^2}\bar{u}^2 u + \frac{8\kappa_1}{a\bar{\ell}^2}u^3 = 0$$

where the solution is similar to the one in the isostatic case:

$$u(x,t) = \pm\bar{u}\tanh\left[\frac{x - x_0 - vt}{\left(\frac{a^2}{2\bar{u}}\sqrt{\frac{\kappa_1}{\tilde{\kappa}}}\right)\sqrt{1 - \frac{v^2}{c^2}}}\right]$$

but in difference now both solutions, kink and anti-kink, have non-zero energy. The kink solution, which in the isostatic case propagates with zero energy, now propagates with an energy V_{kink} which to first order in κ_2 is given by

$$\frac{V_{kink}}{\kappa_1 a^2} = \frac{4\kappa_2}{3\bar{\ell}^2}\left[a^2 r^3 \sin^3\bar{\theta}\tanh(2\kappa_1 r\sin\bar{\theta})\right]\left[\tanh^2(2\kappa_1 r\sin\bar{\theta}) - 3\right]$$

Despite that this is finite energy, we are still interested in knowing if this energy propagates along the chain with smaller energy than the linear oscillations, which is our current work in this problem.

Chapter 6

Conclusions

In this thesis, we have studied if the topological zero-frequency modes, which were relegated to isostatic systems, can be extended in some manner to hyperstatic systems. Based on a recent model which describes topological soft modes in a particular hyperstatic system, we came across the limits of its scheme, but also we were able to generalize this scheme out of this regime, and we reach several new promising problems.

Our work in Chapter 4 allows us to build a system where the DOF number remains constant but the number of constrain can grow, in principle to infinity. This system supports topologically protected soft modes which are characterized by a topological invariant controlled by a single c value, that arises from a generalization of the topological invariant described in the single chain case. In this problem, there are several open questions to answer. We are still not sure how the number of chains is related to the decay length of the interface modes. Based on the results for a big number of chains which shows that the decay rates decrease as the number of chains increases, we conjecture that the mode at the interface may not be supported in the limit of an infinite number of chains

In addition, we have looking for new generalizations of this system and possible topological generalizations. For instance, we can consider several chains placed in the same line as in the multiple chain system, instead of coupling the chains with the same angle θ, we can consider that each chain has a different rotation ratio, and analyze under what condition similar modes can appear. On the other hand, we have been working in a possible localized mode near $c = -1$ for the regular hyperstatic chain, where the chain also supports ZM as in $c = 1$ and where our initial calculations suggest that in an interface between two different values c_L and c_R, where $c_L + c_L = -2$ the system also exhibit a localized mode. However, this problem still requires further analysis, a review of all the details and additional numerical simulations.

In the variable stiffness hyperstatic chain, a possible topological characterization for the encountered modes has been searched, since it also appears to be robust to geometrical changes in c if the elastic constant κ_L remains small enough. In principle, we could think that this eventual topological characterization should differentiate the different sets of c values for which the state is exponentially localized.

Finally in Chapter 5 we generalize the non-linear waves described in the isostatic chain in the limit of rigid springs, where in the hyperstatic case the analog is built by taking one rigid and one normal spring per unit cell. In difference to the isostatic case, where the system supports a zero-energy solution that propagates along the chain(the kink), in the hyperstatic case all the solutions have finite energy. We still have to verify if the kink solution in this case can propagate with an smaller energy than the required by the linear waves. If this is the case, this solution is still an interesting mode to take into account, despite that is not a zero-energy mode anymore.

In summary, our work has been fruitful, since we have been able to demonstrate that the topological phenomena that emerge from the zero energy modes in an isostatic system seem to extend to an hyperstatic chain and finite frequency modes. However, it is not yet clear whether there is any way to construct a more general theoretical framework that would allow us to study the topology more generically. What we can state without a doubt is that if we look for the effects that emerge as reminiscent of zero-energy modes in hyperstatic systems, they will inevitably be associated with rectangular equilibrium and compatibility matrices, and therefore it is inevitable to take into account the topology of these matrices, as we did in the generalization of the hyperstatic chain.

Bibliography

[1] Mikio Nakahara. *Geometry, Topology, and Physics*. 2nd ed. Graduate Student Series in Physics. Bristol ; Philadelphia: Institute of Physics Publishing, 2003. 573 pp. ISBN: 978-0-7503-0606-5 (cit. on pp. 1, 2).

[2] James R. Munkres. *Topology*. 2nd ed. Upper Saddle River, NJ: Prentice Hall, Inc, 2000. 537 pp. ISBN: 978-0-13-181629-9 (cit. on pp. 1–3).

[3] Christopher T. J. Dodson and Phillip E. Parker. *A User's Guide to Algebraic Topology*. eng. Mathematics and Its Applications 387. Dordrecht: Kluwer Academic Publishers, 1997. 405 pp. ISBN: 978-0-7923-4293-9 978-0-7923-4292-2 (cit. on pp. 1, 38, 48).

[4] János K. Asbóth, László Oroszlány, and András Pályi. *A Short Course on Topological Insulators*. en. Vol. 919. Lecture Notes in Physics. Cham: Springer International Publishing, 2016. DOI: 10.1007/978-3-319-25607-8 (cit. on pp. 1, 5, 8).

[5] M. Z. Hasan and C. L. Kane. "*Colloquium* : Topological Insulators". en. In: *Reviews of Modern Physics* 82.4 (2010), pp. 3045–3067. DOI: 10.1103/RevModPhys.82.3045 (cit. on pp. 1, 4, 5, 23).

[6] R. Shankar. *Topological Insulators – A Review*. en. 2018. arXiv: 1804.06471 [cond-mat]. preprint (cit. on pp. 1, 23).

[7] Andreas W W Ludwig. "Topological Phases: Classification of Topological Insulators and Superconductors of Non-Interacting Fermions, and Beyond". en. In: *Physica Scripta* T168 (2016), p. 014001. DOI: 10.1088/0031-8949/2015/T168/014001 (cit. on p. 1).

[8] Ching-Kai Chiu, Jeffrey C. Y. Teo, Andreas P. Schnyder, and Shinsei Ryu. "Classification of Topological Quantum Matter with Symmetries". en. In: *Reviews of Modern Physics* 88.3 (2016), p. 035005. DOI: 10.1103/RevModPhys.88.035005 (cit. on pp. 1, 23).

[9] Shinsei Ryu, Andreas P Schnyder, Akira Furusaki, and Andreas W W Ludwig. "Topological Insulators and Superconductors: Tenfold Way and Dimensional Hierarchy". en. In: *New Journal of Physics* 12.6 (2010), p. 065010. DOI: 10.1088/1367-2630/12/6/065010 (cit. on pp. 1, 23).

[10] Muamer Kadic, Tiemo Bückmann, Robert Schittny, and Martin Wegener. "Metamaterials beyond Electromagnetism". In: *Reports on Progress in Physics* 76.12 (2013), p. 126501. DOI: 10.1088/0034-4885/76/12/126501 (cit. on pp. 1, 10, 12).

[11] Pierre A. Deymier, ed. *Acoustic Metamaterials and Phononic Crystals*. en. Vol. 173. Springer Series in Solid-State Sciences. Berlin, Heidelberg: Springer Berlin Heidelberg, 2013. DOI: 10.1007/978-3-642-31232-8 (cit. on pp. 1, 11).

[12] Arthur R. McGurn. *Introduction to Photonic and Phononic Crystals and Metamaterials*. en. Synthesis Lectures on Materials and Optics. Cham: Springer International Publishing, 2020. DOI: 10.1007/978-3-031-02384-2 (cit. on p. 1).

[13] Emilio Barchiesi, Mario Spagnuolo, and Luca Placidi. "Mechanical Metamaterials: A State of the Art". en. In: *Mathematics and Mechanics of Solids* 24.1 (2019), pp. 212–234. DOI: 10.1177/1081286517735695 (cit. on pp. 1, 10, 12).

[14] Sebastian D. Huber. "Topological Mechanics". en. In: *Nature Physics* 12.7 (2016), pp. 621–623. DOI: 10.1038/nphys3801 (cit. on pp. 1, 10, 12, 14, 21).

[15] Xiaoming Mao and Tom C. Lubensky. "Maxwell Lattices and Topological Mechanics". en. In: *Annual Review of Condensed Matter Physics* 9.1 (2018), pp. 413–433. DOI: 10/gc4nh9 (cit. on pp. 1, 10, 14, 19, 26, 32).

[16] Li Xin, Yu Siyuan, Liu Harry, Lu Minghui, and Chen Yanfeng. "Topological Mechanical Metamaterials: A Brief Review". en. In: *Current Opinion in Solid State and Materials Science* 24.5 (2020), p. 100853. DOI: 10.1016/j.cossms.2020.100853 (cit. on pp. 1, 10, 12, 14).

[17] Shengjie Zheng, Guiju Duan, and Baizhan Xia. "Progress in Topological Mechanics". en. In: *Applied Sciences* 12.4 (2022), p. 1987. DOI: 10.3390/app12041987 (cit. on pp. 1, 10, 12, 14).

[18] Guancong Ma, Meng Xiao, and C. T. Chan. "Topological Phases in Acoustic and Mechanical Systems". en. In: *Nature Reviews Physics* 1.4 (2019), pp. 281–294. DOI: 10.1038/s42254-019-0030-x (cit. on pp. 1, 10, 14).

[19] Paul Renteln and Alan Dundes. "Foolproof: A Sampling of Mathematical Folk Humor". en. In: 52.1 (2005) (cit. on p. 3).

[20] K. V. Klitzing, G. Dorda, and M. Pepper. "New Method for High-Accuracy Determination of the Fine-Structure Constant Based on Quantized Hall Resistance". en. In: *Physical Review Letters* 45.6 (1980), pp. 494–497. DOI: 10.1103/PhysRevLett.45.494 (cit. on p. 4).

[21] Richard E. Prange and Steven M. Girvin, eds. *The Quantum Hall Effect*. Red. by Joseph L. Birman, H. Faissner, and Jeffrey W. Lynn. Graduate Texts in Contemporary Physics. New York, NY: Springer New York, 1990. DOI: 10.1007/978-1-4612-3350-3 (cit. on pp. 4, 5, 10).

[22] D. J. Thouless, M. Kohmoto, M. P. Nightingale, and M. Den Nijs. "Quantized Hall Conductance in a Two-Dimensional Periodic Potential". en. In: *Physical Review Letters* 49.6 (1982), pp. 405–408. DOI: 10.1103/PhysRevLett.49.405 (cit. on p. 4).

[23] Marvin E. Cage, Ronald F. Dziuba, and Bruce F. Field. "A Test of the Quantum Hall Effect as a Resistance Standard". In: *IEEE Transactions on Instrumentation and Measurement* IM-34.2 (1985), pp. 301–303. DOI: 10.1109/TIM.1985.4315329 (cit. on p. 5).

[24] W. P. Su, J. R. Schrieffer, and A. J. Heeger. "Solitons in Polyacetylene". en. In: *Physical Review Letters* 42.25 (1979), pp. 1698–1701. DOI: 10.1103/PhysRevLett.42.1698 (cit. on p. 6).

[25] Alexei Kitaev, Vladimir Lebedev, and Mikhail Feigel'man. "Periodic Table for Topological Insulators and Superconductors". en. In: *AIP Conference Proceedings*. Advances in Theoretical Physics: Landau Memorial Conference. Chernogolokova (Russia): AIP, 2009, pp. 22–30. DOI: 10.1063/1.3149495 (cit. on pp. 10, 23, 37).

[26] Joel E. Moore. "The Birth of Topological Insulators". en. In: *Nature* 464.7286 (2010), pp. 194–198. DOI: 10.1038/nature08916 (cit. on p. 10).

[27] Sławomir P. Łepkowski. "Advances in Topological Materials: Fundamentals, Challenges and Outlook". en. In: *Nanomaterials* 12.19 (2022), p. 3522. DOI: 10.3390/nano12193522 (cit. on p. 10).

[28] Vanda M. Pereira et al. "Challenges of Topological Insulator Research: Bi $_2$ Te $_3$ Thin Films and Magnetic Heterostructures". en. In: *physica status solidi (b)* 258.1 (2021), p. 2000346. DOI: 10.1002/pssb.202000346 (cit. on p. 10).

[29] Ling Lu, John D. Joannopoulos, and Marin Soljačić. "Topological Photonics". en. In: *Nature Photonics* 8.11 (2014), pp. 821–829. DOI: 10.1038/nphoton.2014.248 (cit. on p. 10).

[30] Daria Smirnova, Daniel Leykam, Yidong Chong, and Yuri Kivshar. "Nonlinear Topological Photonics". en. In: *Applied Physics Reviews* 7.2 (2020), p. 021306. DOI: 10.1063/1.5142397 (cit. on p. 10).

[31] Tomoki Ozawa et al. "Topological Photonics". In: *Reviews of Modern Physics* 91.1 (2019), p. 015006. DOI: 10.1103/RevModPhys.91.015006 (cit. on p. 10).

[32] Jinwoong Cha, Kun Woo Kim, and Chiara Daraio. "Experimental Realization of On-Chip Topological Nanoelectromechanical Metamaterials". en. In: *Nature* 564.7735 (2018), pp. 229–233. DOI: 10.1038/s41586-018-0764-0 (cit. on pp. 10, 14).

[33] Ze-Guo Chen and Ying Wu. "Tunable Topological Phononic Crystals". en. In: *Physical Review Applied* 5.5 (2016), p. 054021. DOI: 10.1103/PhysRevApplied.5.054021 (cit. on pp. 10, 14).

[34] Yingjie Chen, Bin Wu, Jian Li, Stephan Rudykh, and Weiqiu Chen. "Low-Frequency Tunable Topological Interface States in Soft Phononic Crystal Cylinders". en. In: *International Journal of Mechanical Sciences* 191 (2021), p. 106098. DOI: 10.1016/j.ijmecsci.2020.106098 (cit. on pp. 10, 14).

[35] Sai Sanjit Ganti, Ting-Wei Liu, and Fabio Semperlotti. "Topological Edge States in Phononic Plates with Embedded Acoustic Black Holes". en. In: *Journal of Sound and Vibration* 466 (2020), p. 115060. DOI: 10.1016/j.jsv.2019.115060 (cit. on pp. 10, 14).

[36] Nan Gao, Sichao Qu, Liang Si, Jiao Wang, and Weiqiu Chen. "Broadband Topological Valley Transport of Elastic Wave in Reconfigurable Phononic Crystal Plate". en. In: *Applied Physics Letters* 118.6 (2021), p. 063502. DOI: 10.1063/5.0036840 (cit. on pp. 10, 14).

[37] Yilan Huang, Yang Huang, Weiqiu Chen, and Ronghao Bao. "Flexible Manipulation of Topologically Protected Waves in One-Dimensional Soft Periodic Plates". en. In: *International Journal of Mechanical Sciences* 170 (2020), p. 105348. DOI: 10.1016/j.ijmecsci.2019.105348 (cit. on pp. 10, 14).

[38] Hongbo Huang, Zhuhua Tan, Shaoyong Huo, Luyang Feng, Jiujiu Chen, and Xu Han. "Topologically Protected Zero Refraction of Elastic Waves in Pseudospin-Hall Phononic Crystals". en. In: *Communications Physics* 3.1 (2020), p. 46. DOI: 10.1038/s42005-020-0314-6 (cit. on pp. 10, 14).

[39] Hongbo Huang, Shaoyong Huo, and Jiujiu Chen. "Subwavelength Elastic Topological Negative Refraction in Ternary Locally Resonant Phononic Crystals". en. In: *International Journal of Mechanical Sciences* 198 (2021), p. 106391. DOI: 10.1016/j.ijmecsci.2021.106391 (cit. on pp. 10, 14).

[40] Shao-yong Huo, Jiu-jiu Chen, Hong-bo Huang, Yong-jian Wei, Zhu-hua Tan, Lu-yang Feng, and Xiao-ping Xie. "Experimental Demonstration of Valley-Protected Backscattering Suppression and Interlayer Topological Transport for Elastic Wave in Three-Dimensional Phononic Crystals". en. In: *Mechanical Systems and Signal Processing* 154 (2021), p. 107543. DOI: 10.1016/j.ymssp.2020.107543 (cit. on pp. 10, 14).

[41] Yabin Jin, Wan Wang, Zhihui Wen, Daniel Torrent, and Bahram Djafari-Rouhani. "Topological States in Twisted Pillared Phononic Plates". en. In: *Extreme Mechanics Letters* 39 (2020), p. 100777. DOI: 10.1016/j.eml.2020.100777 (cit. on pp. 10, 14).

[42] S. Hossein Mousavi, Alexander B. Khanikaev, and Zheng Wang. "Topologically Protected Elastic Waves in Phononic Metamaterials". en. In: *Nature Communications* 6.1 (2015), p. 8682. DOI: 10.1038/ncomms9682 (cit. on pp. 10, 14).

[43] Muhammad, Weijian Zhou, and C.W. Lim. "Topological Edge Modeling and Localization of Protected Interface Modes in 1D Phononic Crystals for Longitudinal and Bending Elastic Waves". en. In: *International Journal of Mechanical Sciences* 159 (2019), pp. 359–372. DOI: 10.1016/j.ijmecsci.2019.05.020 (cit. on pp. 10, 14).

[44] D. Zeb Rocklin, Shangnan Zhou, Kai Sun, and Xiaoming Mao. "Transformable Topological Mechanical Metamaterials". en. In: *Nature Communications* 8.1 (1 2017), p. 14201. DOI: 10.1038/ncomms14201 (cit. on pp. 10, 14).

[45] Olaf Stenull, C. L. Kane, and T. C. Lubensky. "Topological Phonons and Weyl Lines in Three Dimensions". In: *Physical Review Letters* 117.6 (2016), p. 068001. DOI: 10.1103/PhysRevLett.117.068001 (cit. on pp. 10, 14).

[46] Roman Süsstrunk and Sebastian D. Huber. "Observation of Phononic Helical Edge States in a Mechanical Topological Insulator". In: *Science* 349.6243 (2015), pp. 47–50. DOI: 10.1126/science.aab0239 (cit. on pp. 10, 14).

[47] Roman Süsstrunk and Sebastian D. Huber. "Classification of Topological Phonons in Linear Mechanical Metamaterials". en. In: *Proceedings of the National Academy of Sciences* 113.33 (2016). DOI: 10.1073/pnas.1605462113 (cit. on pp. 10, 14, 21, 23).

[48] Pai Wang, Ling Lu, and Katia Bertoldi. "Topological Phononic Crystals with One-Way Elastic Edge Waves". en. In: *Physical Review Letters* 115.10 (2015), p. 104302. DOI: 10.1103/PhysRevLett.115.104302 (cit. on pp. 10, 11, 13, 14, 21, 24).

[49] Wei Wang, Bernard Bonello, Bahram Djafari-Rouhani, and Yan Pennec. "Topological Valley, Pseudospin, and Pseudospin-Valley Protected Edge States in Symmetric Pillared Phononic Crystals". en. In: *Physical Review B* 100.14 (2019), p. 140101. DOI: 10.1103/PhysRevB.100.140101 (cit. on pp. 10, 14).

[50] Zhen Wang and Qi Wei. “An Elastic Higher-Order Topological Insulator Based on Kagome Phononic Crystals”. en. In: *Journal of Applied Physics* 129.3 (2021), p. 035102. DOI: 10.1063/5.0031377 (cit. on pp. 10, 14).

[51] Meng Xiao, Guancong Ma, Zhiyu Yang, Ping Sheng, Z. Q. Zhang, and C. T. Chan. “Geometric Phase and Band Inversion in Periodic Acoustic Systems”. en. In: *Nature Physics* 11.3 (2015), pp. 240–244. DOI: 10.1038/nphys3228 (cit. on pp. 10, 14).

[52] Zhan Xiong, Hai-Xiao Wang, Hao Ge, Jinjie Shi, Jie Luo, Yun Lai, Ming-Hui Lu, and Jian-Hua Jiang. “Topological Node Lines in Mechanical Metacrystals”. en. In: *Physical Review B* 97.18 (2018), p. 180101. DOI: 10.1103/PhysRevB.97.180101 (cit. on pp. 10, 14).

[53] Jianfei Yin, Massimo Ruzzene, Jihong Wen, Dianlong Yu, Li Cai, and Linfeng Yue. “Band Transition and Topological Interface Modes in 1D Elastic Phononic Crystals”. en. In: *Scientific Reports* 8.1 (2018), p. 6806. DOI: 10.1038/s41598-018-24952-5 (cit. on pp. 10, 14).

[54] Si-Yuan Yu, Cheng He, Zhen Wang, Fu-Kang Liu, Xiao-Chen Sun, Zheng Li, Hai-Zhou Lu, Ming-Hui Lu, Xiao-Ping Liu, and Yan-Feng Chen. “Elastic Pseudospin Transport for Integratable Topological Phononic Circuits”. en. In: *Nature Communications* 9.1 (2018), p. 3072. DOI: 10.1038/s41467-018-05461-5 (cit. on pp. 10, 14).

[55] Ziqi Yu, Zongqing Ren, and Jaeho Lee. “Phononic Topological Insulators Based on Six-Petal Holey Silicon Structures”. en. In: *Scientific Reports* 9.1 (2019), p. 1805. DOI: 10.1038/s41598-018-38387-5 (cit. on pp. 10, 14).

[56] Hongbo Zhang, Bilong Liu, Xilong Zhang, Qianqian Wu, and Xingang Wang. “Zone Folding Induced Tunable Topological Interface States in One-Dimensional Phononic Crystal Plates”. en. In: *Physics Letters A* 383.23 (2019), pp. 2797–2801. DOI: 10.1016/j.physleta.2019.05.045 (cit. on pp. 10, 14).

[57] Jiaming Zhao, Shaoyong Huo, Hongbo Huang, and Jiujiu Chen. “Topological Interface States of Shear Horizontal Guided Wave in One-Dimensional Phononic Quasicrystal Slabs”. en. In: *physica status solidi (RRL) - Rapid Research Letters* 12.10 (2018), p. 1800322. DOI: 10.1002/pssr.201800322 (cit. on pp. 10, 14).

[58] Cheng He, Hua-Shan Lai, Bo He, Si-Yuan Yu, Xiangyuan Xu, Ming-Hui Lu, and Yan-Feng Chen. “Acoustic Analogues of Three-Dimensional Topological Insulators”. en. In: *Nature Communications* 11.1 (2020), p. 2318. DOI: 10.1038/s41467-020-16131-w (cit. on pp. 10, 14).

[59] Lisa M. Nash, Dustin Kleckner, Alismari Read, Vincenzo Vitelli, Ari M. Turner, and William T. M. Irvine. “Topological Mechanics of Gyroscopic Metamaterials”. en. In: *Proceedings of the National Academy of Sciences* 112.47 (2015), pp. 14495–14500. DOI: 10.1073/pnas.1507413112. arXiv: 1504.03362 [cond-mat] (cit. on pp. 10, 14, 21, 24).

[60] Xu Ni, Cheng He, Xiao-Chen Sun, Xiao-ping Liu, Ming-Hui Lu, Liang Feng, and Yan-Feng Chen. “Topologically Protected One-Way Edge Mode in Networks of Acoustic Resonators with Circulating Air Flow”. In: *New Journal of Physics* 17.5 (2015), p. 053016. DOI: 10.1088/1367-2630/17/5/053016 (cit. on pp. 10, 14).

[61] D. Zeb Rocklin, Bryan Gin–ge Chen, Martin Falk, Vincenzo Vitelli, and T. C. Lubensky. "Mechanical Weyl Modes in Topological Maxwell Lattices". In: *Physical Review Letters* 116.13 (2016), p. 135503. DOI: 10.1103/PhysRevLett.116.135503 (cit. on pp. 10, 14).

[62] Zhaoju Yang, Fei Gao, Xihang Shi, Xiao Lin, Zhen Gao, Yidong Chong, and Baile Zhang. "Topological Acoustics". en. In: *Physical Review Letters* 114.11 (2015), p. 114301. DOI: 10.1103/PhysRevLett.114.114301 (cit. on pp. 10, 12, 14).

[63] Zhiwang Zhang, Qi Wei, Ying Cheng, Ting Zhang, Dajian Wu, and Xiaojun Liu. "Topological Creation of Acoustic Pseudospin Multipoles in a Flow-Free Symmetry-Broken Metamaterial Lattice". en. In: *Physical Review Letters* 118.8 (2017), p. 084303. DOI: 10.1103/PhysRevLett.118.084303 (cit. on pp. 10, 14).

[64] Xiujuan Zhang, Meng Xiao, Ying Cheng, Ming-Hui Lu, and Johan Christensen. "Topological Sound". en. In: *Communications Physics* 1.1 (2018), p. 97. DOI: 10.1038/s42005-018-0094-4 (cit. on pp. 10, 12, 14).

[65] Hasan Al Ba'ba'a, Kunhao Yu, and Qiming Wang. "Elastically-Supported Lattices for Tunable Mechanical Topological Insulators". en. In: *Extreme Mechanics Letters* 38 (2020), p. 100758. DOI: 10.1016/j.eml.2020.100758 (cit. on pp. 10, 14).

[66] Bryan Gin-ge Chen, Nitin Upadhyaya, and Vincenzo Vitelli. "Nonlinear Conduction via Solitons in a Topological Mechanical Insulator". en. In: *Proceedings of the National Academy of Sciences* 111.36 (2014), pp. 13004–13009. DOI: 10.1073/pnas.1405969111 (cit. on pp. 10, 12, 14, 59).

[67] Bryan Gin-ge Chen, Bin Liu, Arthur A. Evans, Jayson Paulose, Itai Cohen, Vincenzo Vitelli, and C. D. Santangelo. "Topological Mechanics of Origami and Kirigami". In: *Physical Review Letters* 116.13 (2016), p. 135501. DOI: 10.1103/PhysRevLett.116.135501 (cit. on pp. 10, 14).

[68] H. Chen, H. Nassar, and G. L. Huang. "A Study of Topological Effects in 1D and 2D Mechanical Lattices". en. In: *Journal of the Mechanics and Physics of Solids* 117 (2018), pp. 22–36. DOI: 10.1016/j.jmps.2018.04.013 (cit. on pp. 10, 14).

[69] Yi Chen, Xiaoning Liu, and Gengkai Hu. "Topological Phase Transition in Mechanical Honeycomb Lattice". en. In: *Journal of the Mechanics and Physics of Solids* 122 (2019), pp. 54–68. DOI: 10.1016/j.jmps.2018.08.021 (cit. on pp. 10, 14).

[70] Ananya Ghatak, Martin Brandenbourger, Jasper Van Wezel, and Corentin Coulais. "Observation of Non-Hermitian Topology and Its Bulk–Edge Correspondence in an Active Mechanical Metamaterial". en. In: *Proceedings of the National Academy of Sciences* 117.47 (2020), pp. 29561–29568. DOI: 10.1073/pnas.2010580117 (cit. on pp. 10, 14).

[71] Yabin Jin, Wan Wang, and Bahram Djafari-Rouhani. "Asymmetric Topological State in an Elastic Beam Based on Symmetry Principle". en. In: *International Journal of Mechanical Sciences* 186 (2020), p. 105897. DOI: 10.1016/j.ijmecsci.2020.105897 (cit. on pp. 10, 14).

[72] C. L. Kane and T. C. Lubensky. "Topological Boundary Modes in Isostatic Lattices". en. In: *Nature Physics* 10.1 (2014), pp. 39–45. DOI: 10.1038/nphys2835. arXiv: 1308.0554 [cond-mat] (cit. on pp. 10, 13, 14, 25, 26, 33).

[73] Hridesh Kedia, Anton Souslov, and D. Zeb Rocklin. "Soft Topological Modes Protected by Symmetry in Rigid Mechanical Metamaterials". In: *Physical Review B* 103.6 (2021), p. L060104. DOI: 10.1103/PhysRevB.103.L060104 (cit. on pp. 10, 14, 34, 38, 41, 43).

[74] Bin Liu, Jesse L. Silverberg, Arthur A. Evans, Christian D. Santangelo, Robert J. Lang, Thomas C. Hull, and Itai Cohen. "Topological Kinematics of Origami Metamaterials". en. In: *Nature Physics* 14.8 (8 2018), pp. 811–815. DOI: 10.1038/s41567-018-0150-8 (cit. on pp. 10, 14).

[75] Yijie Liu, Liang Jin, Hongfa Wang, Dongying Liu, and Yingjing Liang. "Topological Interface States in Translational Metamaterials for Sub-Wavelength in-Plane Waves". en. In: *International Journal of Mechanical Sciences* 197 (2021), p. 106308. DOI: 10.1016/j.ijmecsci.2021.106308 (cit. on pp. 10, 14).

[76] Anne S. Meeussen, Jayson Paulose, and Vincenzo Vitelli. "Geared Topological Metamaterials with Tunable Mechanical Stability". In: *Physical Review X* 6.4 (2016), p. 041029. DOI: 10.1103/PhysRevX.6.041029 (cit. on pp. 10, 14).

[77] Jayson Paulose, Bryan Gin-ge Chen, and Vincenzo Vitelli. "Topological Modes Bound to Dislocations in Mechanical Metamaterials". en. In: *Nature Physics* 11.2 (2 2015), pp. 153–156. DOI: 10.1038/nphys3185 (cit. on pp. 10, 14).

[78] Emil Prodan and Camelia Prodan. "Topological Phonon Modes and Their Role in Dynamic Instability of Microtubules". In: *Physical Review Letters* 103.24 (2009), p. 248101. DOI: 10.1103/PhysRevLett.103.248101 (cit. on pp. 10, 12, 14).

[79] K. Roychowdhury, D.Z. Rocklin, and M.J. Lawler. "Topology and Geometry of Spin Origami". English. In: *Physical Review Letters* 121.17 (2018). DOI: 10.1103/PhysRevLett.121.177201 (cit. on pp. 10, 14, 37).

[80] Lea Sirota, Roni Ilan, Yair Shokef, and Yoav Lahini. "Non-Newtonian Topological Mechanical Metamaterials Using Feedback Control". en. In: *Physical Review Letters* 125.25 (2020), p. 256802. DOI: 10.1103/PhysRevLett.125.256802 (cit. on pp. 10, 14).

[81] Yao-Ting Wang, Pi-Gang Luan, and Shuang Zhang. "Coriolis Force Induced Topological Order for Classical Mechanical Vibrations". In: *New Journal of Physics* 17.7 (2015), p. 073031. DOI: 10.1088/1367-2630/17/7/073031 (cit. on pp. 10, 14).

[82] Wei Wang, Yabin Jin, Wan Wang, Bernard Bonello, Bahram Djafari-Rouhani, and Romain Fleury. "Robust Fano Resonance in a Topological Mechanical Beam". en. In: *Physical Review B* 101.2 (2020), p. 024101. DOI: 10.1103/PhysRevB.101.024101 (cit. on pp. 10, 14).

[83] Li-Yang Zheng, Georgios Theocharis, Vincent Tournat, and Vitalyi Gusev. "Quasitopological Rotational Waves in Mechanical Granular Graphene". en. In: *Physical Review B* 97.6 (2018), p. 060101. DOI: 10.1103/PhysRevB.97.060101 (cit. on pp. 10, 14).

[84] Yujie Zhou, Bryan Gin-ge Chen, Nitin Upadhyaya, and Vincenzo Vitelli. "Kink-Antikink Asymmetry and Impurity Interactions in Topological Mechanical Chains". en. In: *Physical Review E* 95.2 (2017), p. 022202. DOI: 10.1103/PhysRevE.95.022202. arXiv: 1608.02127 [cond-mat] (cit. on pp. 10, 12, 14).

[85] Steven A. Cummer, Johan Christensen, and Andrea Alù. "Controlling Sound with Acoustic Metamaterials". en. In: *Nature Reviews Materials* 1.3 (2016), p. 16001. DOI: 10.1038/natrevmats.2016.1 (cit. on p. 10).

[86] Xianglong Yu, Ji Zhou, Haiyi Liang, Zhengyi Jiang, and Lingling Wu. "Mechanical Metamaterials Associated with Stiffness, Rigidity and Compressibility: A Brief Review". en. In: *Progress in Materials Science* 94 (2018), pp. 114–173. DOI: 10.1016/j.pmatsci.2017.12.003 (cit. on pp. 10, 12).

[87] James Utama Surjadi, Libo Gao, Huifeng Du, Xiang Li, Xiang Xiong, Nicholas Xuanlai Fang, and Yang Lu. "Mechanical Metamaterials and Their Engineering Applications". en. In: *Advanced Engineering Materials* 21.3 (2019), p. 1800864. DOI: 10.1002/adem.201800864 (cit. on p. 10).

[88] Mahmoud I. Hussein, Michael J. Leamy, and Massimo Ruzzene. "Dynamics of Phononic Materials and Structures: Historical Origins, Recent Progress, and Future Outlook". en. In: *Applied Mechanics Reviews* 66.4 (2014), p. 040802. DOI: 10.1115/1.4026911 (cit. on pp. 10, 11).

[89] Katia Bertoldi, Pedro M. Reis, Stephen Willshaw, and Tom Mullin. "Negative Poisson's Ratio Behavior Induced by an Elastic Instability". In: *Advanced Materials* 22.3 (2010), pp. 361–366. DOI: 10.1002/adma.200901956 (cit. on pp. 11, 12).

[90] T. A. Schaedler, A. J. Jacobsen, A. Torrents, A. E. Sorensen, J. Lian, J. R. Greer, L. Valdevit, and W. B. Carter. "Ultralight Metallic Microlattices". en. In: *Science* 334.6058 (2011), pp. 962–965. DOI: 10.1126/science.1211649 (cit. on p. 11).

[91] M. Thota and K. W. Wang. "Reconfigurable Origami Sonic Barriers with Tunable Bandgaps for Traffic Noise Mitigation". en. In: *Journal of Applied Physics* 122.15 (2017), p. 154901. DOI: 10.1063/1.4991026 (cit. on p. 11).

[92] Xin Ren, Raj Das, Phuong Tran, Tuan Duc Ngo, and Yi Min Xie. "Auxetic Metamaterials and Structures: A Review". In: *Smart Materials and Structures* 27.2 (2018), p. 023001. DOI: 10.1088/1361-665X/aaa61c (cit. on p. 11).

[93] Dong Han, Xin Ren, Yi Zhang, Xiang Yu Zhang, Xue Gang Zhang, Chen Luo, and Yi Min Xie. "Lightweight Auxetic Metamaterials: Design and Characteristic Study". en. In: *Composite Structures* 293 (2022), p. 115706. DOI: 10.1016/j.compstruct.2022.115706 (cit. on p. 11).

[94] Daniel Acuna, Francisco Gutiérrez, Rodrigo Silva, Humberto Palza, Alvaro S. Nunez, and Gustavo Düring. "A Three Step Recipe for Designing Auxetic Materials on Demand". en. In: *Communications Physics* 5.1 (2022), p. 113. DOI: 10.1038/s42005-022-00876-5 (cit. on p. 11).

[95] Andrew L. Goodwin, David A. Keen, and Matthew G. Tucker. "Large Negative Linear Compressibility of $Ag_3[Co(CN)_6]$". en. In: *Proceedings of the National Academy of Sciences* 105.48 (2008), pp. 18708–18713. DOI: 10.1073/pnas.0804789105 (cit. on p. 11).

[96] Matthias Mecklenburg, Arnim Schuchardt, Yogendra Kumar Mishra, Sören Kaps, Rainer Adelung, Andriy Lotnyk, Lorenz Kienle, and Karl Schulte. "Aerographite: Ultra Lightweight, Flexible Nanowall, Carbon Microtube Material with Outstanding Mechanical Performance". en. In: *Advanced Materials* 24.26 (2012), pp. 3486–3490. DOI: 10.1002/adma.201200491 (cit. on p. 11).

[97] Liuxian Zhao, Eitan Laredo, Olivia Ryan, Amirhossein Yazdkhasti, Hyun-Tae Kim, Randy Ganye, Timothy Horiuchi, and Miao Yu. "Ultrasound Beam Steering with Flattened Acoustic Metamaterial Luneburg Lens". In: *Applied Physics Letters* 116.7 (2020), p. 071902. DOI: 10.1063/1.5140467 (cit. on p. 11).

[98] Guancong Ma and Ping Sheng. "Acoustic Metamaterials: From Local Resonances to Broad Horizons". In: *Science Advances* 2.2 (2016), e1501595. DOI: 10.1126/sciadv.1501595 (cit. on p. 11).

[99] Yan-Feng Wang, Ting-Ting Wang, Jin-Ping Liu, Yue-Sheng Wang, and Vincent Laude. "Guiding and Splitting Lamb Waves in Coupled-Resonator Elastic Waveguides". en. In: *Composite Structures* 206 (2018), pp. 588–593. DOI: 10.1016/j.compstruct.2018.08.088 (cit. on p. 11).

[100] Bogdan-Ioan Popa, Lucian Zigoneanu, and Steven A. Cummer. "Experimental Acoustic Ground Cloak in Air". In: *Physical Review Letters* 106.25 (2011), p. 253901. DOI: 10.1103/PhysRevLett.106.253901 (cit. on p. 11).

[101] Ying Cheng, Fan Yang, Jian Yi Xu, and Xiao Jun Liu. "A Multilayer Structured Acoustic Cloak with Homogeneous Isotropic Materials". In: *Applied Physics Letters* 92.15 (2008), p. 151913. DOI: 10.1063/1.2903500 (cit. on p. 11).

[102] Peng Yang, Jingzhi Wu, Rongrong Zhao, and Jianning Han. "Research on Local Sound Field Control Technology Based on Acoustic Metamaterial Triode Structure". en. In: *Crystals* 10.3 (3 2020), p. 204. DOI: 10.3390/cryst10030204 (cit. on p. 11).

[103] Lingling Wu, Yong Wang, Zirui Zhai, Yi Yang, Deepakshyam Krishnaraju, Junqiang Lu, Fugen Wu, Qianxuan Wang, and Hanqing Jiang. "Mechanical Metamaterials for Full-Band Mechanical Wave Shielding". en. In: *Applied Materials Today* 20 (2020), p. 100671. DOI: 10.1016/j.apmt.2020.100671 (cit. on p. 11).

[104] Xin Fang, Jihong Wen, Bernard Bonello, Jianfei Yin, and Dianlong Yu. "Ultra-Low and Ultra-Broad-Band Nonlinear Acoustic Metamaterials". en. In: *Nature Communications* 8.1 (1 2017), p. 1288. DOI: 10.1038/s41467-017-00671-9 (cit. on p. 11).

[105] Ganesh U. Patil and Kathryn H. Matlack. "Review of Exploiting Nonlinearity in Phononic Materials to Enable Nonlinear Wave Responses". en. In: *Acta Mechanica* 233.1 (2022), pp. 1–46. DOI: 10.1007/s00707-021-03089-z (cit. on p. 12).

[106] Claudio Findeisen, Jörg Hohe, Muamer Kadic, and Peter Gumbsch. "Characteristics of Mechanical Metamaterials Based on Buckling Elements". en. In: *Journal of the Mechanics and Physics of Solids* 102 (2017), pp. 151–164. DOI: 10.1016/j.jmps.2017.02.011 (cit. on p. 12).

[107] Bolei Deng, Jian Li, Vincent Tournat, Prashant K. Purohit, and Katia Bertoldi. "Dynamics of Mechanical Metamaterials: A Framework to Connect Phonons, Nonlinear Periodic Waves and Solitons". en. In: *Journal of the Mechanics and Physics of Solids* 147 (2021), p. 104233. DOI: 10.1016/j.jmps.2020.104233 (cit. on p. 12).

[108] R Chaunsali, E Kim, A Thakkar, PG Kevrekidis, and J Yang. "Demonstrating an In Situ Topological Band Transition in Cylindrical Granular Chains". English. In: *Physical Review Letters* 119.2 (2017). DOI: 10.1103/PhysRevLett.119.024301 (cit. on pp. 13, 14).

[109] M. Miniaci, R. K. Pal, B. Morvan, and M. Ruzzene. "Experimental Observation of Topologically Protected Helical Edge Modes in Patterned Elastic Plates". en. In: *Physical Review X* 8.3 (2018), p. 031074. DOI: 10.1103/PhysRevX.8.031074 (cit. on pp. 13, 14).

[110] HB Huang, JJ Chen, and SY Huo. "Simultaneous Topological Bragg and Locally Resonant Edge Modes of Shear Horizontal Guided Wave in One-Dimensional Structure". English. In: *Journal of Physics D: Applied Physics* 50.27 (2017). DOI: 10.1088/1361-6463/aa7619 (cit. on p. 14).

[111] J Vila, GH Paulino, and M Ruzzene. "Role of Nonlinearities in Topological Protection: Testing Magnetically Coupled Fidget Spinners". English. In: *Physical Review B* 99.12 (2019). DOI: 10.1103/PhysRevB.99.125116 (cit. on p. 14).

[112] SF Li, DG Zhao, H Niu, XF Zhu, and JF Zang. "Observation of Elastic Topological States in Soft Materials". English. In: *Nature Communications* 9 (2018). DOI: 10.1038/s41467-018-03830-8 (cit. on p. 14).

[113] YW Tsai, YT Wang, PG Luan, and TJ Yen. "Topological Phase Transition in a One-Dimensional Elastic String System". English. In: *Crystals* 9.6 (2019). DOI: 10.3390/cryst9060313 (cit. on p. 14).

[114] Di Zhou, Leyou Zhang, and Xiaoming Mao. "Topological Boundary Floppy Modes in Quasicrystals". en. In: *Physical Review X* 9.2 (2019), p. 021054. DOI: 10.1103/PhysRevX.9.021054 (cit. on p. 17).

[115] T C Lubensky, C L Kane, Xiaoming Mao, A Souslov, and Kai Sun. "Phonons and Elasticity in Critically Coordinated Lattices". en. In: *Reports on Progress in Physics* 78.7 (2015), p. 073901. DOI: 10.1088/0034-4885/78/7/073901 (cit. on pp. 17–19, 33).

[116] Di Zhou, Leyou Zhang, and Xiaoming Mao. "Topological Edge Floppy Modes in Disordered Fiber Networks". en. In: *Physical Review Letters* 120.6 (2018), p. 068003. DOI: 10.1103/PhysRevLett.120.068003 (cit. on p. 17).

[117] S Guest. "On the Determinacy of Repetitive Structures". en. In: *Journal of the Mechanics and Physics of Solids* 51.3 (2003), pp. 383–391. DOI: 10.1016/S0022-5096(02)00107-2 (cit. on p. 18).

[118] Kenneth Hoffman and Ray Alden Kunze. *Linear Algebra*. 2d ed. Englewood Cliffs, N.J: Prentice-Hall, 1971. 407 pp. ISBN: 978-0-13-536797-1 (cit. on p. 18).

[119] J. Clerk Maxwell. "L. *On the Calculation of the Equilibrium and Stiffness of Frames*". en. In: *The London, Edinburgh, and Dublin Philosophical Magazine and Journal of Science* 27.182 (1864), pp. 294–299. DOI: 10.1080/14786446408643668 (cit. on p. 19).

[120] C.R. Calladine. "Buckminster Fuller's "Tensegrity" Structures and Clerk Maxwell's Rules for the Construction of Stiff Frames". en. In: *International Journal of Solids and Structures* 14.2 (1978), pp. 161–172. DOI: 10.1016/0020-7683(78)90052-5 (cit. on p. 19).

[121] Steven H. Simon. *The Oxford Solid State Basics*. 1st ed. Oxford: Oxford University Press, 2013. 290 pp. ISBN: 978-0-19-968077-1 978-0-19-968076-4 (cit. on p. 19).

[122] Krishanu Roychowdhury and Michael J. Lawler. "Classification of Magnetic Frustration and Metamaterials from Topology". en. In: *Physical Review B* 98.9 (2018), p. 094432. DOI: 10.1103/PhysRevB.98.094432 (cit. on p. 38).

[123] Mariya Lizunova and Jasper Van Wezel. "An Introduction to Kinks in $\varphî4$-Theory". In: *SciPost Physics Lecture Notes* (2021), p. 23. DOI: 10.21468/SciPostPhysLectNotes.23 (cit. on p. 62).